

GPS RECEIVER SELF SURVEY AND ATTITUDE  
DETERMINATION USING PSEUDOLITE SIGNALS

A Dissertation

by

KEUN JOO PARK

Submitted to the Office of Graduate Studies of  
Texas A&M University  
in partial fulfillment of the requirements for the degree of

DOCTOR OF PHILOSOPHY

August 2004

Major Subject: Aerospace Engineering

© 2004

KEUN JOO PARK

ALL RIGHTS RESERVED

GPS RECEIVER SELF SURVEY AND ATTITUDE  
DETERMINATION USING PSEUDOLITE SIGNALS

A Dissertation

by

KEUN JOO PARK

Submitted to Texas A&M University  
in partial fulfillment of the requirements  
for the degree of

DOCTOR OF PHILOSOPHY

Approved as to style and content by:

---

John L. Crassidis  
(Co-Chair of Committee)

---

Daniele Mortari  
(Co-Chair of Committee)

---

John L. Junkins  
(Member)

---

Srinivas R. Vadali  
(Member)

---

Don R. Halverson  
(Member)

---

Walter E. Haisler  
(Head of Department)

August 2004

Major Subject: Aerospace Engineering

## ABSTRACT

GPS Receiver Self Survey and Attitude

Determination Using Pseudolite Signals. (August 2004)

Keun Joo Park, B.S., Inha University;

M.S., Inha University

Co-Chairs of Advisory Committee: Dr. John L. Crassidis  
Dr. Daniele Mortari

This dissertation explores both the estimation of various parameters from a multiple antenna GPS receiver, which is used as an attitude sensor, and attitude determination using GPS-like Pseudolite signals. To use a multiple antenna GPS receiver as an attitude sensor, parameters such as baselines, integer ambiguities, line biases, and attitude, should be resolved beforehand. Also, due to a cycle slip problem a subsystem to correct this problem should be implemented. All of these tasks are called a self survey. A new algorithm to estimate these parameters from a GPS receiver is developed using nonlinear batch filtering methods. For convergence issues, both the nonlinear least squares (NLS) and Levenberg-Marquardt (LM) methods are applied in the estimation. A comparison of the NLS and LM methods shows that the convergence of the LM method for the large initial errors is more robust than that of the NLS. In the proximity of the International Space Station (ISS), Pseudolite signals replace the GPS signals since almost all signals are blocked. Since the Pseudolite signals have spherical wavefronts, a new observation model should be applied. A nonlinear predictive filter, an extended Kalman filter (EKF), and an unscented filter (UF) are developed and compared using Pseudolite signals. A nonlinear predictive

filter can provide a deterministic solution; however, it cannot be used for the moving case. Instead, the EKF or the UF can be used with the angular rate measurements. A comparison of EKF and UF shows that the convergence of the UF for the large initial errors is more robust than that of the EKF. Also, an alternative global navigation constellation is presented by using the Flower Constellation (FC) scheme. A comparison of FC global navigation constellation and other GPS constellations, U.S. GPS, Galileo, and GLONASS, shows that position and attitude errors of the FC constellation are smaller than those of the others.

To whom I love . . .

## ACKNOWLEDGMENTS

As far as the laws of mathematics refer to reality, they are not certain; and as far as they are certain, they do not refer to reality.

Albert Einstein

For the last 20 years I have been a student. As I'm concluding my student life, I cannot help agreeing with the above words of Einstein. In fact, I always feel I need to learn something more. Without the encouragement of many people, I could not have completed this dissertation. Here, I'd like to remember some very special people who helped to make my journey to the Ph.D. degree possible.

First of all, I'd like to thank both of my advisors. Without their support, I could not have finished my goal. Dr. John L. Crassidis always gave support and guidance to me. Following his advice, every problem was clarified and resolved. Dr. Daniele Mortari also helped me and introduced me to new problems. Then, I thank all the other committee members. Dr. John L. Junkins always gave kind advice and helped to strengthen my understanding of dynamics and kinematics. Dr. Srinivas R. Vadali helped me to build the concept of optimality and is a model scholar. Dr. Don R. Halverson was very understanding.

For the research, I thank Ms. Janet Bell of NASA's Johnson Space Center for her management of the project. Also, I thank many researchers at Navigation Systems and Technology Laboratory for their helpful advice and cooperation.

Then, I should thank Dr. Jane Sell for her valuable advice and support. She was a perfect mentor whenever I was in difficulty due to cultural shock. Also, I have to thank Dr. Jinho Kim who was the advisor of my master's thesis. Without his encouragement to study in the United States, my dissertation would never have been initiated.

Especially, I thank my parents, Hee Hong Park and Chung Ae Lee, for their never ending sacrifice and support. Without their love, I couldn't have started this academic journey. My brother is also a wonderful supporter. The encouragement of my friends is appreciated as well.

Finally, the most and grateful thanks to my wife, Hye Jin, she shares the sweet and bitter with me from the beginning.

I thank you all again!



## TABLE OF CONTENTS

CHAPTER		Page
I	INTRODUCTION . . . . .	1
II	ESTIMATION TECHNIQUES . . . . .	7
	2.1 Least Squares . . . . .	7
	2.1.1 Weighted Least Squares . . . . .	8
	2.1.2 Sequential Least Squares . . . . .	9
	2.1.3 Nonlinear Least Squares . . . . .	9
	2.2 Levenberg-Marquardt Algorithm . . . . .	12
	2.3 Maximum Likelihood Estimation . . . . .	12
	2.4 The Cramér-Rao Inequality . . . . .	13
	2.5 Extended Kalman Filtering . . . . .	13
	2.6 Nonlinear Predictive Filtering . . . . .	14
	2.7 Unscented Filtering . . . . .	16
	2.8 Summary . . . . .	19
III	ATTITUDE DETERMINATION PROBLEM . . . . .	20
	3.1 Attitude Parameters . . . . .	20
	3.1.1 Euler Angles . . . . .	20
	3.1.2 Quaternions . . . . .	21
	3.1.3 Modified Rodrigues Parameters . . . . .	23
	3.2 Process Error Covariance . . . . .	24
	3.3 Solutions of Wahba Problem . . . . .	25
	3.4 Summary . . . . .	27
IV	THE GLOBAL POSITIONING SYSTEM . . . . .	28
	4.1 GPS Overview . . . . .	28
	4.2 GPS Data Format . . . . .	30
	4.3 GPS Signals . . . . .	30
	4.4 GPS Errors . . . . .	31
	4.4.1 Multipath Error . . . . .	31
	4.4.2 Cycle Ambiguity . . . . .	32
	4.4.3 Line Bias . . . . .	32
	4.4.4 Cycle Slip . . . . .	32

CHAPTER	Page
4.4.5 Dilution of Precision . . . . .	32
4.4.5.1 Geometric DOP . . . . .	32
4.4.5.2 Attitude DOP . . . . .	33
4.5 Alternative GPS Constellation . . . . .	33
4.5.1 Flower Constellation . . . . .	35
4.5.1.1 Background . . . . .	35
4.5.1.2 GNFC Constellation . . . . .	37
4.5.2 Simulation and Result . . . . .	39
4.5.3 Conclusion . . . . .	46
V SELF SURVEY . . . . .	48
5.1 Problem Statement . . . . .	48
5.2 Previous Work . . . . .	49
5.2.1 Integer Ambiguity Resolution . . . . .	50
5.2.1.1 Geometric Constraint . . . . .	51
5.2.1.2 Cost Minimization . . . . .	52
5.2.2 Survey Window . . . . .	55
5.3 New Approach . . . . .	60
5.3.1 Cycle Slip Detection and Repair . . . . .	60
5.3.2 Integer Ambiguity Resolution . . . . .	62
5.3.2.1 Double Differences . . . . .	63
5.3.2.2 Geometric Constraint for Double Differences . . . . .	65
5.3.2.3 Integer Ambiguity Resolution . . . . .	65
5.3.3 Nonlinear Least Squares . . . . .	67
5.3.4 Baseline Estimation . . . . .	69
5.3.5 Covariance Study . . . . .	69
5.3.5.1 Integer Ambiguity Resolution . . . . .	70
5.3.5.2 Nonlinear Least Squares . . . . .	70
5.3.5.3 Baseline/Line Biases Estimation . . . . .	70
5.4 Implementation . . . . .	71
5.4.1 STK/Chains . . . . .	71
5.4.2 GPS Almanac . . . . .	72
5.5 Simulation and Result . . . . .	75
5.6 Real Data Application . . . . .	80
5.7 Summary . . . . .	88
VI PSEUDOLITE SIGNALS APPLICATION . . . . .	89
6.1 Problem Statement . . . . .	89

CHAPTER	Page
6.2 Previous Work . . . . .	91
6.3 New Approach . . . . .	91
6.4 Implementation . . . . .	92
6.4.1 Nonlinear Least Squares . . . . .	92
6.4.2 Levenberg-Marquardt Method . . . . .	93
6.4.3 Nonlinear Predictive Filter . . . . .	93
6.4.4 Extended Kalman Filter . . . . .	97
6.4.5 Unscented Filter . . . . .	99
6.5 Simulation . . . . .	101
6.5.1 NLS and LM . . . . .	104
6.5.2 Nonlinear Predictive Filter . . . . .	105
6.5.2.1 Static Case . . . . .	105
6.5.2.2 Moving Cases . . . . .	111
6.5.3 EKF and UF . . . . .	119
6.5.3.1 Monte Carlo Simulation . . . . .	119
6.5.3.2 Large Initial Errors . . . . .	123
6.6 Summary . . . . .	127
VII CONCLUSION . . . . .	128
REFERENCES . . . . .	130
APPENDIX A . . . . .	140
VITA . . . . .	142

## LIST OF TABLES

TABLE		Page
4.1	Example GNFC Parameters . . . . .	37
4.2	GNFC Parameters: $\Omega_k$ and $M_k$ (In Degrees) . . . . .	38
4.3	Parameters Used in Simulation . . . . .	39
4.4	Percent Changes in GDOP vs. GNFC . . . . .	43
4.5	Percent Changes in ADOP vs. GNFC . . . . .	46
5.1	Survey Window Types . . . . .	57
5.2	WGS84 System Values . . . . .	74
5.3	GPS Almanac Ephemeris URE . . . . .	74
5.4	SEM GPS Almanac Data Format . . . . .	74
5.5	Convergence of Nonlinear Least Squares . . . . .	81
5.6	Integer Ambiguities . . . . .	83
5.7	Line Biases (Unit: Cycles) . . . . .	83
6.1	Locations of Transceivers and Antennas . . . . .	103
6.2	Angular Velocities and Weighting Matrices for Each Case . . . . .	105
6.3	Mean and Standard Deviation Values . . . . .	111

## LIST OF FIGURES

FIGURE		Page
2.1	Procedure of Nonlinear Least Squares . . . . .	11
4.1	Example of GPS Status Data . . . . .	29
4.2	GPS Observation Data Example . . . . .	30
4.3	Example of GPS Navigation Data . . . . .	31
4.4	Half GNFC . . . . .	38
4.5	Complete GNFC . . . . .	38
4.6	The GNFC Constellation (Polar View) . . . . .	39
4.7	The GNFC Constellation (Isometric View) . . . . .	40
4.8	Example Accesses Computed by STK for the GNFC Constellation and Receiver Locations (Shaded Boxes) . . . . .	41
4.9	Number of GNFC Satellites in Connection . . . . .	42
4.10	Number of U.S. GPS Satellites in Connection . . . . .	43
4.11	GDOP History for Selected Latitude Locations . . . . .	44
4.12	GDOP Comparison . . . . .	45
4.13	ADOP Comparison . . . . .	47
4.14	GNFC GDOPs for Whole Earth Locations . . . . .	47
5.1	Planar Phase Measurement Model . . . . .	49
5.2	An Example of Survey Window . . . . .	56
5.3	Availability of Survey Window . . . . .	57
5.4	Covariance of Baseline Estimation Error for Each Type . . . . .	58
5.5	Covariance of Line Bias Estimation Error for Each Type . . . . .	59
5.6	Flow Chart of Self Survey . . . . .	61
5.7	Measured and Cycle Slips Repaired $\Delta\phi$ Example . . . . .	62

FIGURE	Page
5.8	Measured and Estimated $\Delta\dot{\phi}$ Example . . . . . 63
5.9	Cycle Slips Detection and Repair Block Diagram . . . . . 64
5.10	STK Main Window for GPS Constellation . . . . . 72
5.11	GPS Constellation Simulation Using STK (2-D Map) . . . . . 73
5.12	SEM GPS Almanac Data . . . . . 75
5.13	Attitude Error Comparison Between NLS and LM . . . . . 76
5.14	Line Bias Error Comparison Between NLS and LM . . . . . 77
5.15	Baseline Error Comparison Between NLS and LM . . . . . 78
5.16	Iteration Number Comparison Between NLS and LM . . . . . 79
5.17	Convergence Comparison Between NLS and LM . . . . . 79
5.18	Baselines in the ENU Coordinate System . . . . . 80
5.19	TANS Vector GPS Receiver Phase Measurements . . . . . 82
5.20	The Residual Error of $\widetilde{\Delta\phi}_{i2} - \Delta\phi_{i2}$ for $i = 1, 2, 3$ . . . . . 84
5.21	The Residual Error of $\widetilde{\Delta\phi}_{i4} - \Delta\phi_{i4}$ for $i = 1, 2, 3$ . . . . . 85
5.22	The Residual Error of $\widetilde{\Delta\phi}_{i7} - \Delta\phi_{i7}$ for $i = 1, 2, 3$ . . . . . 85
5.23	The Residual Error of $\widetilde{\Delta\phi}_{i8} - \Delta\phi_{i8}$ for $i = 1, 2, 3$ . . . . . 86
5.24	The Residual Error of $\widetilde{\Delta\phi}_{i11} - \Delta\phi_{i11}$ for $i = 1, 2, 3$ . . . . . 86
5.25	The Residual Error of $\widetilde{\Delta\phi}_{i19} - \Delta\phi_{i19}$ for $i = 1, 2, 3$ . . . . . 87
5.26	The Residual Error of $\widetilde{\Delta\phi}_{i24} - \Delta\phi_{i24}$ for $i = 1, 2, 3$ . . . . . 87
6.1	Non-Planar Pseudolite Carrier Phase Measurement Model . . . . . 90
6.2	USQUE Procedure . . . . . 102
6.3	Geometric Configuration of Simulation . . . . . 103
6.4	Euler Angle Errors of NLS/LM Estimation (Static) . . . . . 104
6.5	Attitude History Comparison . . . . . 106

FIGURE	Page
6.6	Attitude Error Comparison in the Roll Axis . . . . . 107
6.7	Attitude Error Comparison in the Pitch Axis . . . . . 107
6.8	Attitude Error Comparison in the Yaw Axis . . . . . 108
6.9	Attitude History Comparison . . . . . 109
6.10	Attitude Error Distribution in the Roll Axis . . . . . 109
6.11	Attitude Error Distribution in the Pitch Axis . . . . . 110
6.12	Attitude Error Distribution in the Yaw Axis . . . . . 110
6.13	Attitude History Comparison (Moving-1) . . . . . 112
6.14	Attitude Error Comparison in the Roll Axis (Moving-1) . . . . . 112
6.15	Attitude Error Comparison in the Pitch Axis (Moving-1) . . . . . 113
6.16	Attitude Error Comparison in the Yaw Axis (Moving-1) . . . . . 113
6.17	Attitude History Comparison (Moving-2) . . . . . 114
6.18	Attitude Error Comparison in the Roll Axis (Moving-2) . . . . . 115
6.19	Attitude Error Comparison in the Pitch Axis (Moving-2) . . . . . 115
6.20	Attitude Error Comparison in the Yaw Axis (Moving-2) . . . . . 116
6.21	Attitude History Comparison (Moving-3) . . . . . 117
6.22	Attitude Error Comparison in the Roll Axis (Moving-3) . . . . . 117
6.23	Attitude Error Comparison in the Pitch Axis (Moving-3) . . . . . 118
6.24	Attitude Error Comparison in the Yaw Axis (Moving-3) . . . . . 118
6.25	EKF vs. UF Roll Error . . . . . 120
6.26	EKF vs. UF Pitch Error . . . . . 121
6.27	EKF vs. UF Yaw Error . . . . . 121
6.28	EKF vs. UF $\beta_1$ Error . . . . . 122
6.29	EKF vs. UF $\beta_2$ Error . . . . . 122
6.30	EKF vs. UF $\beta_3$ Error . . . . . 123
6.31	UF Attitude Estimation Errors . . . . . 124

FIGURE		Page
6.32	EKF Attitude Estimation Errors . . . . .	125
6.33	UF Bias Estimation Errors . . . . .	126
6.34	EKF Bias Estimation Errors . . . . .	126



## CHAPTER I

## INTRODUCTION

The definition of attitude determination is to estimate the attitude parameters of a body fixed coordinate frame, which is fixed to a vehicle body, relative to a reference coordinate frame, such as the Earth Centered Inertial (ECI) reference coordinates system. Due to the sensor type, attitude determination algorithms are largely divided into two approaches: static methods and filtering methods. Static methods give a point-by-point attitude solution, while filtering methods combine dynamic and/or kinematic models. Both methods use the measurements of the attitude sensors, such as a sun sensor, earth sensor, Three-Axis Magnetometer (TAM), and/or star sensor.

Vector observation methods usually use Line-Of-Sight (LOS) vectors as measurements. All static methods provide an attitude information without a priori information when at least two sets of unparallel LOS vector measurements are available.<sup>1-6</sup> These methods are divided into two sub-approaches. The simple and deterministic method is the TRIAD method that determines the attitude matrix by discarding part of the measurement information.<sup>1-3,5,7</sup> The main drawback of the TRIAD algorithm is that it cannot handle multiple measurement sets. However, a spacecraft usually has more than two attitude sensors for redundancy. An optimal problem using more than two sensor measurements was first proposed by Wahba in 1965.<sup>8</sup> Wahba's problem needs to determine the attitude matrix that minimizes a cost function. In 1968 Davenport posed the q-Method to solve Wahba's problem that determines the optimal quaternion by computing the maximum eigenvalue and its corresponding eigenvector of the  $\mathbf{K}$  matrix.<sup>1,3</sup> However, this approach requires a large computation burden because the computation of the eigenvectors requires complex matrix factorization methods such as a QR factorization or a Singular Value Decomposition

---

This dissertation follows the style and format of the *Journal of Guidance, Control, and Dynamics*.

(SVD). In 1981 Shuster and Oh presented the QUEST algorithm that determines the maximum eigenvalue using one or two Newton-Raphson iterations to the  $\mathbf{K}$  matrix characteristic equation and, then, the optimal quaternion is estimated by applying the Cayley-Hamilton theorem together with the Gibbs vector.<sup>2,3</sup> Since the use of the Gibbs vector introduces a singularity for the principal angle close to  $\pi$ , the technique of sequential rotations is also proposed.<sup>2,3</sup> In 1992 Markley proposed the Fast Optimal Attitude Matrix (FOAM) algorithm that directly determines the attitude matrix minimizing Wahba's cost function.<sup>4</sup> In 2000 Mortari developed the second EStimator of the Optimal Quaternion (ESOQ2) that is a faster attitude estimation method fully complying with Wahba's optimality criterion.<sup>3,9,10</sup>

In case of eclipse or existing bright objects in the Field-Of-View (FOV) of the attitude sensors, static methods can often not determine an attitude solution, while other approaches combining dynamic and/or kinematic models with attitude sensor data can still predict attitude information.<sup>11-16</sup> These filtering algorithms can determine the attitude using even only one set of attitude sensor observation if the LOS vector has significant motion, such like a TAM.<sup>17</sup> Among methods using dynamics and/or kinematic models, the most common technique for attitude estimation is the Kalman filtering. These are also divided into two sub-approaches. One uses the gyro measurements with kinematic models.<sup>7,12,13,16-28</sup> The other algorithms use a dynamic model instead of angular rate measurements.<sup>29-33</sup> In general, the dynamic model is inaccurate since perfect information of moments of inertia, external torques, and disturbances cannot be obtained. Also, the angular rate measurements using gyros have either systematic or random errors.<sup>11,13,15</sup> Thus, other attitude sensors should be used to compensate the prediction errors. The estimation techniques that determine the state of a stochastic differential equations representing system dynamics from noisy observations have been investigated. Kalman and Bucy studied the problem for linear systems and showed that Kalman filter provides the optimal solution for maintaining a consistent estimate of the first two moments of the state distribution.<sup>11,13,15,34-36</sup> However, linear filtering theory cannot be applied directly to the attitude determination problem since the system model and the observation model are nonlinear. The Extended Kalman Filter (EKF) based on the linearized model is widely used in at-

titude estimation. Several parameterizations can be used to represent the attitude, such as Euler angles, quaternions, and Modified Rodrigues Parameters (MRP).<sup>37,38</sup> Among those quaternions are especially appealing since no singularities are present and the kinematics equation is bilinear.<sup>37,38</sup> However, the quaternion must obey a normalization constraint, which can be violated by the linear measurement updates associated with the standard EKF approach.<sup>26</sup> The most common approach to overcome this shortfall involves using a multiplicative error quaternion summarized by Lefferts, Markley, and Shuster.<sup>18,26,27</sup> Crassidis developed an EKF using MRPs.<sup>17</sup> Although the EKF has become a standard for nonlinear estimation, it has several drawbacks. The EKF uses a Gaussian approximation on the process and observation error. Also, it may be unstable for large initial errors since the EKF uses a first order linearization approximation. Also, the Jacobians of process and observation model should exist. Julier, Uhlmann, and Durrant-Whyte have developed an alternative to EKF, which is called the Unscented Filter (UF).<sup>35,39</sup> The UF involves more computations than the EKF, however, it has several advantages. Mainly, the UF is more robust for large initial errors than EKF and knowledge of Jacobian matrices can be avoided.<sup>20,34-36,39-42</sup> In the attitude determination applications, however, the quaternion based UF will fail because the sigma points will violate the quaternion normalization constraint. Crassidis and Markley developed the USQUE algorithm that is based on the UF.<sup>34</sup> The USQUE is proven to be more robust for large initial attitude errors than EKF. However, the UF still uses Gaussian assumption with known covariance in the process and observation model error. Crassidis et al. proposed a predictive filter that determines the model error during the estimation process,<sup>43</sup> which can estimate for non-Gaussian errors.

The Global Positioning System (GPS) was originally developed for the purpose of navigation. With the pseudorange measurements of the GPS receiver the instantaneous positions and velocities are determined as well as the precise time. No other instrument can provide this information with both the accuracy and bandwidth achievable with GPS. In addition to orbit determination, the capability of GPS to provide attitude information makes it increasingly applied in the attitude subsystem of modern spacecraft.<sup>23,24,29,44-59</sup> Since GPS receivers can also measure the signal

carrier phases, GPS receivers have been applied as attitude sensors with multiple antenna sets. However, when using the phase measurements the solution becomes more complicated since the phase measurements contain integer ambiguities.<sup>42,45,53,60–67</sup>

Furthermore, to utilize a GPS receiver as an attitude sensor, the system parameters such as baselines and line biases need to be determined, as well as integer ambiguities.<sup>53,68</sup> This operation is called the self survey. In general, the self survey requires 6 to 8 hours of data to estimate baselines, line biases, integer ambiguities, and attitude because the sightlines, i.e., the LOS vector between the GPS satellites and the receiver, are moving slowly.<sup>47,53,69</sup> The orbit period of GPS satellites is approximately 12 sidereal hours. Since the GPS satellites are moving, the connections between GPS satellites and receiver will be on and off repeatedly. When a new GPS satellite signal is available, the integer ambiguities should be resolved first. Also, the GPS signals are often blocked and jammed for up to ten minutes. This causes cycle slips or jumps in the phase measurements since the receiver accumulates the cycles of the carrier phase.<sup>67</sup> For the correct estimation, cycle slip free measurements should be obtained. Altmayer enhanced the integrity of an integrated GPS/INS system by cycle slip detection and correction.<sup>70</sup> Since the phases change slowly, cycle slips can be successfully detected and repaired by using a low-order polynomial fitting method.<sup>53</sup> As a result, several subsystem aspects such as an integer ambiguity resolution routine to determine the integer number wavelengths in the phase measurements and cycle slip detection and repair algorithm are needed for correct estimation. Once a self survey is accomplished, the attitude determination problem then can be solved.

Integer ambiguities are determined two approaches.<sup>61,63,71</sup> One is the instantaneous method that finds integer sets that minimizes a loss function by searching all possible integer sets.<sup>66,69</sup> Since the searching requires much time, Lightsey et al. proposed a geometric constraint that reduces the search space.<sup>63</sup> Also, they determined integer ambiguities when the baselines are coplanar. However, the minimum residual does not guarantee correct integers due to the measurement noise. Dynamic techniques that are more robust than instantaneous methods have also been developed. Cohen developed quasi-static integer resolution algorithm that uses a linearization approximation of observation model,<sup>71</sup> but requires a priori attitude information. An

attitude independent algorithm is developed by Crassidis.<sup>61,72</sup> Lightsey and Crassidis developed a real-time algorithm for attitude independent integer ambiguity resolution.<sup>42</sup>

In the key application by Cohen and Trimble Navigation, Ltd. in the late 1980's the GPS receivers, TANS Vector and TANS Quadrex, are designed primarily for airborne applications, tracking up to six satellites on four separate antennas.<sup>47</sup> Cohen has developed an iterative nonlinear least squares using Euler angles. When three non-coplanar baselines exist, Cohen showed that the solution based on Wahba's problem is almost an order faster than a nonlinear least squares algorithm. Still, an SVD that is computationally expensive should be performed. Bar-Itzhack et al. show another analytical conversion of the GPS phase difference measurements into unit vectors to be used in QUEST algorithm.<sup>46</sup> However, it only used two baselines sets. Crassidis and Markley have developed a generalized deterministic attitude solution using GPS phase difference measurements.<sup>50,51</sup> Crassidis et al. have proposed an efficient and optimal algorithm based on nonlinear predictive filter scheme first introduced by Crassidis and Markley.<sup>48,49</sup> This algorithm, called Attitude-Lean-Loping-Estimator using GPS Recursive Operations (ALLEGRO), has several advantages: 1) the ALLEGRO is non-iterative, 2) an optimal attitude is provided even for coplanar baseline configurations, and 3) it guarantees convergence even for poor initial conditions.<sup>52</sup>

Estimator-based filtering methods such as the EKF have also been developed for GPS attitude determination applications. The main advantage of using filtering techniques is that the three-axis attitude solution can be achieved using less than three baseline sets as long as there is sufficient vehicle motion. Also, line biases can be estimated concurrently with the attitude. Fujikawa and Zimbelman developed an EKF using GPS signal phase differences to estimate the attitude and line biases using one baseline.<sup>73</sup> Crassidis et al. have proposed a new filter based on nonlinear predictive filter scheme.<sup>48,49,52</sup> This filter does not assume that the external torque is modeled by a zero-mean Gaussian process. Instead, it is determined during the estimation process. In the GPS receiver data defined by a RINEX format the Signal-to-Noise Ratio (SNR) of GPS signal is also measured. Axelrad and Behre have developed an attitude determination algorithm using GPS SNR measurements.<sup>44</sup> Lightsey and Madsen

developed an EKF algorithm using canted antenna SNR measurements.<sup>56</sup> However, the attitude errors of the SNR measurements methods are larger than those of using carrier phase measurements.

All of the various attitude determination approaches have been tested on a number of actual spacecraft.<sup>74-78</sup> Currently, the International Space Station (ISS) uses GPS for both orbit and attitude determination. However, significant GPS signal outages occur due to various structures near the ISS. Gaylor et al. showed that GPS signals below 10 meters from the ISS are blocked 99.99%.<sup>54</sup> Therefore, Pseudolite techniques are being developing by the Navigation Systems and Technology Laboratory (NSTL) in NASA Johnson Space Center (JSC) and Texas A&M university to replace GPS signals near the proximity of the ISS.<sup>53</sup> The Pseudolite Transceivers (PLTX) are used to transmit GPS-like signals. However, this leads to more complicated solutions because the pseudolite signals have spherical wavefronts. These non-planar (or spherical) wavefronts effects were investigated for the rendezvous problem by Zimmerman.<sup>79,80</sup> In the attitude determination algorithms, these effects should be resolved.

Therefore, in this dissertation two tasks are presented. First, the self survey algorithm using GPS signals is considered because the attitude determination using GPS receivers is not possible without knowing baselines, line biases, and integer ambiguity information. Optimal algorithms that are more efficient and reliable than conventional approaches are presented. The algorithms are implemented using MATLAB<sup>81</sup> and extensive simulations are executed for various simulation conditions. Furthermore, a comparison of the self-survey results with the commercial receiver results is presented. Then, optimal attitude determination algorithms using pseudolite signals are investigated. Nonlinear least squares, predictive filter, EKF, and UF based algorithms are derived and analyzed with realistic simulations.

## CHAPTER II

## ESTIMATION TECHNIQUES

Even for a simple spacecraft control system, angular rate information is needed to determine the control. We can use a system model, numerical derivatives, and gyro outputs for angular velocity. However, a model is often inaccurate, although some properties are known well. Also, gyro measurements contain either systematic or random errors. The estimation problem is to obtain the optimal state that minimizes a cost function constructed by the residual error between the true state and the estimated state.<sup>12</sup> Since the true state is unknown in the real world, it is replaced by the residual between the estimate and the measurement.<sup>14</sup> Once this residual is minimized, the residual between the true and the estimate is also considered to be minimized.<sup>14</sup> This chapter reviews some common estimation techniques.

## 2.1 Least Squares

Assume that the measurement model and the estimated output of a linear system are given by

$$\tilde{\mathbf{y}} = \mathbf{H}\mathbf{x} + \boldsymbol{\nu} \quad (2.1a)$$

$$\hat{\mathbf{y}} = \mathbf{H}\hat{\mathbf{x}} \quad (2.1b)$$

where the  $(\tilde{\cdot})$  represents the measurement, the  $(\hat{\cdot})$  denotes the estimate, and  $\boldsymbol{\nu}$  is the measurement error. Define the residual error as

$$\mathbf{e}_r \equiv \tilde{\mathbf{y}} - \hat{\mathbf{y}} \quad (2.2)$$

Then, the least squares by Gauss determines the optimal  $\hat{\mathbf{x}}$  that minimizes the sum square of the residual errors,<sup>14</sup> given by

$$J = \frac{1}{2} \mathbf{e}_r^\top \mathbf{e}_r \quad (2.3)$$

where the constant  $J$  is the loss function. An optimal  $\hat{\mathbf{x}}$  satisfies

$$\frac{\partial J}{\partial \mathbf{x}} = \mathbf{H}^\top \mathbf{H} \hat{\mathbf{x}} - \mathbf{H}^\top \tilde{\mathbf{y}} = \mathbf{0} \quad (2.4a)$$

$$\frac{\partial^2 J}{\partial \mathbf{x} \partial \mathbf{x}^\top} = \mathbf{H}^\top \mathbf{H} > 0 \quad (2.4b)$$

where Eq. (2.4a) is the necessary conditions and Eq. (2.4b) is the sufficient conditions. For a minimum of  $J$ , the matrix  $\mathbf{H}^\top \mathbf{H}$  must be positive definite. Then, the necessary conditions of Eq. (2.4a) yield the normal equations

$$(\mathbf{H}^\top \mathbf{H}) \hat{\mathbf{x}} = \mathbf{H}^\top \tilde{\mathbf{y}} \quad (2.5)$$

By using the direct inversion we obtain

$$\hat{\mathbf{x}} = (\mathbf{H}^\top \mathbf{H})^{-1} \mathbf{H}^\top \tilde{\mathbf{y}} \quad (2.6)$$

For the overdetermined case that the dimension of the measurements is larger than that of the state, and the numerical methods to solve the least squares are well explained in Ref. [82]. As for speed and accuracy, the QR factorization approach is the best algorithm to compute the least squares solution. If the measurements are fewer than the state dimension, a minimum norm solution can still be obtained by applying a Lagrange multiplier.<sup>82</sup>

### 2.1.1 Weighted Least Squares

Since the measurements might be made with unequal precision, the weights of the reciprocal of the measurement error variance in Eq. (2.3) are considered to yield a statistically optimal solution.<sup>12,14</sup> Then, the new loss function to be minimized is given by

$$J = \frac{1}{2} \mathbf{e}_r^\top \mathbf{W} \mathbf{e}_r \quad (2.7)$$

where the matrix  $\mathbf{W}$  is symmetric and positive definite of which components are given by

$$w_{ij} = \sigma_{ij}^{-2} \quad (2.8)$$

where  $\sigma_{ij}^2 (i = j)$  are the variances, and  $\sigma_{ij}^2 (i \neq j)$  are the cross-correlation terms. Then, from the necessary conditions, the optimal estimate is given by

$$\hat{\mathbf{x}} = (\mathbf{H}^\top \mathbf{W} \mathbf{H})^{-1} \mathbf{H}^\top \mathbf{W} \tilde{\mathbf{y}} \quad (2.9)$$



### 2.1.2 Sequential Least Squares

Assume two subsets of measurement data are given by

$$\tilde{\mathbf{y}}_1 = \mathbf{H}_1 \mathbf{x} + \boldsymbol{\nu}_1 \quad (2.10a)$$

$$\tilde{\mathbf{y}}_2 = \mathbf{H}_2 \mathbf{x} + \boldsymbol{\nu}_2 \quad (2.10b)$$

The least squares solution using the data subset in Eq. (2.10a) yields the estimate

$$\hat{\mathbf{x}}_1 = (\mathbf{H}_1^\top \mathbf{W}_1 \mathbf{H}_1)^{-1} \mathbf{H}_1^\top \mathbf{W}_1 \tilde{\mathbf{y}}_1 \quad (2.11)$$

Then, by using this information, the update estimate using the data subset in Eq. (2.10b) can be expressed by

$$\hat{\mathbf{x}}_2 = \hat{\mathbf{x}}_1 + \mathbf{P}_2 \mathbf{H}_2^\top \mathbf{W}_2 (\tilde{\mathbf{y}}_2 - \mathbf{H}_2 \hat{\mathbf{x}}_1) \quad (2.12)$$

Therefore, a large matrix inversion can be avoided. The general form, known as the Kalman update, is given by

$$\hat{\mathbf{x}}_{k+1} = \hat{\mathbf{x}}_k + \mathbf{K}_{k+1} (\tilde{\mathbf{y}}_{k+1} - \mathbf{H}_{k+1} \hat{\mathbf{x}}_k) \quad (2.13a)$$

$$\mathbf{K}_{k+1} = \mathbf{P}_{k+1} \mathbf{H}_{k+1}^\top \mathbf{W}_{k+1} \quad (2.13b)$$

$$\mathbf{P}_{k+1}^{-1} = \mathbf{P}_k^{-1} + \mathbf{H}_{k+1}^\top \mathbf{W}_{k+1} \mathbf{H}_{k+1} \quad (2.13c)$$

If the dimension of measurement is less than that of the state, an alternative form can be used to reduce the computation of the matrix inverses,<sup>12,14</sup> given by

$$\hat{\mathbf{x}}_{k+1} = \hat{\mathbf{x}}_k + \mathbf{K}_{k+1} (\tilde{\mathbf{y}}_{k+1} - \mathbf{H}_{k+1} \hat{\mathbf{x}}_k) \quad (2.14a)$$

$$\mathbf{K}_{k+1} = \mathbf{P}_k \mathbf{H}_{k+1}^\top (\mathbf{H}_{k+1} \mathbf{P}_k \mathbf{H}_{k+1}^\top + \mathbf{W}_{k+1}^{-1})^{-1} \quad (2.14b)$$

$$\mathbf{P}_{k+1} = (\mathbf{I} - \mathbf{K}_{k+1} \mathbf{H}_{k+1}) \mathbf{P}_k \quad (2.14c)$$

### 2.1.3 Nonlinear Least Squares

Although the optimal solutions for the linear system are available, many real estimation problems are generally nonlinear. To solve a nonlinear estimation problem, a successive approximation procedure, such as a least square differential correction, developed by Gauss can be used.<sup>12</sup> However, the convergence of the multi-dimensional

case is guaranteed only under requirements on the functions that the first two partial derivatives should exist and the initial guesses are close to the true values.<sup>12,14</sup>

The nonlinear least squares algorithm using Newton's method is shown here. Assume the output model is

$$\mathbf{y} = \mathbf{f}(\mathbf{x}) \quad (2.15)$$

where  $\mathbf{f}$  is the model function whose first partial derivatives should be single-valued, continuous, and at least once differentiable. Then, the measurement and the estimate are given by

$$\tilde{\mathbf{y}} = \mathbf{f}(\mathbf{x}) + \boldsymbol{\nu} \quad (2.16a)$$

$$\hat{\mathbf{y}} = \mathbf{f}(\hat{\mathbf{x}}) \quad (2.16b)$$

Let the residual error be  $\mathbf{e}_r = \tilde{\mathbf{y}} - \hat{\mathbf{y}}$ . Then, the loss function to be minimized is given by

$$J = \frac{1}{2} \mathbf{e}_r^T \mathbf{W} \mathbf{e}_r = \frac{1}{2} [\tilde{\mathbf{y}} - \mathbf{f}(\hat{\mathbf{x}})]^T \mathbf{W} [\tilde{\mathbf{y}} - \mathbf{f}(\hat{\mathbf{x}})] \quad (2.17)$$

Since it is difficult to find the solution of the nonlinear function  $\mathbf{f}(\hat{\mathbf{x}})$  explicitly, assume the estimate of the unknown is given by

$$\hat{\mathbf{x}} = \mathbf{x}_c + \Delta \mathbf{x} \quad (2.18)$$

where  $\mathbf{x}_c$  is the nominal state and  $\Delta \mathbf{x}$  is the correction. Then, by linearizing the model  $\mathbf{f}(\hat{\mathbf{x}})$  the correction can be obtained if the correction is sufficiently small.<sup>14</sup> A 1st-order Taylor series expansion of the model about  $\mathbf{x}_c$  is given by

$$\mathbf{f}(\hat{\mathbf{x}}) \approx \mathbf{f}(\mathbf{x}_c) + \mathbf{H} \Delta \mathbf{x} \quad (2.19)$$

where the Jacobian matrix is

$$\mathbf{H} \equiv \left. \frac{\partial \mathbf{f}}{\partial \mathbf{x}} \right|_{\mathbf{x}_c} \quad (2.20)$$

The measurement residual can be rewritten as

$$\mathbf{e}_r = \tilde{\mathbf{y}} - \mathbf{f}(\hat{\mathbf{x}}) \approx \tilde{\mathbf{y}} - \mathbf{f}(\mathbf{x}_c) - \mathbf{H} \Delta \mathbf{x} = \Delta \mathbf{y} - \mathbf{H} \Delta \mathbf{x} \quad (2.21)$$

where

$$\Delta \mathbf{y} \equiv \tilde{\mathbf{y}} - \mathbf{f}(\mathbf{x}_c) \quad (2.22)$$

To seek the optimal  $\Delta \mathbf{x}$ , a loss function to be minimized is given by

$$\Delta J = \frac{1}{2} (\Delta \mathbf{y} - \mathbf{H} \Delta \mathbf{x})^T \mathbf{W} (\Delta \mathbf{y} - \mathbf{H} \Delta \mathbf{x}) \quad (2.23)$$

Therefore,

$$\Delta \mathbf{x} = (\mathbf{H}^T \mathbf{W} \mathbf{H})^{-1} \mathbf{H}^T \mathbf{W} \Delta \mathbf{y} \quad (2.24)$$

Then, the new nominal state is updated as

$$\mathbf{x}_c = \mathbf{x}_c + \Delta \mathbf{x} \quad (2.25)$$

This procedure repeats until a certain stopping condition is met. A stopping condition with an accuracy dependent tolerance for minimization of  $J$  is given by

$$\frac{\Delta J}{J} < \frac{\epsilon}{\|\mathbf{W}\|} \quad (2.26)$$

where  $\epsilon$  is predetermined tolerance and  $\|\cdot\|$  denotes a matrix norm. The procedure of nonlinear least squares is shown in Fig. 2.1.

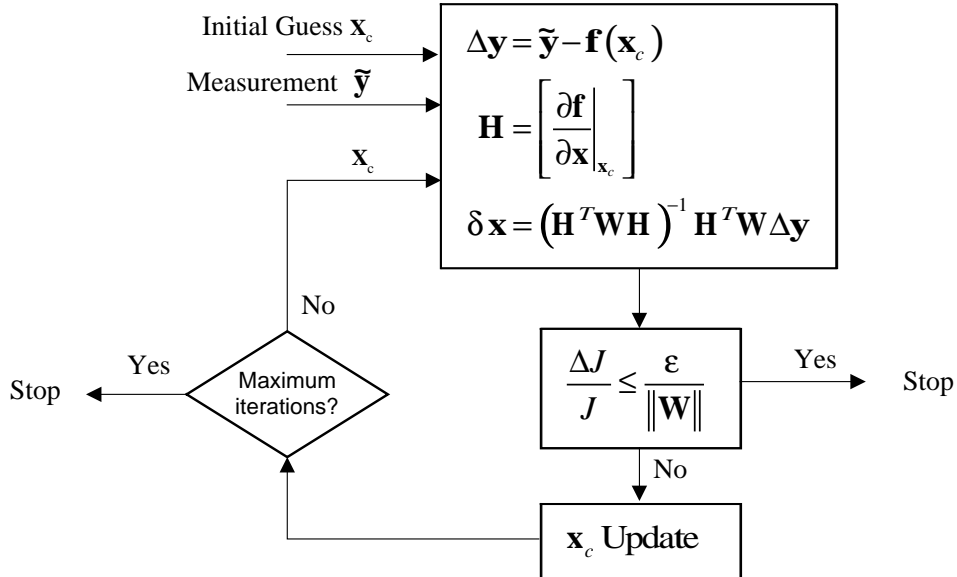


Fig. 2.1. Procedure of Nonlinear Least Squares

## 2.2 Levenberg-Marquardt Algorithm

For some nonlinear problems the nonlinear least squares may not converge to correct solutions unless the initial guess is close to a minimum in the loss function. The method of steepest descent may help to avoid this problem, however, the convergence is very poor close to the solution.<sup>83</sup> These difficulties can be overcome by Levenberg-Marquardt(LM) method.<sup>12,84</sup> In the LM method, the normal equations in Eq. (2.24) are modified as

$$\Delta \mathbf{x} = (\mathbf{H}^T \mathbf{W} \mathbf{H} + \eta \mathcal{H})^{-1} \mathbf{H}^T \mathbf{W} \Delta \mathbf{y} \quad (2.27)$$

where  $\eta$  is a scaling factor, and  $\mathcal{H}$  is a diagonal matrix with entries given by the diagonal elements of  $\mathbf{H}^T \mathbf{W} \mathbf{H}$ . By using Eq. (2.27) the search direction is intermediate between the steepest descent and the differential correction direction. As  $\eta \rightarrow 0$ , Eq. (2.27) is equivalent to the differential correction method, however, as  $\eta \rightarrow \infty$  Eq. (2.27) becomes a steepest descent search along the negative gradient of  $J$ . Thus, the LM algorithm is as follows:

1. Do an update using Eq. (2.27).
2. Evaluate the loss function in Eq. (2.17) using new parameters.
3. If the cost has increased, then reset the update and increase  $\eta$  by a factor of  $f$ , where  $f$  is a specified integer. Then go back to 1. and try an update again.
4. If the cost has decreased, then accept new parameters as an update and decrease  $\eta$  by a factor of  $f$ .

## 2.3 Maximum Likelihood Estimation

The objective of Maximum Likelihood Estimation (MLE) is to maximize the probability of obtaining an observed set of data. Let the likelihood function given by

$$L(\tilde{\mathbf{y}}, \mathbf{x}) = \prod_{i=1}^N f_i(\tilde{\mathbf{y}}, \mathbf{x}) \quad (2.28)$$

where  $N$  is the total number of probability density functions (p.d.f.). Generally, many p.d.f. involve exponential terms. Since the natural logarithm function is monotonic,

maximizing  $\ln L$  is equivalent to maximizing  $L$ . Thus, the necessary and sufficient conditions are

$$\frac{\partial}{\partial \mathbf{x}} \left\{ \ln L(\tilde{\mathbf{y}}, \mathbf{x}) \right\} \Big|_{\mathbf{x}=\hat{\mathbf{x}}} = \mathbf{0} \quad (2.29a)$$

$$\frac{\partial^2}{\partial \mathbf{x} \partial \mathbf{x}^\top} \left\{ \ln L(\tilde{\mathbf{y}}, \mathbf{x}) \right\} \Big|_{\mathbf{x}=\hat{\mathbf{x}}} \leq \mathbf{0} \quad (2.29b)$$

It is known that MLE can produce biased estimates, however, if a large number of data is used then the MLE is approximately unbiased and has the same variance that approaches the smallest that can be achieved by any estimator. Also, the estimation errors in a maximum likelihood estimate is asymptotically Gaussian no matter what p.d.f. is used. For a zero-mean, Gaussian noise process, both the MLE and minimum variance estimate yield the same result.

## 2.4 The Cramér-Rao Inequality

The Cramér-Rao Inequality is used to represent the lower bound of the estimation errors. For an unbiased estimate, the Cramér-Rao Inequality is given by

$$\mathbf{P} \equiv E \left\{ (\hat{\mathbf{x}} - \mathbf{x})(\hat{\mathbf{x}} - \mathbf{x})^\top \right\} \geq \mathbf{F}^{-1} \quad (2.30)$$

where  $\mathbf{P}$  is the covariance matrix and  $\mathbf{F}$  is the Fisher information matrix, which is given by

$$\mathbf{F} \equiv E \left\{ \left[ \frac{\partial}{\partial \mathbf{x}} \ln L(\tilde{\mathbf{y}}, \mathbf{x}) \right] \left[ \frac{\partial}{\partial \mathbf{x}} \ln L(\tilde{\mathbf{y}}, \mathbf{x}) \right]^\top \right\} \quad (2.31)$$

Any estimator is said optimal if  $\mathbf{P} = \mathbf{F}^{-1}$ .

## 2.5 Extended Kalman Filtering

For a linear system, the optimality of the Kalman filter is well proven.<sup>11</sup> For the case of a nonlinear system, by using a linearized model of the nonlinear system, we can still use the Kalman filter if the errors are assumed small. Let the model be

$$\dot{\mathbf{x}} = \mathbf{f}(\mathbf{x}) + \mathbf{g}(\mathbf{x}) \mathbf{w} \quad (2.32a)$$

$$\tilde{\mathbf{y}}_k = \mathbf{h}(\mathbf{x}_k) + \mathbf{v}_k \quad (2.32b)$$

where  $\mathbf{f}(\mathbf{x}) \in \mathbb{R}^n \rightarrow \mathbb{R}^n$  is the assumed model vector,  $\mathbf{x} \in \mathbb{R}^n$  is the true state vector,  $\mathbf{g} \in \mathbb{R}^{n \times p}$  is the process noise distribution matrix,  $\tilde{\mathbf{y}}_k \in \mathbb{R}^m$  is the measurement vector,  $\mathbf{h}(\mathbf{x}_k) \in \mathbb{R}^n \rightarrow \mathbb{R}^m$  is the observation model vector, and  $\mathbf{w}$  and  $\mathbf{v}_k$  are zero-mean Gaussian noise processes with the properties given by

$$\mathbf{w} = \mathcal{N}(\mathbf{0}, \mathbf{Q}) \quad (2.33a)$$

$$\mathbf{v}_k = \mathcal{N}(\mathbf{0}, \mathbf{R}_k) \quad (2.33b)$$

where  $\mathbf{Q}$  and  $\mathbf{R}_k$  are the covariance matrices. The prediction between measurements is given by

$$\dot{\hat{\mathbf{x}}} = \mathbf{f}(\hat{\mathbf{x}}) \quad (2.34a)$$

$$\dot{\mathbf{P}} = \mathbf{f}_x \mathbf{P} + \mathbf{P} \mathbf{f}_x^\top + \mathbf{g}_x \mathbf{Q} \mathbf{g}_x^\top \quad (2.34b)$$

where  $\hat{\mathbf{x}} \in \mathbb{R}^n$  is the estimated state vector,  $\mathbf{P}$  is the error covariance matrix, and  $\mathbf{f}_x$  and  $\mathbf{g}_x$  are Jacobian matrices. The updates are

$$\hat{\mathbf{x}}_k^+ = \hat{\mathbf{x}}_k^- + \mathbf{K}_k [\tilde{\mathbf{y}}_k - \mathbf{h}(\hat{\mathbf{x}}_k^-)] \quad (2.35a)$$

$$\mathbf{P}_k^+ = [\mathbf{I} - \mathbf{K}_k \mathbf{H}_k] \mathbf{P}_k^- \quad (2.35b)$$

$$\mathbf{K}_k = \mathbf{P}_k^- \mathbf{H}_k^\top [\mathbf{H}_k \mathbf{P}_k^- \mathbf{H}_k^\top + \mathbf{R}_k]^{-1} \quad (2.35c)$$

where the ‘+’ sign denotes the updated state, the ‘-’ sign represents the propagated state, and the observation sensitivity matrix  $\mathbf{H}_k$  is given by

$$\mathbf{H}_k = \left. \frac{\partial \mathbf{h}}{\partial \mathbf{x}} \right|_{\mathbf{x}_k = \hat{\mathbf{x}}_k^-} \quad (2.36)$$

## 2.6 Nonlinear Predictive Filtering

The major advantage of the predictive filter is that the model error is not assumed to be represented by a zero-mean Gaussian noise process with known covariance, but instead is determined during the estimation process.<sup>43</sup> Crassidis et al. have proposed the nonlinear predictive filter by simultaneously solving system optimality conditions and an output error constraint. Since the multipath GPS signal error is known to have non-Gaussian components, this approach is fit for Pseudolite case because the multipath effect of using Pseudolite is more severe than those of using GPS signals.

In the predictive filter, the state and output estimates are given by a preliminary model and a to-be-determined model error vector,<sup>30</sup> which are given by

$$\dot{\hat{\mathbf{x}}}(t) = \mathbf{f}[\hat{\mathbf{x}}(t), t] + \mathbf{G}[\hat{\mathbf{x}}(t)] \mathbf{d}(t) \quad (2.37a)$$

$$\hat{\mathbf{y}}(t) = \mathbf{c}[\hat{\mathbf{x}}(t), t] \quad (2.37b)$$

where  $\mathbf{f} \in \mathbb{R}^n \rightarrow \mathbb{R}^n$  is sufficiently differentiable,  $\hat{\mathbf{x}}(t) \in \mathbb{R}^n$  is the state estimate vector,  $\mathbf{d}(t) \in \mathbb{R}^q$  is the model error vector,  $\mathbf{G}[\hat{\mathbf{x}}(t)] \in \mathbb{R}^n \rightarrow \mathbb{R}^{n \times q}$  is the model-error distribution matrix,  $\mathbf{c}[\hat{\mathbf{x}}(t), t] \in \mathbb{R}^n \rightarrow \mathbb{R}^m$  is the measurement vector, and  $\hat{\mathbf{y}} \in \mathbb{R}^m$  is the output estimate vector. The Taylor series expansion of the output estimate in Eq. (2.37b) is given by

$$\hat{\mathbf{y}}(t + \Delta t) \approx \hat{\mathbf{y}}(t) + \mathbf{z}[\hat{\mathbf{x}}(t), t] + \mathbf{\Lambda}(\Delta t) \mathbf{S}[\hat{\mathbf{x}}(t)] \mathbf{d}(t) \quad (2.38)$$

where  $\Delta t$  is the measurement sampling interval, and the matrix  $\mathbf{S}[\hat{\mathbf{x}}(t)]$  is a generalized sensitivity matrix, and  $\mathbf{\Lambda}(\Delta t) \in \mathbb{R}^{m \times m}$  is a diagonal matrix with elements given by

$$\lambda_{ii} = \Delta t^{p_i} / p_i! \quad i = 1, 2, \dots, m \quad (2.39)$$

where  $p_i$ ,  $i = 1, 2, \dots, m$  is the lowest order of the derivative of  $c_i[\hat{\mathbf{x}}(t)]$  in which any component of  $\mathbf{d}(t)$  first appears due to successive differentiation and substitution for  $\dot{\hat{\mathbf{x}}}(t)$  on the right side of Eq. (2.37a). The  $i$ -th component of vector  $\mathbf{z}[\hat{\mathbf{x}}(t), t]$  is given by

$$z_i(\hat{\mathbf{x}}, \Delta t) = \sum_{k=1}^{p_i} \frac{\Delta t_k}{k!} L_f^k(c_i) \quad (2.40)$$

where  $L_f^k(c_i)$  is the  $k$ -th Lie derivative.

A cost function consisting of the weighted sum square of the measurement-minus-estimate residual plus the weighted sum square of the model correction term is given by<sup>43,49</sup>

$$J[\mathbf{d}(t)] = \frac{1}{2} [\tilde{\mathbf{y}}(t + \Delta t) - \hat{\mathbf{y}}(t + \Delta t)]^T \mathbf{R}^{-1} [\tilde{\mathbf{y}}(t + \Delta t) - \hat{\mathbf{y}}(t + \Delta t)] + \frac{1}{2} \mathbf{d}^T(t) \mathbf{W} \mathbf{d}(t) \quad (2.41)$$

where  $\mathbf{W} \in \mathbb{R}^{q \times q}$  is positive semi-definite. The optimal model error can be obtained by minimizing Equation (2.41) with respect to  $\mathbf{d}(t)$ , given by

$$\mathbf{d}(t) = - \left\{ [\mathbf{\Lambda}(\Delta t) \mathbf{S}(\hat{\mathbf{x}})]^\top \mathbf{R}^{-1} \mathbf{\Lambda}(\Delta t) \mathbf{S}(\hat{\mathbf{x}}) + \mathbf{W} \right\}^{-1} [\mathbf{\Lambda}(\Delta t) \mathbf{S}(\hat{\mathbf{x}})]^\top \mathbf{R}^{-1} [\mathbf{z}(\hat{\mathbf{x}}, \Delta t) - \tilde{\mathbf{y}}(t + \Delta t) + \hat{\mathbf{y}}(t)] \quad (2.42)$$

where  $\mathbf{d}(t)$  in Eq. (2.42) is used to perform a nonlinear propagation of the state estimates in Eq. (2.37a) to time  $t_k$ . Then, the measurement is processed at time  $t_{k+1}$  to find the new  $\mathbf{d}(t)$  in  $[t_k, t_{k+1}]$ , and then the state estimates are propagated to time  $t_{k+1}$ . As  $\mathbf{W}$  decreases, more model error is added to correct the model, so that the estimates more closely follow the measurements. As  $\mathbf{W}$  increases, less model error is added, so that the estimates more closely follow the propagated model.

## 2.7 Unscented Filtering

The EKF may fail to estimate the correct estimates because it uses a linearization of the nonlinear system. Therefore, errors in truncating the Taylor series to first order should be small. Also, a zero-mean Gaussian random process is assumed. Therefore, the mean and covariance used in EKF are propagated by using only the first-order truncated linearization of the nonlinear system. The third and higher order moments are thus all zero. Therefore, the EKF has an error in the covariance expression when the fourth-order moments of the Gaussian distribution (kurtosis) is not zero.

A better mean and covariance expression can be obtained by using the *Unscented Filter* (UF) developed by Julier, Uhlmann and Durrant-Whyte.<sup>35,36,39,85,86</sup> The UF uses the same structure as the EKF, however, the mean and covariance propagations are different. The main idea of UF is that with a fixed number of parameters it should be easier to approximate a Gaussian distribution than to approximate an arbitrary nonlinear function. Although the UF needs more computations than the EKF, it has several advantages; 1) the expected error is lower than the EKF and 2) the UF avoids the derivation of Jacobian matrices. In fact, the UF is accurate to third order for Gaussian inputs for all nonlinearities and at least to second order for non-Gaussian inputs.<sup>36</sup>



Let the system model be given by

$$\mathbf{x}_{k+1} = \mathbf{f}(\mathbf{x}_k, \mathbf{w}_{k+1}, k+1) \quad (2.43a)$$

$$\tilde{\mathbf{y}}_{k+1} = \mathbf{h}(\mathbf{x}_{k+1}, \mathbf{v}_{k+1}, k+1) \quad (2.43b)$$

where  $\mathbf{w}_{k+1}$  and  $\mathbf{v}_{k+1}$  are assumed zero-mean Gaussian noise processes with covariances given by  $\mathbf{Q}_{k+1}$  and  $\mathbf{R}_{k+1}$ , respectively. The update equations are rewritten as

$$\hat{\mathbf{x}}_{k+1}^+ = \hat{\mathbf{x}}_{k+1}^- + \mathbf{K}_{k+1} \boldsymbol{\nu}_{k+1} \quad (2.44a)$$

$$\mathbf{P}_{k+1}^+ = \mathbf{P}_{k+1}^- - \mathbf{K}_{k+1} \mathbf{P}_{k+1}^{\nu\nu} \mathbf{K}_{k+1}^\top \quad (2.44b)$$

where  $\boldsymbol{\nu}_{k+1}$  is the innovations process, given by

$$\boldsymbol{\nu}_{k+1}^+ \equiv \tilde{\mathbf{y}}_{k+1} - \hat{\mathbf{y}}_{k+1}^- = \tilde{\mathbf{y}}_{k+1} - \mathbf{h}(\hat{\mathbf{x}}_{k+1}^-, k+1) \quad (2.45)$$

The covariance of  $\boldsymbol{\nu}_{k+1}$  is defined by  $\mathbf{P}_{k+1}^{\nu\nu}$ . The gain  $\mathbf{K}_{k+1}$  is computed by

$$\mathbf{K}_{k+1} = \mathbf{P}_{k+1}^{xy} (\mathbf{P}_{k+1}^{\nu\nu})^{-1} \quad (2.46)$$

where  $\mathbf{P}_{k+1}^{xy}$  is the cross-correlation matrix between  $\hat{\mathbf{x}}_{k+1}^-$  and  $\hat{\mathbf{y}}_{k+1}^-$ .

As can be seen the structure is the same as the EKF, however, the UF uses a different propagation of covariance matrix. Given a covariance matrix  $\mathbf{P}$ , a set of order  $n$  points can be generated from the columns (or rows) of the matrices  $\pm\sqrt{(n+\kappa)\mathbf{P}}$ , given by

$$\boldsymbol{\sigma}_k \leftarrow 2n \text{ columns from } \pm\sqrt{(n+\lambda)\mathbf{P}_k} \quad (2.47a)$$

$$\boldsymbol{\chi}_k(0) = \hat{\mathbf{x}}_k \quad (2.47b)$$

$$\boldsymbol{\chi}_k(i) = \boldsymbol{\sigma}_k(i) + \hat{\mathbf{x}}_k \quad (2.47c)$$

where  $n$  is the dimension of the state and  $\lambda = \{\alpha^2(n+\kappa) - n\}$  is a scaling parameter. The parameter  $\kappa$  is a secondary scaling parameter which is usually set to 0. The parameter  $\alpha$  is usually set to a small positive value, and  $\beta$  is used to compensate the higher-order moments. Setting  $\beta = 2$  is optimal for Gaussian distributions. Efficiently methods to compute the matrix square root can be found by using the Cholesky decomposition. If an orthogonal matrix square root is used, then the sigma points lie along the eigenvectors of the covariance matrix. Note that there are a

total of  $2n$  values for  $\sigma_k$  (the positive and negative square roots). The mean and covariance of these points are known.<sup>39</sup> Since this set of points is symmetric, its odd central moments are zero, so its first three moments are the same as the original Gaussian distribution.

The transformed set of sigma points are evaluated for each of the points by

$$\boldsymbol{\chi}_{k+1}(i) = \mathbf{f}(\boldsymbol{\chi}_k(i), k) \quad (2.48)$$

The predicted mean for the state estimate is calculated by

$$\hat{\boldsymbol{x}}_{k+1}^- = \frac{1}{n + \lambda} \left[ \lambda \boldsymbol{\chi}_k(0) + \frac{1}{2} \sum_{i=1}^{2n} \boldsymbol{\chi}_{k+1}(i) \right] \quad (2.49)$$

The predicted covariance is given by

$$\begin{aligned} \mathbf{P}_{k+1}^- &= \frac{1}{n + \lambda} \left\{ [\lambda + (1 - \alpha^2 + \beta)(n + \lambda)] [\boldsymbol{\chi}_{k+1}(0) - \hat{\boldsymbol{x}}_{k+1}^-] [\boldsymbol{\chi}_{k+1}(0) - \hat{\boldsymbol{x}}_{k+1}^-]^\top \right. \\ &\quad \left. + \frac{1}{2} \sum_{i=1}^{2n} [\boldsymbol{\chi}_{k+1}(i) - \hat{\boldsymbol{x}}_{k+1}^-] [\boldsymbol{\chi}_{k+1}(i) - \hat{\boldsymbol{x}}_{k+1}^-]^\top \right\} \end{aligned} \quad (2.50)$$

By using these equations, third-order estimation errors (at the very least) of the state and process noise can be obtained.

The mean observation is given by

$$\hat{\boldsymbol{y}}_{k+1}^- = \frac{1}{n + \lambda} \left[ \lambda \boldsymbol{\gamma}_{k+1}(0) + \frac{1}{2} \sum_{i=1}^{2n} \boldsymbol{\gamma}_{k+1}(i) \right] \quad (2.51)$$

where

$$\boldsymbol{\gamma}_{k+1}(i) = \mathbf{h}(\boldsymbol{\chi}_{k+1}(i), k + 1) \quad (2.52)$$

The output covariance is given by

$$\begin{aligned} \mathbf{P}_{k+1}^{yy} &= \frac{1}{n + \lambda} \left\{ [\lambda + (1 - \alpha^2 + \beta)(n + \lambda)] [\boldsymbol{\gamma}_{k+1}(0) - \hat{\boldsymbol{y}}_{k+1}^-] [\boldsymbol{\gamma}_{k+1}(0) - \hat{\boldsymbol{y}}_{k+1}^-]^\top \right. \\ &\quad \left. + \frac{1}{2} \sum_{i=1}^{2n} [\boldsymbol{\gamma}_{k+1}(i) - \hat{\boldsymbol{y}}_{k+1}^-] [\boldsymbol{\gamma}_{k+1}(i) - \hat{\boldsymbol{y}}_{k+1}^-]^\top \right\} \end{aligned} \quad (2.53)$$

Then the innovations covariance is given by

$$\mathbf{P}_{k+1}^{\nu\nu} = \mathbf{P}_{k+1}^{yy} + \mathbf{R}_{k+1} \quad (2.54)$$

The cross covariance matrix is determined using

$$\mathbf{P}_{k+1}^{xy} = \frac{1}{n+\lambda} \left\{ [\lambda + (1 - \alpha^2 + \beta)(n + \lambda)] [\boldsymbol{\chi}_{k+1}(0) - \hat{\boldsymbol{x}}_{k+1}^-] [\boldsymbol{\gamma}_{k+1}(0) - \hat{\boldsymbol{y}}_{k+1}^-]^\top + \frac{1}{2} \sum_{i=1}^{2n} [\boldsymbol{\chi}_{k+1}(i) - \hat{\boldsymbol{x}}_{k+1}^-] [\boldsymbol{\gamma}_{k+1}(i) - \hat{\boldsymbol{y}}_{k+1}^-]^\top \right\} \quad (2.55)$$

The filter gain is then computed using Eq. (2.46), and the state vector can now be updated using Eq. (2.44).

## 2.8 Summary

Some common estimation techniques are reviewed in this chapter. Both batch and recursive algorithms are described for either linear or nonlinear systems.

## CHAPTER III

## ATTITUDE DETERMINATION PROBLEM

## 3.1 Attitude Parameters

Many parameters can be used to represent the attitude. Each has its own relative merits and demerits. Among them the quaternions and the modified Rodrigues parameters (MRP) are used in this dissertation to describe the system model. Also, Euler angles are used to represent the attitude errors. The four component quaternion seems to be the best selection since it is singularity free and has a quasi-linear representation of the attitude, although it is not a minimum parameter representation. As for MRP, it is a minimum parameter representation. Therefore, it has a singularity at  $360^\circ$ , but we can switch to a “shadow” image to avoid the singularity.<sup>38</sup> The MRP is used in the self survey and quaternion is used for EKF and predictive filtering. Both the MRP and quaternion are used in the UF.

## 3.1.1 Euler Angles

Euler angles describe the attitude of a reference frame  $\mathcal{B}$  relative to the frame  $\mathcal{N}$  through three successive rotation angles about the sequentially displaced body fixed axes. A direction cosine matrix, which is called an attitude matrix, in terms of the (3-2-1) Euler angles  $(\psi, \theta, \phi)$  is defined by

$$\mathbf{A} = \begin{bmatrix} \cos \psi \cos \theta & \sin \psi \cos \theta & -\sin \theta \\ \cos \psi \sin \theta \sin \phi - \sin \psi \cos \phi & \sin \psi \sin \theta \sin \phi + \cos \psi \cos \phi & \cos \theta \sin \phi \\ \cos \psi \sin \theta \cos \phi + \sin \psi \cos \phi & \sin \psi \sin \theta \cos \phi - \cos \psi \sin \phi & \cos \theta \cos \phi \end{bmatrix} \quad (3.1)$$

Euler angles can be determined from the attitude matrix by

$$\phi = \tan^{-1} \left( \frac{A_{23}}{A_{33}} \right) \quad (3.2a)$$

$$\theta = \sin^{-1} (-A_{13}) \quad (3.2b)$$

$$\psi = \tan^{-1} \left( \frac{A_{12}}{A_{11}} \right) \quad (3.2c)$$

Although Euler angles have a singularity and contain trigonometric functions to express attitude matrix, they can be used to visualize the attitude errors for small angle rotations.

### 3.1.2 Quaternions

The attitude matrix is parameterized by quaternions, defined by

$$\mathbf{q} = \begin{bmatrix} \mathbf{q}_{13} \\ q_4 \end{bmatrix} \quad (3.3)$$

with

$$\mathbf{q}_{13} \equiv [q_1, q_2, q_3]^\top = \hat{\mathbf{e}} \sin(\varphi/2) \quad (3.4a)$$

$$q_4 = \cos(\varphi/2) \quad (3.4b)$$

where  $\hat{\mathbf{e}}$  is the principal axis, a unit vector corresponding to the axis of rotation, and  $\varphi$  is the principal angle, the angle of rotation. The quaternions satisfy the constraint given by

$$\mathbf{q}^\top \mathbf{q} = \mathbf{q}_{13}^\top \mathbf{q}_{13} + q_4^2 = 1 \quad (3.5)$$

The attitude matrix is related to the quaternion by

$$\mathbf{A}(\mathbf{q}) = \mathbf{\Xi}^\top(\mathbf{q}) \mathbf{\Psi}(\mathbf{q}) \quad (3.6)$$

where

$$\mathbf{\Xi}(\mathbf{q}) \equiv \begin{bmatrix} q_4 \mathbf{I}_{3 \times 3} + [\mathbf{q}_{13} \times] \\ \dots\dots\dots \\ -\mathbf{q}_{13}^\top \end{bmatrix} \quad (3.7a)$$

$$\mathbf{\Psi}(\mathbf{q}) \equiv \begin{bmatrix} q_4 \mathbf{I}_{3 \times 3} - [\mathbf{q}_{13} \times] \\ \dots\dots\dots \\ -\mathbf{q}_{13}^\top \end{bmatrix} \quad (3.7b)$$

with

$$[\mathbf{q}_{13} \times] = \begin{bmatrix} 0 & -q_3 & q_2 \\ q_3 & 0 & -q_1 \\ -q_2 & q_1 & 0 \end{bmatrix} \quad (3.8)$$

The transformation from attitude matrix to quaternion is obtained by the Stanley algorithm.<sup>87</sup> First, the largest  $q_i$  is chosen by computing the following equations:

$$\begin{aligned}
q_1^2 &= \frac{1}{4} (1 + 2A_{11} - \text{trace}[\mathbf{A}]) \\
q_2^2 &= \frac{1}{4} (1 + 2A_{22} - \text{trace}[\mathbf{A}]) \\
q_3^2 &= \frac{1}{4} (1 + 2A_{33} - \text{trace}[\mathbf{A}]) \\
q_4^2 &= \frac{1}{4} (1 + \text{trace}[\mathbf{A}])
\end{aligned} \tag{3.9}$$

The sign of the largest  $q_i$  is set to positive and then the other three quaternion parameters are determined using the relation given by

$$\begin{aligned}
q_4 q_1 &= (A_{23} - A_{32}) / 4 \\
q_4 q_2 &= (A_{31} - A_{13}) / 4 \\
q_4 q_3 &= (A_{12} - A_{21}) / 4 \\
q_2 q_3 &= (A_{23} + A_{32}) / 4 \\
q_3 q_1 &= (A_{31} + A_{13}) / 4 \\
q_1 q_2 &= (A_{12} + A_{21}) / 4
\end{aligned} \tag{3.10}$$

Successive rotations can be accomplished using quaternion multiplication in the same order as the attitude matrix multiplication, given by

$$\mathbf{A}(\mathbf{q}') \mathbf{A}(\mathbf{q}) = \mathbf{A}(\mathbf{q}' \otimes \mathbf{q}) \tag{3.11}$$

where the composition of the quaternions is bilinear, with

$$\mathbf{q}' \otimes \mathbf{q} = \begin{bmatrix} \Psi(\mathbf{q}') & \vdots & \mathbf{q}' \end{bmatrix} \mathbf{q} = \begin{bmatrix} \Xi(\mathbf{q}) & \vdots & \mathbf{q} \end{bmatrix} \mathbf{q}' \tag{3.12}$$

The attitude kinematics in terms of quaternions is given by

$$\dot{\mathbf{q}} = \frac{1}{2} \Omega(\boldsymbol{\omega}) \mathbf{q} \tag{3.13}$$

where  $\boldsymbol{\omega}$  is the  $3 \times 1$  angular velocity vector and

$$\Omega(\boldsymbol{\omega}) \equiv \begin{bmatrix} -[\boldsymbol{\omega} \times] & \vdots & \boldsymbol{\omega} \\ \dots\dots\dots & & \\ -\boldsymbol{\omega}^\top & \vdots & 0 \end{bmatrix} \tag{3.14}$$

The angular velocity can be considered constant during the integration. Therefore, the discrete-form kinematics equation is given by<sup>88</sup>

$$\begin{aligned}\mathbf{q}_{k+1} &= \exp\left(\frac{1}{2}\boldsymbol{\Omega}(\boldsymbol{\omega})\Delta t\right)\mathbf{q}_k \\ &= \left[\cos\left(\frac{1}{2}\omega\Delta t\right)\mathbf{I} + \sin\left(\frac{1}{2}\omega\Delta t\right)\omega^{-1}\boldsymbol{\Omega}(\boldsymbol{\omega})\right]\mathbf{q}_k\end{aligned}\quad (3.15)$$

where  $\omega = |\boldsymbol{\omega}|$  and  $\Delta t$  is the sampling interval.

### 3.1.3 Modified Rodrigues Parameters

The modified Rodrigues parameter is defined by<sup>37,38</sup>

$$\mathbf{p} = \hat{\mathbf{e}} \tan\left(\frac{\varphi}{4}\right) \quad (3.16)$$

where  $\hat{\mathbf{e}}$  is the principal axis and  $\varphi$  is the principal angle. The MRPs can be obtained from quaternions, which are given by

$$p_i = \frac{q_i}{1 + q_4}, \quad \text{for } i = 1, 2, 3 \quad (3.17)$$

Inversely, the quaternions can be obtained from MRPs, given by

$$\mathbf{q}_{13} = \frac{2\mathbf{p}}{1 + p^2} \quad (3.18a)$$

$$q_4 = \frac{1 - p^2}{1 + p^2} \quad (3.18b)$$

where  $p^2 = \mathbf{p}^\top \mathbf{p}$ . As can be seen from the definition of the MRP in Eq. (3.16), the MRPs have a geometric singularity at  $\varphi = \pm 2\pi$ . However, this problem can be resolved by using the shadow image MRPs, given by

$$\mathbf{p}^s = \frac{-\mathbf{q}_{13}}{1 - q_4} = \frac{-\mathbf{p}}{p^2} \quad (3.19)$$

The shadow image MRP can be written in terms of the principal axis and angle as

$$\mathbf{p}^s = \hat{\mathbf{e}} \tan\left(\frac{\varphi - 2\pi}{4}\right) \quad (3.20)$$

Also, the mapping between an MRP time derivative and its shadow image counterpart is given by

$$\dot{\mathbf{p}}^s = -\frac{\dot{\mathbf{p}}}{p^2} + \frac{1}{2}\left(\frac{1 + p^2}{p^4}\right)\mathbf{p}\mathbf{p}^\top \boldsymbol{\omega} \quad (3.21)$$

Thus, the singularity can be avoided by switching the MRPs at  $\varphi = \pm\pi$ . The kinematics equation of the MRPs is given by

$$\dot{\mathbf{p}} = \frac{1}{4} \left[ (1 - p^2) \mathbf{I} + 2[\mathbf{p}\times] + 2\mathbf{p}\mathbf{p}^\top \right] \boldsymbol{\omega} \quad (3.22)$$

The attitude matrix representation by using MRPs is given by

$$\mathbf{A}(\mathbf{p}) = \mathbf{I} + \frac{8[\mathbf{p}\times]^2 - 4(1 - p^2)[\mathbf{p}\times]}{(1 + p^2)^2} \quad (3.23)$$

The overall MRP of two successive rotations having MRPs  $\mathbf{p}'$  and  $\mathbf{p}''$  is defined by

$$\mathbf{p} = \frac{(1 - \mathbf{p}' \cdot \mathbf{p}') \mathbf{p}'' + (1 - \mathbf{p}'' \cdot \mathbf{p}'') \mathbf{p}' - 2\mathbf{p}'' \times \mathbf{p}'}{1 + \mathbf{p}'' \cdot \mathbf{p}'' \mathbf{p}' \cdot \mathbf{p}' - 2\mathbf{p}'' \cdot \mathbf{p}'} \quad (3.24)$$

### 3.2 Process Error Covariance

For the attitude estimation problem using gyro measurements, the estimated attitude contains an error originated by the drift rate and zero-mean additive Gaussian white noise  $\boldsymbol{w}$ . The process error covariance is related to the attitude and gyro drift rate estimation errors.

The gyro-measured angular velocity is modeled by

$$\tilde{\boldsymbol{\omega}} = \boldsymbol{\omega} + \boldsymbol{\beta} + \boldsymbol{\eta}_v \quad (3.25a)$$

$$\dot{\boldsymbol{\beta}} = \boldsymbol{\eta}_u \quad (3.25b)$$

where  $\boldsymbol{\omega}$  is the true angular velocity,  $\boldsymbol{\beta}$  is the gyro drift vector,  $\boldsymbol{\eta}_v$  and  $\boldsymbol{\eta}_u$  are zero-mean Gaussian white-noise processes with covariances given by  $\sigma_v^2 \mathbf{I}$  and  $\sigma_u^2 \mathbf{I}$ , respectively. With the approximation of  $\|\boldsymbol{\omega}\| \ll 1$ , the state transition matrix can be approximated by

$$\Phi(\Delta t) = \begin{bmatrix} \mathbf{I}_{3 \times 3} & -\Delta t \mathbf{I}_{3 \times 3} \\ \mathbf{0}_{3 \times 3} & \mathbf{I}_{3 \times 3} \end{bmatrix} \quad (3.26)$$

Then, the discrete process noise covariance is given by<sup>89</sup>

$$\mathbf{Q}_k = \begin{bmatrix} (\sigma_v^2 \Delta t + \frac{1}{3} \sigma_u^2 \Delta t^3) \mathbf{I}_{3 \times 3} & -\frac{1}{2} \sigma_u^2 \Delta t^2 \mathbf{I}_{3 \times 3} \\ -\frac{1}{2} \sigma_u^2 \Delta t^2 \mathbf{I}_{3 \times 3} & \sigma_u^2 \Delta t \mathbf{I}_{3 \times 3} \end{bmatrix} \quad (3.27)$$



For the application of the UF, Crassidis proposed a modified covariance matrix which is given by<sup>34</sup>

$$\mathbf{Q}_k = \frac{\Delta t}{2} \begin{bmatrix} (\sigma_v^2 - \frac{1}{6}\sigma_u^2\Delta t^2) \mathbf{I}_{3\times 3} & \mathbf{0}_{3\times 3} \\ \mathbf{0}_{3\times 3} & \sigma_u^2 \mathbf{I}_{3\times 3} \end{bmatrix} \quad (3.28)$$

This matrix is achieved by applying a trapezoidal approximation in the covariance propagation.

### 3.3 Solutions of Wahba Problem

Wahba's problem finds a proper orthogonal matrix that minimizes the scalar weighted norm-squared residual between sets of  $3 \times 1$  observed LOS vectors in the body frame and  $3 \times 1$  ephemerides in the reference frame. However, the GPS carrier phase measurements is not in the form of a LOS vector, so finding attitude using GPS signals is more difficult.

The general loss function which was used by Cohen is given by<sup>71</sup>

$$J(\mathbf{A}) = \frac{1}{2} \sum_{i=1}^M \sum_{j=1}^N w_{ij} (\Delta\phi_{ij} - \mathbf{b}_i^T \mathbf{A} \mathbf{s}_j)^2 \quad (3.29)$$

where  $M$  represents the number of baselines,  $N$  represents the number of observed GPS spacecraft, and the parameter  $w_{ij}$  serves to weight each individual phase measurement. In Cohen's method, the integer ambiguities are assumed to be resolved beforehand. Cohen proposed a linearized least squares technique that is numerically efficient, but is sensitive to initial guesses.<sup>71</sup>

A new method using vectorized phase measurements was proposed by Crassidis et al.<sup>51,53</sup> The vectorized measurement problem involves determining the sightline vector in the body frame, denoted by  $\tilde{\mathbf{s}}_j \equiv \mathbf{A} \mathbf{s}_j$ , or the baseline in a reference frame, denoted by  $\bar{\mathbf{b}}_i \equiv \mathbf{A}^T \mathbf{b}_i$ . For the sightline case, the following loss function is minimized

$$J_j(\tilde{\mathbf{s}}_j) = \frac{1}{2} \sum_{i=1}^M \frac{1}{\bar{w}_{ij}^2} (\Delta\phi_{ij} - \mathbf{b}_i^T \tilde{\mathbf{s}}_j)^2 \quad \text{for } j = 1, 2, \dots, N \quad (3.30)$$

where  $\bar{w}_{ij}$  is the standard deviation of noise. The minimization of Eq. (3.30) is straightforward and leads to

$$\tilde{\mathbf{s}}_j = \mathbf{M}_j^{-1} \mathbf{y}_j \quad (3.31)$$

where

$$\mathbf{M}_j = \sum_{i=1}^M \frac{1}{\bar{w}_{ij}^2} \mathbf{b}_i \mathbf{b}_i^\top \quad \text{for } j = 1, 2, \dots, N \quad (3.32a)$$

$$\mathbf{y}_j = \sum_{i=1}^M \frac{1}{\bar{w}_{ij}^2} \Delta\phi_{ij} \mathbf{b}_i \quad \text{for } j = 1, 2, \dots, N \quad (3.32b)$$

As can be seen in Eq. (3.31), at least three non-coplanar baselines are required to determine the sightlines in the body frame. However, when only two non-coplanar baselines exist, a solution is again possible as long as three non-coplanar sightlines exist. This approach determines the baselines in the reference frame by minimizing the following loss function given by

$$J_i(\bar{\mathbf{b}}_i) = \frac{1}{2} \sum_{j=1}^N \frac{1}{\bar{w}_{ij}^2} (\Delta\phi_{ij} - \bar{\mathbf{b}}_i^\top \mathbf{s}_j)^2 \quad \text{for } i = 1, 2, \dots, M \quad (3.33)$$

The minimization of Eq. (3.33) is again straightforward and leads to

$$\bar{\mathbf{b}}_i = \mathbf{N}_i^{-1} \mathbf{z}_i \quad (3.34)$$

where

$$\mathbf{N}_i = \sum_{j=1}^N \frac{1}{\bar{w}_{ij}^2} \mathbf{s}_j \mathbf{s}_j^\top \quad \text{for } j = 1, 2, \dots, N \quad (3.35a)$$

$$\mathbf{z}_i = \sum_{j=1}^N \frac{1}{\bar{w}_{ij}^2} \Delta\phi_{ij} \mathbf{s}_j \quad \text{for } j = 1, 2, \dots, N \quad (3.35b)$$

Then, the attitude can be determined by minimizing the following loss function:

$$J(\mathbf{A}) = \frac{1}{2} \sum_{j=1}^N (\tilde{\mathbf{s}}_j - \mathbf{A} \mathbf{s}_j)^\top \mathbf{M}_j (\tilde{\mathbf{s}}_j - \mathbf{A} \mathbf{s}_j) \quad (3.36)$$

Determining the attitude using sightlines in the body frame is very similar to that using reference baselines, so the former case is considered here. To compare with Wahba's problem, this loss function is not identical to Wahba's problem since the quartic dependency in the quaternions does not cancel, unless the baselines form an orthogonal basis so that  $\mathbf{M}_j$  is given by a scalar times the identity matrix,  $\mathbf{M}_j = m_j \mathbf{I}$ .

The loss function in Eq. (3.36) is in fact equivalent to the general loss function in Eq. (3.29). However, the loss function of Wahba's problem is

$$J(\mathbf{A}) = \sum_{i=1}^N w_i |\mathbf{u}_B^i - \mathbf{A}\mathbf{u}_R^i|^2 \quad (3.37)$$

where  $\mathbf{u}_R^i$  is the  $i$ -th vector in the reference frame,  $\mathbf{u}_B^i$  is in the body frame, and  $w_i$  is a scalar weight.<sup>1</sup> Crassidis et al. convert the loss function in Eq. (3.36) into Eq. (3.37) by assigning the sightline vectors in Eq. (3.31) as

$$\mathbf{u}_B^j = \tilde{\mathbf{s}}_j \quad , \quad \mathbf{u}_R^j = \mathbf{s}_j \quad \text{for } j = 1, 2, \dots, N \quad (3.38)$$

If 3 sightlines are available, we assign the baseline vectors in Eq. (3.34) as

$$\mathbf{u}_B^i = \mathbf{b}_i \quad , \quad \mathbf{u}_R^i = \bar{\mathbf{b}}_i \quad \text{for } i = 1, 2, \dots, M \quad (3.39)$$

After a number of simulations, it was shown that when 2 sightlines and 3 baselines are used, the initial attitude obtained by minimizing Eq. (3.29) and assigning vectors as in Eq. (3.38) is fairly close to the true value.<sup>51,53</sup>

### 3.4 Summary

Attitude parameters, Euler angles, quaternion, and MRP, are reviewed. Kinematic equations and transformation between them are described. For the case of using gyro measurements, the process covariance matrix is presented. Finally, an attitude determination algorithm, similar to the solution of Wahba's problem, is described for either coplanar or non-coplanar baselines.

## CHAPTER IV

### THE GLOBAL POSITIONING SYSTEM

The Global Positioning System (GPS) is an application of Earth satellites for navigation around Earth surface. The GPS was developed by the U.S. Department of Defense to support capabilities of U.S. military forces, however, it is now in widespread use for public and commercial applications as well.

#### 4.1 GPS Overview

The first GPS satellite, named NAVSTAR, was launched in 1978. With ten more satellites after it, they consist of the Block I. The Block II satellites were launched from 1989 and composed of 9 satellites. The slightly improved 15 satellites, named Block IIA, are also in orbit. The full 24-satellite operation constellation was completed on March 9th 1994. Since the lifetime of Block II and IIA satellites is 7 years, Block IIRs began replacing older Block II/IAs on 22 July 1997. Block II, IIA and IIR satellites make up the current constellation. Block IIR satellites boast dramatic improvements over the previous blocks. Eight Block IIR satellites are being modified to radiate the new military (M-Code) signal on both the L1 and L2 channels as well as the more robust civil signal (L2C) on the L2 channel. The M-Code signal is a more robust and capable signal architecture. The first modified Block IIR (designated as the IIR-M) is planned for launch in 2004. Block IIF satellites are the next generation of GPS Space Vehicles. Block IIF provides all the capabilities of the previous blocks with some additional benefits as well. Improvements include an extended design life of 12 years, faster processors with more memory, and a new civil signal on a third frequency. The first Block IIF satellite is scheduled to launch in 2006. As of March 22nd 2004, 28 satellites are operational and the current status of GPS is shown in Fig. 4.1.<sup>90</sup>

```

GPS OPERATIONAL ADVISORY      082.OA1
SUBJ: GPS STATUS      22 MAR 2004

1. SATELLITES, PLANES, AND CLOCKS (CS=CESIUM RB=RUBIDIUM):
A. BLOCK I : NONE
B. BLOCK II: PRNS  1,  2,  3,  4,  5,  6,  7,  8,  9, 10, 11, 13, 14, 15
   PLANE   : SLOT F4, B5, C2, D4, B4, C1, C4, A3, A1, E3, D2, F3, F1, D5
   CLOCK   :      CS, CS, CS, RB, CS, RB, RB, RB, CS, CS, RB, RB, RB, CS
   BLOCK II: PRNS 16, 17, 18, 20, 21, 22, 24, 25, 26, 27, 28, 29, 30, 31
   PLANE   : SLOT B1, D6, E4, E1, D3, E2, D1, A2, F2, A4, B3, F5, B2, C3
   CLOCK   :      RB, RB, RB, RB, RB, RB, CS, CS, RB, RB, RB, RB, RB, RB
2. CURRENT ADVISORIES AND FORECASTS :
A. FORECASTS:      FOR SEVEN DAYS AFTER EVENT CONCLUDES.
NANU      MSG DATE/TIME      PRN  TYPE      SUMMARY (JDAY/ZULU TIME START - STOP)

2004026   262248Z FEB 2004    27  FCSTMX    064/0500-064/1700
2004027   031914Z MAR 2004    30  FCSTMX    069/1430-070/0230
2004029   040457Z MAR 2004    27  FCSTRESCD 069/0445-069/1645
2004030   040508Z MAR 2004    30  FCSTCANC  069/1430-/
2004032   091115Z MAR 2004    27  FCSTSUMM  069/0514-069/1111
2004033   121717Z MAR 2004    05  FCSTDV    077/1430-078/0230
2004035   180027Z MAR 2004    05  FCSTSUMM  077/1452-078/0023
B. ADVISORIES:
NANU      MSG DATE/TIME      PRN  TYPE      SUMMARY (JDAY/ZULU TIME START - STOP)

2004025   221045Z FEB 2004    02  UNUSUFN   053/1037-/
2004028   040101Z MAR 2004    31  UNUSUFN   064/0014-/
2004031   051817Z MAR 2004    31  UNUSABLE  064/0014-065/1818
2004034   171530Z MAR 2004    06  UNUSUFN   077/1531-/
C. GENERAL:
NANU      MSG DATE/TIME      PRN  TYPE      SUMMARY (JDAY/ZULU TIME START - STOP)

2004036   221843Z MAR 2004      GENERAL  /-/-
3. REMARKS:
A. THE POINT OF CONTACT FOR GPS MILITARY OPERATIONAL SUPPORT IS THE GPS
SUPPORT CENTER AT (719)567-2541 OR DSN 560-2541.
B. CIVILIAN: FOR INFORMATION, CONTACT US COAST GUARD NAVCEN AT
COMMERCIAL (703)313-5900 24 HOURS DAILY AND INTERNET
HTTP://WWW.NAVCEN.USCG.GOV
C. MILITARY SUPPORT WEBPAGES CAN BE FOUND AT THE FOLLOWING
HTTP://WWW.SCHRIEVER.AF.MIL/GPS OR HTTP://WWW.SCHRIEVER.AF.MIL/GPSSUPPORTCENTER

```

Fig. 4.1. Example of GPS Status Data

These 28 satellites are placed in 6 orbital planes and guarantee a minimum of 4 satellites anywhere on Earth. The information of position and time can be obtained by using 4 satellite positions and time information as well as 4 pseudo-range measurements. Although the primary use of GPS signals is for navigation purposes, they can be used for attitude estimation. By using multiple sets of antennas and GPS signal carrier phase measurements the attitude can be obtained as well as the navigation information.

## 4.2 GPS Data Format

GPS receiver collects data using the RINEX data format.<sup>91</sup> An example of the GPS observation data in RINEX 2.10 format is shown in Fig. 4.2.

```

1 11 5 17 55 19.9134373 0 10G 1G29G20G22G25R 1R29R20R22R25 0.000000007
40367413.39806| -1607757.67106 1871.83600 1036201.00 0
40432269.66805| 1637825.36205 -2388.14100 582952.00 1
39156278.21907| 121733.29807 -679.97800 1119821.00 2
38002320.42708| 127080.70007 -689.19300 803856.00 3
40649177.27507| 439260.30206 -2301.84200 1162194.00 5
40367416.97505| -1609228.35105 1871.38300 1036176.00 6
40432258.93704| 1618013.62304 -2388.76100 583027.00 7
39156274.78506| 124558.48506 -679.90100 1119845.00 8
38002317.56507| 125081.90607 -687.32200 803876.00 9
40649173.26905| 427520.65105 -2300.70600 1162222.00 11
1 11 5 17 55 19.9134373 9 5
0.000000006872 -95.751032304 0.060417217342 0.000000326254 0.060708794626
-503.1750709090 1.000 0.000000319
-492608.2409 -5530754.2987 3127706.1758
0.0819 0.2061 -0.1686
29.5566228246 -95.0897383458 -19.6011

```

Fig. 4.2. GPS Observation Data Example

The pseudo-range, L1 carrier phase, and the doppler frequency measurements are shown as well as the navigation data. Among them the dotted boxed data shown in Fig. 4.2 represents the L1 carrier phase measurements of both MA and SA. For attitude applications the original software was changed for crosstalk. The differences of phase measurements between MA and SA correspond the single differenced phase measurements which are used in the attitude estimation. Also, an example of GPS navigation message is shown in Fig. 4.3.<sup>91</sup> The navigation message of the satellites, PRN6 and PRN13, are displayed in RINEX format. These include each GPS satellite orbit ephemeris, clock corrections, and other parameters.

## 4.3 GPS Signals

All GPS satellites including the Block IIR satellites broadcast two microwave carrier signals with timing based on two rubidium and two cesium atomic clocks. The first is called L1 frequency, 1,575.42MHz, and the second is called L2 frequency, 1,227.60MHz. Only L1 frequency is used for civilian use and is known as the Coarse

Acquisition (C/A) signal. This signal carries a 1,023-bit PRN code for the identification of each satellite.

```

2.10          N: GPS NAV DATA          RINEX VERSION / TYPE
XXRINEXN V2.10  AIUB                    3-SEP-99 15:22  PGM / RUN BY / DATE
EXAMPLE OF VERSION 2.10 FORMAT          COMMENT
.1676D-07 .2235D-07 -.1192D-06 -.1192D-06  ION ALPHA
.1208D+06 .1310D+06 -.1310D+06 -.1966D+06  ION BETA
.133179128170D-06 .107469588780D-12  552960    1025 DELTA-UTC: A0,A1,T,W
13                                           LEAP SECONDS
                                           END OF HEADER
6 99  9  2 17 51 44.0 -.839701388031D-03 -.165982783074D-10 .000000000000D+00
.910000000000D+02 .934062500000D+02 .116040547840D-08 .162092304801D+00
.484101474285D-05 .626740418375D-02 .652112066746D-05 .515365489006D+04
.409904000000D+06 -.242143869400D-07 .329237003460D+00 -.596046447754D-07
.111541663136D+01 .326593750000D+03 .206958726335D+01 -.638312302555D-08
.307155651409D-09 .000000000000D+00 .102500000000D+04 .000000000000D+00
.000000000000D+00 .000000000000D+00 .000000000000D+00 .910000000000D+02
.406800000000D+06 .000000000000D+00
13 99  9  2 19  0 0.0 .490025617182D-03 .204636307899D-11 .000000000000D+00
.133000000000D+03 -.963125000000D+02 .146970407622D-08 .292961152146D+01
-.498816370964D-05 .200239347760D-02 .928156077862D-05 .515328476143D+04
.414000000000D+06 -.279396772385D-07 .243031939942D+01 -.558793544769D-07
.110192796930D+01 .271187500000D+03 -.232757915425D+01 -.619632953057D-08
-.785747015231D-11 .000000000000D+00 .102500000000D+04 .000000000000D+00
.000000000000D+00 .000000000000D+00 .000000000000D+00 .389000000000D+03
.410400000000D+06 .000000000000D+00

```

Fig. 4.3. Example of GPS Navigation Data

## 4.4 GPS Errors

Major GPS error sources for attitude estimation are described in the following.

### 4.4.1 Multipath Error

Although a majority of the GPS signal travels directly to the antenna, some signals can reflect off nearby objects and reach the antenna via a longer path. Multipath is the dominant error source in many spacecraft applications, accounting for more than 90% of the total error budget in the carrier phase measurement. Empirically, the carrier phase error for complex reflective surface spacecraft caused by multipath is approximately 5 mm rms.

#### 4.4.2 Cycle Ambiguity

When a receiver is turned on, the fractional part of the phase difference between the satellite transmitted carrier and a receiver generated signal is observed and an integer counter is initialized. However, when the receiver starts operating the initial cycle ambiguities contained in the measurements are not known. This will cause serious errors in the attitude estimation.

#### 4.4.3 Line Bias

Line bias is the nearly constant offset in phase from one antenna to another. Therefore it is assumed constant for a baseline. The length of the cable between the antenna and the receiver is the parameter of the line bias as well as a temperature-dependent component.

#### 4.4.4 Cycle Slip

During tracking the signal, GPS receivers increment the counter by one cycle when the fractional phase varies from  $2\pi$  to 0. However, GPS signals can be lost for a while for various reasons. In this event, a reinitialization of the integer counter must occur, which may cause a jump in the phase measurements. Since false cycle counts will deteriorate the attitude estimation result, the cycle slips should be detected and repaired in real time.

#### 4.4.5 Dilution of Precision

The GPS navigation and attitude determination errors can be expressed by using *Dilution of Precision* (DOP).<sup>69</sup>

##### 4.4.5.1 Geometric DOP

DOP can be defined variously, however, Geometric DOP (GDOP) is the most common. By using GDOP, the single-point solution errors on position and time can be



measured. The  $4 \times 4$  covariance matrix of position and time errors is given by<sup>69</sup>

$$\text{cov}(\text{position}) = (\mathbf{H}^T \mathbf{W} \mathbf{H})^{-1} \quad (4.1)$$

where  $\mathbf{W}$  is the weighting matrix and the sensitivity matrix  $\mathbf{H}$  is defined by

$$\mathbf{H} = \begin{bmatrix} \mathbf{s}_1^T & 1 \\ \vdots & \vdots \\ \mathbf{s}_N^T & 1 \end{bmatrix} \quad (4.2)$$

where the vector  $\mathbf{s}_i$  is the  $i$ -th sightline, which is a unit vector from the receiver to the  $i$ -th GPS satellite. The ranging errors, having the same variance  $\sigma_R^2$ , are assumed to be uncorrelated and contain zero-mean Gaussian noise. This implies that Eq. (4.1) can be rewritten as

$$\text{cov}(\text{position}) = \sigma_R^2 (\mathbf{H}^T \mathbf{H})^{-1} \quad (4.3)$$

The matrix  $(\mathbf{H}^T \mathbf{H})^{-1}$  is known as GDOP matrix. The scalar GDOP is defined as the square root of the trace of the GDOP matrix, which is given by

$$\text{GDOP} = \sqrt{\text{trace} [(\mathbf{H}^T \mathbf{H})^{-1}]} \quad (4.4)$$

#### 4.4.5.2 Attitude DOP

The concept of DOP can also be applied to attitude. The *Attitude Dilution Of Precision* (ADOP), accordingly with the definition given by Crassidis,<sup>51,53</sup> uses the optimal covariance expression of attitude estimation error, which is given by

$$\text{ADOP} = \text{trace} \left( \left[ \sum_{i=1}^M \sum_{j=1}^N [\mathbf{A} \mathbf{s}_j \times] \mathbf{b}_i \mathbf{b}_i^T [\mathbf{A} \mathbf{s}_j \times]^T \right]^{-1} \right) \quad (4.5)$$

where the matrix  $\mathbf{A}$  denotes the attitude matrix and  $\mathbf{b}_i$  denotes the  $i$ -th baseline. The baseline is the vector between two antennas.

## 4.5 Alternative GPS Constellation

Global navigation systems provide navigation and attitude information by using signals broadcast by satellites orbiting the Earth. The current U.S. GPS constellation

uses 28 satellites that are placed into 6 circular orbit planes.<sup>67,69</sup> The GLONASS constellation is constructed by 24 satellites in 3 orbital planes.<sup>92</sup> The Galileo constellation for global navigation, has been recently proposed by the European Commission (EC) and the European Space Agency (ESA), and consists of 30 satellites to be placed into 3 circular orbit planes.<sup>93</sup> For the global navigation purpose, a minimum of 4 satellites are required to be in view at any time, no matter where you are on the Earth. However, the presence of trees, mountains, and buildings, implies that more than the minimum number of satellites in view are required. Furthermore, having only 4 satellites in view is not sufficient for accurate navigation information since the geometry of the sightlines affects the navigation performance. Designing a global navigation system such as GPS or Galileo based on current constellation methods such as the Walker delta pattern may not satisfy all these requirements.

An alternative constellation design scheme that uses the *Flower Constellation* (FC) theory,<sup>94</sup> is applied to design a new global navigation system. The FCs present many interesting features useful for telecommunication, Earth and deep space observations, and global and regional navigation systems. The FCs are built with compatible orbits, thus the satellites follow the same relative trajectory with respect to an Earth fixed system of coordinates. This is a peculiar property of the FCs, an additional characteristic, that will certainly yield into the same advantage. A subset of all the intersections of this relative trajectory with the inertial orbit identifies a set of *admissible positions* for satellites to belong to the same relative trajectory (patent pending). Among all of possibilities to distribute the satellites in these admissible positions (along the relative trajectory), a uniform distribution in time is here selected.

This section, which first includes a brief introduction summarizing the main FC definitions and characteristics, introduces the new *Global Navigation Flower Constellation* (GNFC). After a brief description on the proposed GNFC, it is then compared in terms of GDOP and ADOP with the U.S. GPS, the GLONASS, and the Galileo constellations by selecting a set of fixed Earth sites.

#### 4.5.1 Flower Constellation

An orbit is called *compatible* when the relative trajectory with respect to an Earth-Centered-Earth-Fixed (ECEF) system of coordinates, constitutes a closed-loop that has a given period of repetition. The concept of compatible orbit is more general than the concept of repeated ground track orbit, since any two different equatorial orbits follow the same ground track but, in general, not the same relative trajectory in the ECEF coordinate system. A compatible orbit, which take into account the  $J_2$  effects on the orbital parameters due to the Earth oblateness, has a given number of *admissible positions* for satellites all belonging to the same relative trajectory (patent pending). The *Flower Constellations*<sup>94</sup> are based on the two concepts of *admissible positions in compatible orbits* and on a phasing rule to select a suitable subset of all the admissible positions (satellite distribution rule).

There are two main advantages of using FCs for global navigation purpose. The first one is that the dynamics of a FC is always axial-symmetric (constellation dynamics synchronized with Earth spin rate), while the second one relies on the adoption of compatible orbits (satellite spatial distribution repeats itself with periodicity). The latter implies, for instance, that ground track antennae can synchronize their pointing angles. However, we believe that the adoption of compatible orbits can - in some way unknown to us - bring some additional benefits in the applications. Summarizing, in the ECEF system of coordinates all the FC satellites follow the same repeating relative trajectory on which the satellites are distributed with a given time step and the GNFC spatial configuration repeats itself with the same time step. How one can take advantage of this property will constitute the subject of a future work.

##### 4.5.1.1 Background

An FC is identified by five independent integer parameters,  $N_p$ ,  $N_d$ ,  $N_s$ ,  $F_n$ , and  $F_d$ , and three orbital parameters  $\omega$ ,  $i$ , and  $h_p$ . In particular  $N_p$  is the number of petals,  $N_d$  is the number of sidereal days to complete the relative trajectory,  $N_s$  is the number of satellites,  $F_n$  and  $F_d$  are two integer parameters ruling the satellite distribution in the admissible positions,  $\omega$  is the argument of perigee,  $i$  is the orbit inclination, and

$h_p$  is the perigee altitude. The orbit compatibility is written by

$$N_p T_\Omega = N_d T_\oplus \quad (4.6)$$

where  $T_\Omega$  is the nodal period of the orbit and  $T_\oplus$  is the nodal period of Greenwich. This relation, by including the  $J_2$  perturbation, allows us to evaluate the orbit semi-major axis  $a$ . The relationship to be solved is a nonlinear equation<sup>94,95</sup>

$$\frac{2\pi}{\omega_\oplus} \frac{N_d}{N_p} \left( 1 + 2\xi \frac{n}{\omega_\oplus} \cos i \right)^{-1} \{1 + \xi\chi\} = 2\pi \sqrt{\frac{a^3}{\mu_\oplus}} \quad (4.7)$$

where

$$\chi = 4 + 2\sqrt{1 - e^2} - \left( 5 + 3\sqrt{1 - e^2} \right) \sin^2 i \quad (4.8)$$

and where

$$\xi = \frac{3R_\oplus^2 J_2}{4p^2} \quad \text{and} \quad e = 1 - \frac{R_\oplus + h_p}{a} \quad (4.9)$$

In these equations,  $e$  is the eccentricity,  $p$  is the semilatus rectum,  $n$  is the mean motion, the Earth equatorial radius  $R_\oplus = 6378.1363\text{Km}$ , the Earth spin rate  $\omega_\oplus = 7.29211585530 \times 10^{-5}\text{rad/s}$ , the perturbation coefficient  $J_2 = 1.0826269 \times 10^{-3}$ , and the Earth gravitational constant  $\mu_\oplus = 398600.4415\text{Km}^3/\text{sec}^2$ .

The value of the right ascension of ascending node (RAAN),  $\Omega$ , and the mean anomaly,  $M$ , for each satellite are then to be determined. Mortari et al. proposed the phasing schemes given in Ref. [94]. The phasing of the satellites, the distribution of the  $N_s$  satellites in any kinds of admissible locations, is accomplished by rules proposed by Mortari et al.<sup>94</sup> which are specified by two parameters,  $F_n$  and  $F_d$ . Then, the relation of  $\Omega$  and  $M$  at epoch time is obtained. The general symmetric phasing scheme for an FC is given by

$$\Omega_k = f_\Omega(N_p, N_d, N_s, F_n, F_d, \Omega_o, k) \quad (4.10a)$$

$$M_k = f_M(N_p, N_d, N_s, F_n, F_d, \omega, i, h_p, F_n, F_d, J_{nm}, M_o, k) \quad (4.10b)$$

where, for the  $k$ -th satellite,  $J_{nm}$  represents the geopotential perturbations and the two integer parameters,  $F_n$  and  $F_d$ , can be chosen so that the satellites are uniformly distributed in time along the relative trajectory. In particular, Mortari et al. have introduced the symmetric phasing scheme of FCs by setting  $F_n$  and  $F_d$  as<sup>94</sup>

$$F_n = N_d \quad \text{and} \quad F_d = N_s \quad (4.11)$$

#### 4.5.1.2 GNFC Constellation

There is a set of important constraints to be satisfied in order to design a proper navigation systems. Our proposed navigation system adopts circular orbits only because, if elliptical orbits are to be used, then, in order to minimize the control effort, one of the critical inclinations ( $63.4^\circ$  or  $116.6^\circ$ ) must be adopted in order to avoid the rotation of the apsidal line. Moreover, it is clear that the orbit altitude should be chosen to avoid the Van Allen radiation belt, which ranges from 9,500 Km to 16,000 Km of altitude.<sup>96</sup>

The proposed GNFC constellation<sup>97</sup> is derived from the idea that the shape of a FC relative trajectory can approximate a uniform spatially distribution path and on the fact that a symmetric phasing scheme implies a uniform distribution of satellites along the relative trajectory (uniformly in time). Both of these ideas constitute the basic of our GNFC and the reason why we believe it could enhance the navigation accuracy. In order to prove this idea, several programs have been written in MATLAB, and both, STK and the *Flower Constellation Visualization and Analysis Tool* (FCVAT) software, have been employed. In particular, the JAVA 3-D based FCVAT software constitutes an ad-hoc software to design flower constellations. Actually, without this design tool, the development of the proposed GNFC were not possible.

Through lots of trials by using FCVAT, the proposed FC for the half of a GNFC has been determined. The FC parameters and the relative path are shown in Table 4.1 and Fig. 4.4, respectively.

Table 4.1. Example GNFC Parameters

FC Parameters	Values
$N_p$	2
$N_d$	1 Day
$N_s$	15
$\omega$	180 Deg.
$i$	70 Deg.
$h_p$	20182 Km

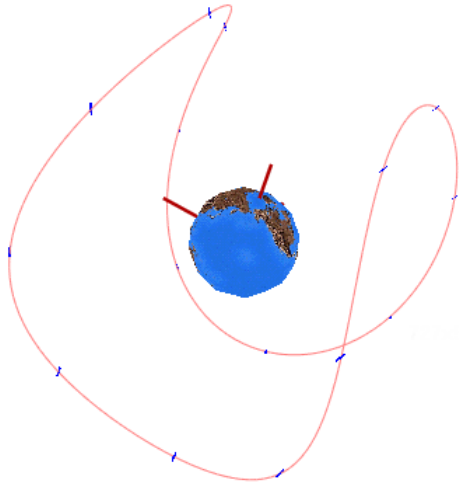


Fig. 4.4. Half GNFC

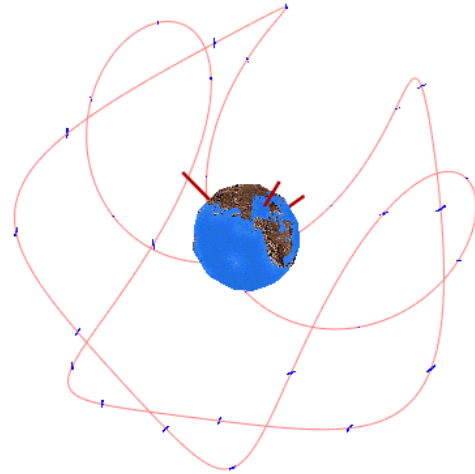


Fig. 4.5. Complete GNFC

The orbit period of each satellite is 11.97 hours. The orbits are circular and have the altitude of 20,182 Km. Figure 4.4 shows the relative path of the FC. By using the symmetric phasing scheme, the satellites in the constellation are distributed uniformly in time along the relative path. The GNFC parameters having symmetric phasing are shown in Table 4.2.

Table 4.2. GNFC Parameters:  $\Omega_k$  and  $M_k$  (In Degrees)

Sat. No.	$\Omega_k$	$M_k$	Sat. No.	$\Omega_k$	$M_k$
1	0	0	2	24.0	311.99
3	48.0	263.99	4	72.0	215.98
5	96.0	167.97	6	120.0	119.96
7	144.0	71.96	8	168.0	23.95
9	192.0	335.94	10	216.0	287.94
11	240.0	239.93	12	264.0	191.92
13	288.0	143.92	14	312.0	95.91
15	336.0	47.90			

The proposed complete GNFC constellation is obtained by combining two half GNFCs. The only difference between the two FCs is that the argument of perigee is  $\omega = 90^\circ$  for one and  $\omega = 180^\circ$  for the other FC. The relative paths of the GNFC constellation, which are generated by the FCVAT program, are shown in Fig. 4.5.

Table 4.3. Parameters Used in Simulation

Parameters	U.S. GPS	GLONASS	Galileo
Number of Satellites	28	24	30
Number of orbit planes	6	3	3
Orbit Inclination	55°	64.8°	56°
Orbit Altitude	20,180 Km	19,100 Km	23,616 Km
Orbit Period	11h 58min	11h 16min	14h

#### 4.5.2 Simulation and Result

The sightlines of GNFC are generated by using the FCVAT design tool, MATLAB,<sup>81</sup> and Satellite Tool Kit (STK).<sup>98</sup> The U.S. GPS constellations are generated by using both GPS Almanac data<sup>90</sup> and STK satellite data. The Galileo and GLONASS constellations are generated by STK using the Walker constellation scheme. Table 4.3 shows the parameters of each constellations.

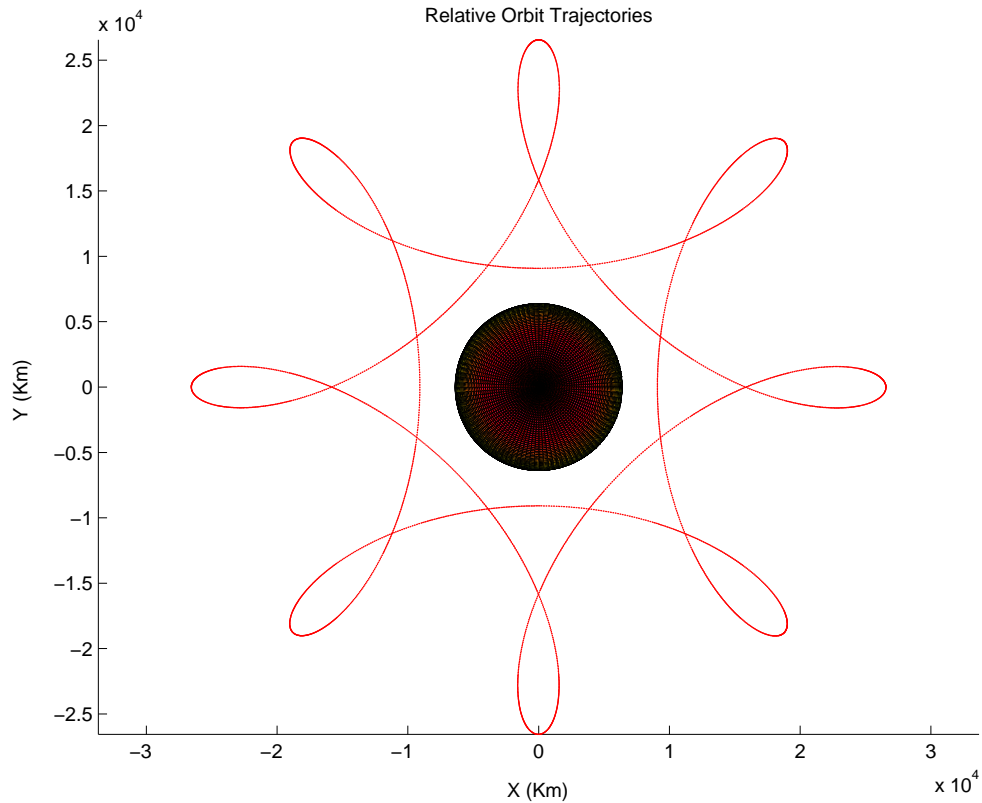


Fig. 4.6. The GNFC Constellation (Polar View)

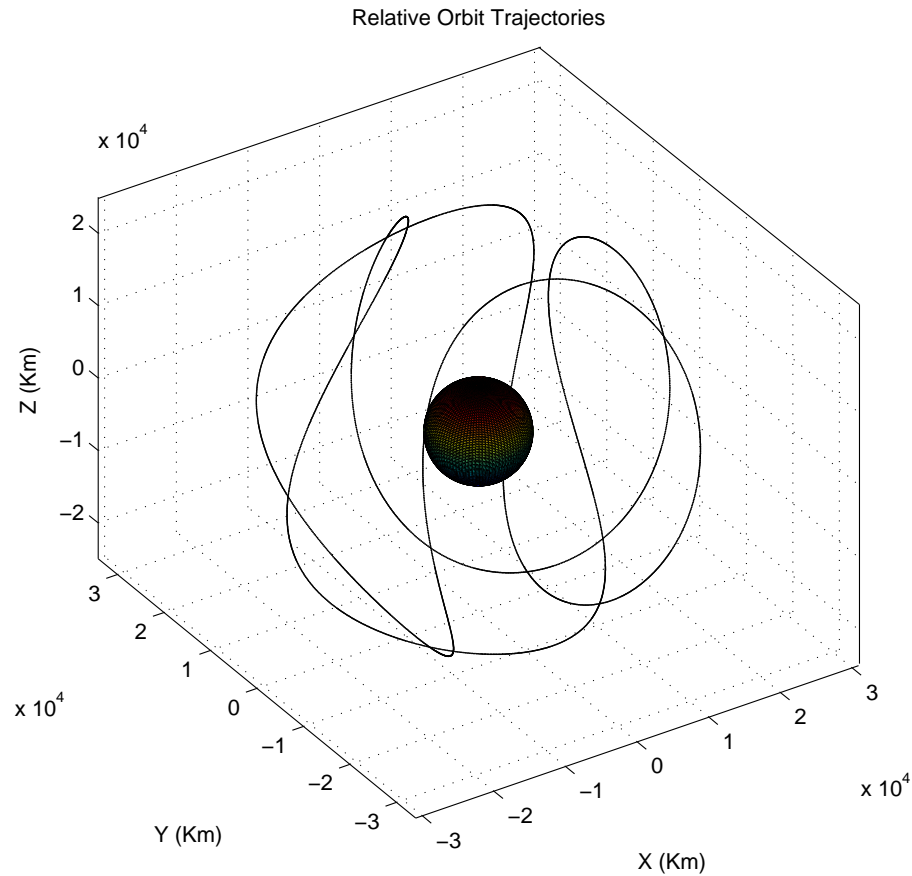


Fig. 4.7. The GNFC Constellation (Isometric View)

The relative path of the GNFC constellation is shown in Fig. 4.6 and Fig. 4.7. The symmetry of the relative path with respect to the Earth spin axis is shown in Fig. 4.6, which shows a projection of the GNFC on the Earth equatorial plane. The same relative path with a different viewpoint is shown Fig. 4.7.

To show the ground tracks of GNFC satellites, the STK software has been used. Figure 4.8 shows the STK generated ground tracks of GNFC satellites. The duration of simulation is 30 days. To include the Earth oblateness effect, the  $J_2$  perturbation has been applied. Accesses between the receiver and the GNFC satellites have been simulated, too. The thick light gray lines in the ground tracks show the access between the receiver and the GNFC satellites. The squares surrounding satellites in thick lines represent those satellites are connected.



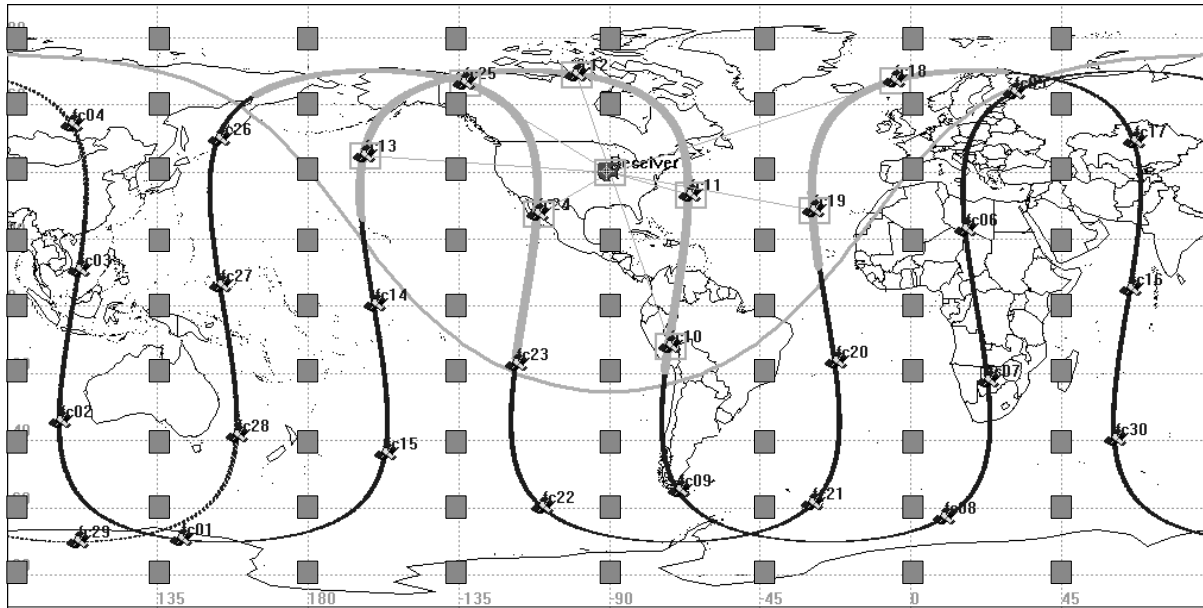


Fig. 4.8. Example Accesses Computed by STK for the GNFC Constellation and Receiver Locations (Shaded Boxes)

Also, the straight lines link a receiver, located in  $90^\circ\text{W}$  longitude and  $40^\circ\text{N}$  latitude, and the connected satellites. We can see 7 satellites are connected to the receiver. The shaded squares in Fig. 4.8 represent the receiver locations used to compute the GDOPs and ADOPs of U.S. GPS, GLONASS, Galileo and GNFC.

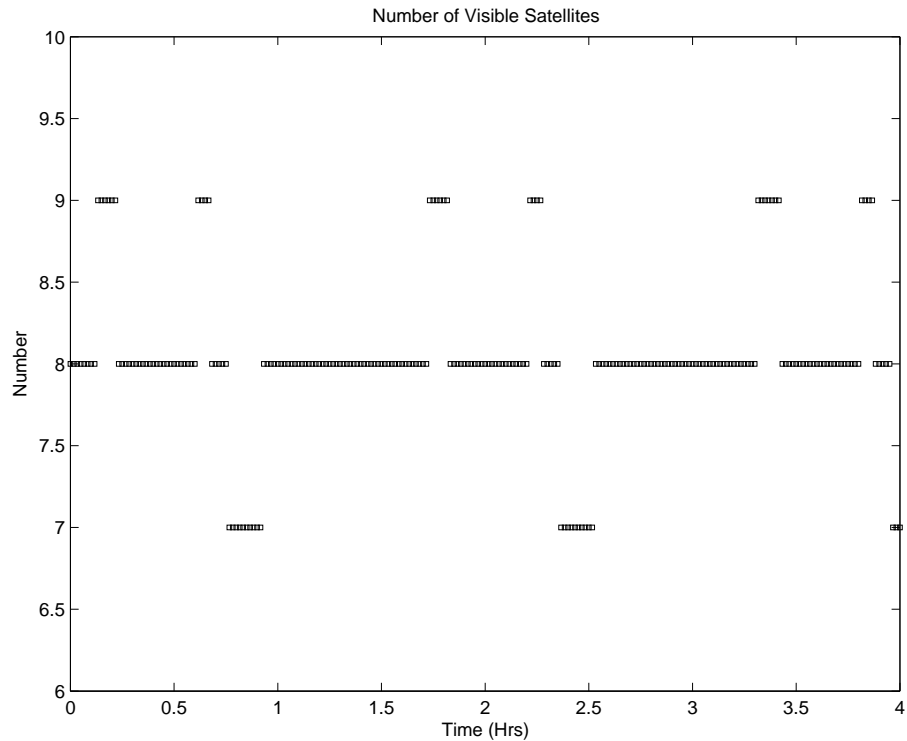


Fig. 4.9. Number of GNFC Satellites in Connection

The total number of the connected GNFC satellites at the receiver location at  $90^\circ\text{W}$  longitude and  $45^\circ\text{N}$  latitude with respect to time is shown in Fig. 4.9. In this case, 7 or more satellites are always in view. Since another satellite repeats the same relative path after  $\omega_{\oplus}\Delta\Omega$  time, simulation of GNFC can be limited in this time range. Thus, we can guarantee these numbers as long as the constellation geometry is maintained. We point out that both the U.S. GPS and GLONASS sometimes only have 4 satellites available during a 24 hour simulation while the Galileo has 6 as few as satellites. A simulation example for GPS is shown in Fig. 4.10.

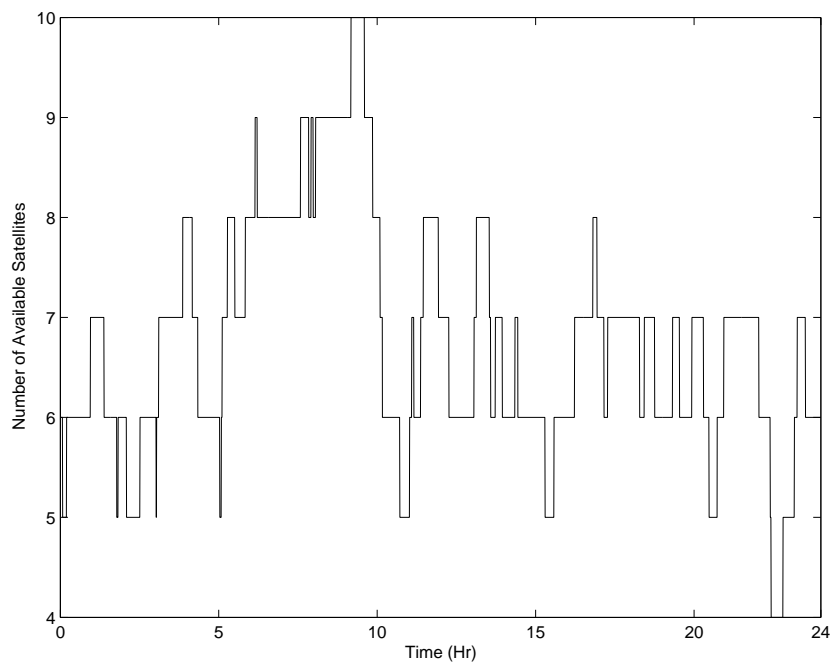


Fig. 4.10. Number of U.S. GPS Satellites in Connection

Table 4.4. Percent Changes in GDOP vs. GNFC

Latitude	U.S. GPS	GLONASS	Galileo
80°N	40.9	23.0	13.1
60°N	64.0	15.3	4.5
40°N	24.5	163.0	2.7
20°N	20.6	97.4	9.7
0°	8.9	136.4	-3.3
20°S	21.0	108.1	7.0
40°S	24.4	182.5	9.9
60°S	61.7	12.9	4.9
80°S	9.7	-1.3	-11.7

To show the effect of the latitude location of the receiver, at  $90^\circ\text{W}$  longitude the scalar GDOPs of the GNFC constellation with respect to latitude are shown in Fig. 4.11. As

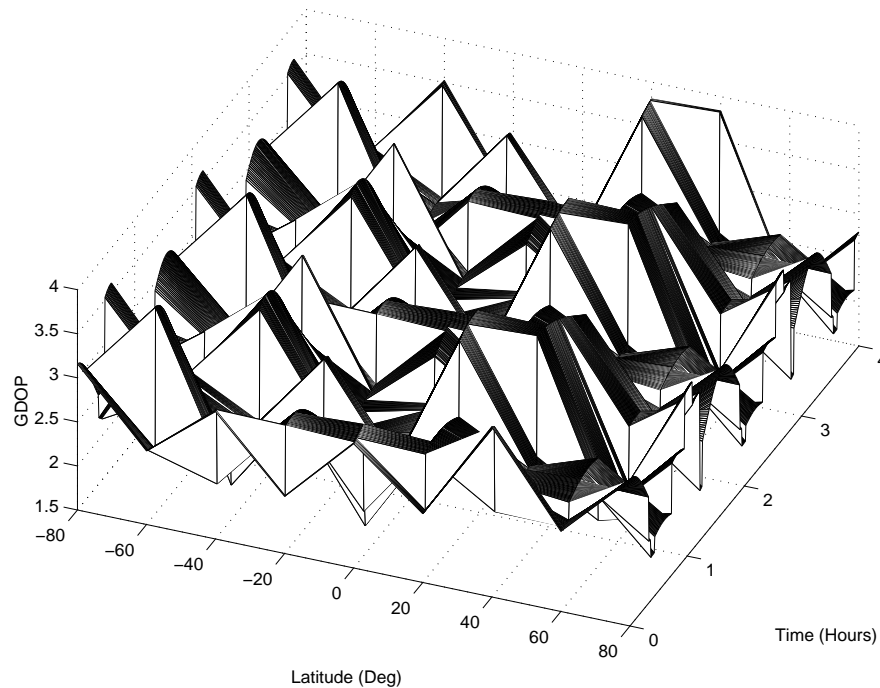


Fig. 4.11. GDOP History for Selected Latitude Locations

time varies, the GDOPs are changing. However, these values are repeating because the ground tracks are the same. Therefore, we can design the GNFC to assign the minimum GDOPs into the most demanding regions. To compare GNFC with U.S. GPS, GLONASS, and Galileo constellations, the time averaged scalar GDOPs are considered. The time averaged GDOPs of four constellations are compared in Fig. 4.12.

The GDOPs of GLONASS for the regions between  $60^\circ\text{S}$  and  $60^\circ\text{N}$  latitude can reach as high as 10 thus, they are not shown in Fig. 4.12 to make the differences among the others distinguishable. The GDOPs of GNFC are predominantly smaller than the other constellations in most regions. The percent changes in GDOPs relative to GNFC, defined as the difference over the average, are shown in Table 4.4. Positive percent changes represent that the constellation has the larger GPS errors. The

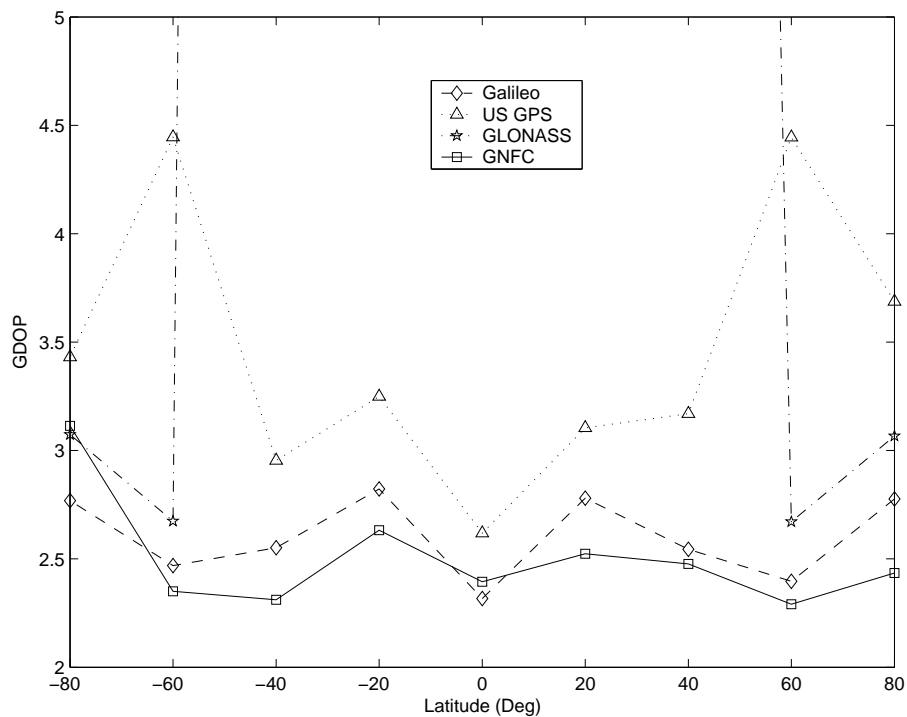


Fig. 4.12. GDOP Comparison

position error of GPS is on average 31 percent larger than that of GNFC. With the comparison of GLONASS, it is 82 percent larger. In comparison to Galileo, the benefit of GNFC is about 4 percent on average. However, the GNFC benefit in the most inhabited regions is about 6 percent.

Figure 4.13 shows the time averaged ADOP comparison with respect to latitude. The GNFC has the smallest ADOPs for most regions except for the regions around the Earth's equator. The percent changes in ADOP relative to GNFC are also investigated in Table 4.5. Note that the GNFC has the smallest ADOPs for the most inhabited regions of the Earth. For example, the comparison of ADOPs at 40°N latitude indicates the attitude error of GPS is 45 percent larger than GNFC. For the GLONASS and the Galileo it is 35 and 25 percent larger, respectively. Thus, GNFC has strong merits over the other constellations.

Table 4.5. Percent Changes in ADOP vs. GNFC

Latitude	U.S. GPS	GLONASS	Galileo
80°N	47.5	33.1	26.1
60°N	64.3	35.3	39.5
40°N	44.5	35.4	25.3
20°N	33.0	43.6	19.3
0°	-20.7	34.1	-36.4
20°S	17.0	27.3	4.1
40°S	50.3	44.2	33.2
60°S	64.9	34.3	40.2
80°S	47.1	31.1	24.2

The GDOPs of GNFC for the all locations in Fig. 4.8 are shown in Fig. 4.14. As can be seen, the longitude also affects the GDOPs of GNFC. Therefore, by obtaining design parameters to assign lower GDOPs for the most required regions the better positioning error characteristic can be achieved.

#### 4.5.3 Conclusion

In the comparison of GPS errors for U.S. GPS, GLONASS, Galileo, and GNFC constellations, the latter demonstrates superior level of service to almost all the regions of the Earth. The GNFC constellation parameters presented in this paper are found by a series of trials. Although the closed-form relationship to build GNFC constellation parameters are not presented here, the FC design scheme has the strong attraction to compensate for the drawbacks of the U.S. GPS, GLONASS, and Galileo constellations.

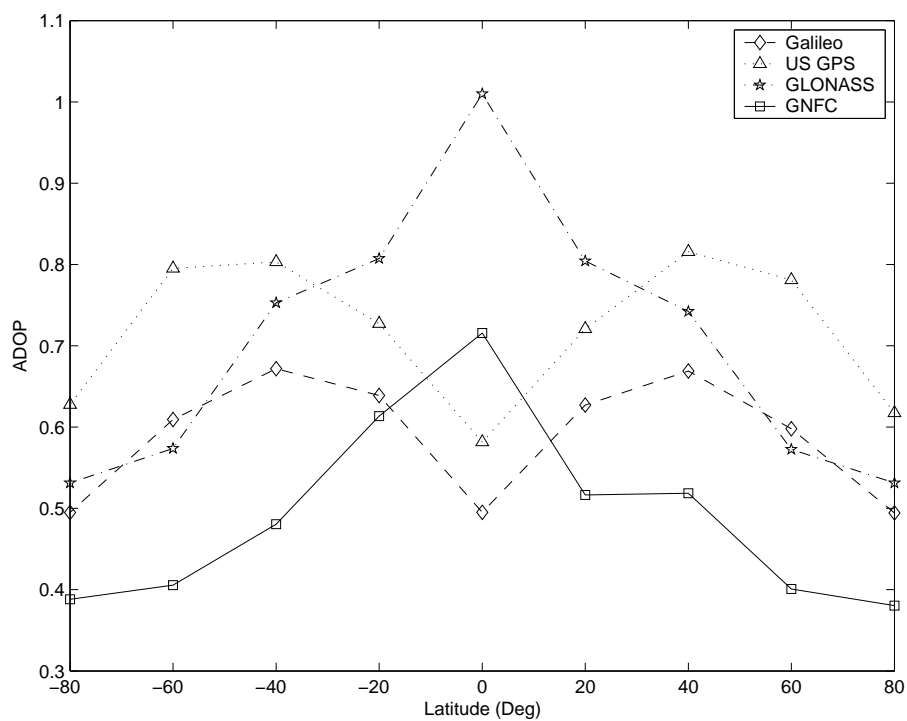


Fig. 4.13. ADOP Comparison

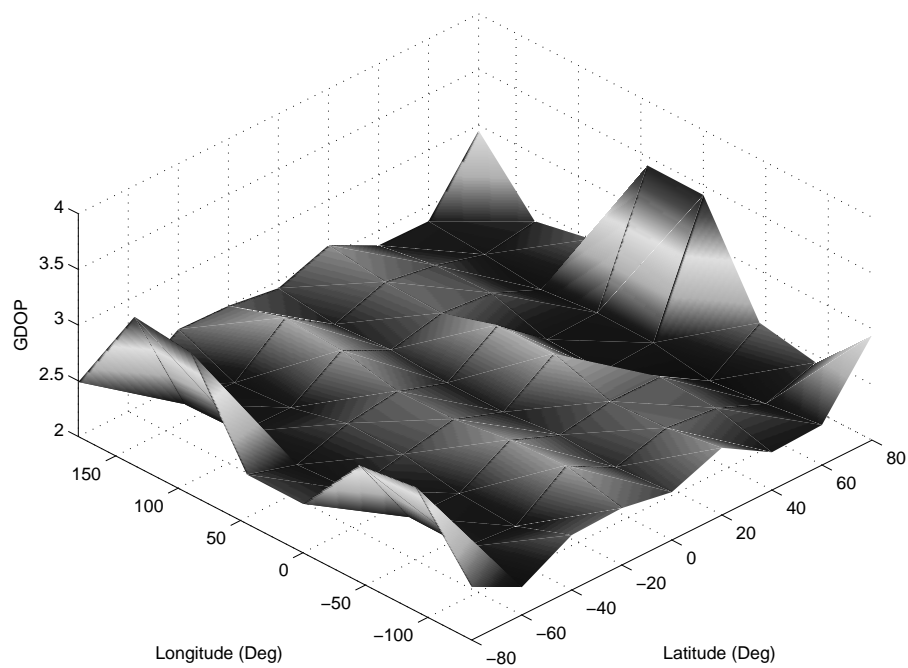


Fig. 4.14. GNFC GDOPs for Whole Earth Locations

## CHAPTER V

## SELF SURVEY

The phase center of each antenna, used to define the baselines, which are the position vectors between the phase center of the master antenna and that of the slave antennas, are required to be determined accurately. Also, line bias errors and integer ambiguities, that cannot be determined previously, need to be resolved before attitude determination using GPS receiver can commence. Then, a GPS receiver with multiple antenna can be used as an attitude sensor. Thus, the objective of GPS receiver self survey is to determine all the unknown parameters such as baselines, line biases, integer ambiguities, and a suboptimal attitude simultaneously.

## 5.1 Problem Statement

The measurement model of the single differenced GPS signal carrier phase between the Master Antenna (MA) and a Slave Antenna (SA) is shown in Fig. 5.1. The  $j$ -th sightline vector,  $\mathbf{s}_j \in \mathbb{R}^3$ , is the unit LOS vector from the receiver to the  $j$ -th GPS satellite in the ECEF reference frame. The  $i$ -th baseline vector,  $\mathbf{b}_i \in \mathbb{R}^3$ , is the relative position vector from the phase center of the MA to that of the  $i$ -th SA, which is represented by cycles in the body frame. Since the wavelength of the L1 frequency of GPS signal carrier is 19.03cm,<sup>67,69</sup> an integer (or cycle) ambiguity,  $n_{ij}$ , could occur either if the baseline is longer than signal wavelength or when cycle slips occur due to signal loss. Since the distance between the receiver and GPS satellites is very far, the wavefronts of GPS signal carrier are considered as planar. Therefore, the single differenced carrier phase between the  $i$ -th baseline and  $j$ -th sightline,  $\Delta\phi_{ij}$ , in Fig. 5.1 can be expressed by

$$\Delta\phi_{ij} = \mathbf{b}_i^\top \mathbf{A} \mathbf{s}_j + n_{ij} + \tau_i \quad (5.1)$$

where  $\mathbf{A} \in \mathbb{R}^{3 \times 3}$  is the attitude matrix between reference frame and body frame, and  $\tau_i$  is the line bias of the  $i$ -th baseline. The self survey determines the attitude  $\mathbf{A}$ ,



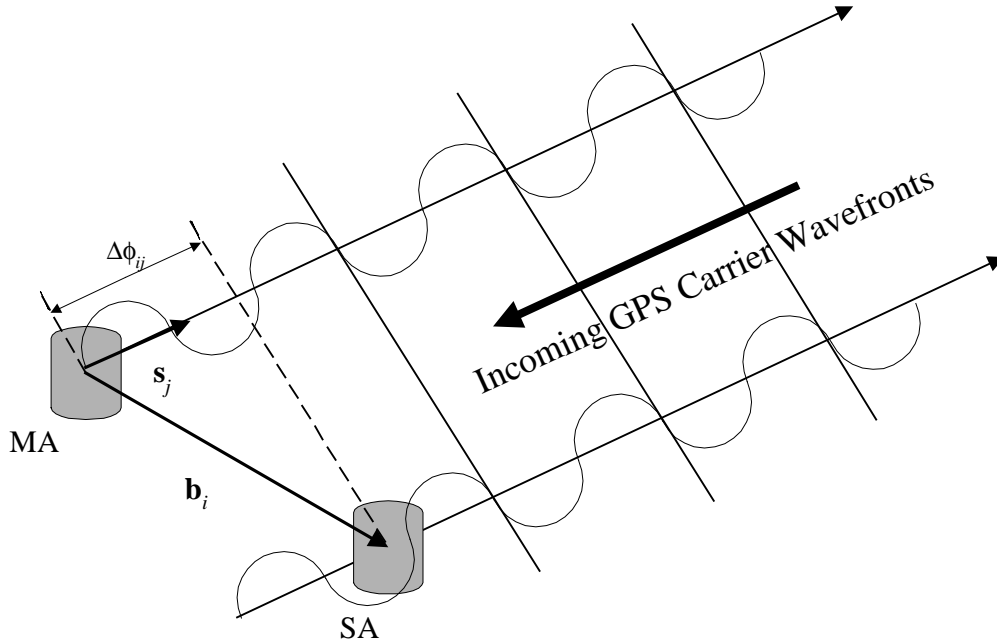


Fig. 5.1. Planar Phase Measurement Model

baseline in the body frame  $\mathbf{b}_i$ , integer ambiguity  $n_{ij}$ , and line bias  $\tau_i$  by using the phase measurement  $\Delta\tilde{\phi}_{ij}$  and the sightline  $\mathbf{s}_j$  information. The sightline information is obtained using the navigation data of the receiver.

## 5.2 Previous Work

As we can see in Eq. (5.1), the self survey is a nonlinear estimation problem. Non-linear least squares or a gradient search method can be used, however, the attitude parameters and the baselines are not independent.<sup>53</sup> Therefore, a singularity in the Hessian matrix occurs. Alternatively, the baselines in the ECEF reference frame and the summation of integer ambiguities and line biases are determined first by using a linear least squares fitting. Then, the integer ambiguities and line biases can be separated without loss of any information by taking the integer parts as the integer ambiguities. Also, a suboptimal attitude information can be estimated by using vector observation methods if 3 non-coplanar baselines exist.<sup>53</sup>

Since the GPS satellites are orbiting earth with a period of 12 hours, the connection between GPS satellites and the receiver will be lost repeatedly. Also, the receivers are often prone to losing GPS signals for several minutes due to hardware and software problems. Since the receiver is accumulating the carrier phase cycles, an incorrect cycle counts can occur when the signals are recovered after the signal connection loss. Therefore, integer ambiguity resolution, cycle slip detection and repair subsystems are required for a successful self survey.

### 5.2.1 *Integer Ambiguity Resolution*

The integer ambiguities can be determined using either instantaneous or dynamic techniques.<sup>71</sup> Instantaneous methods find a solution that minimizes the error residual at a specific time by searching through all possible integers sets. Refinements can be made to the solution by restricting the search space using geometric constraints.<sup>63</sup> This is well suited to short baselines, however, the minimum residual does not guarantee a correct solution in the presence of measurement noise.<sup>61</sup> The algorithm can determine wrong integers as valid ones. This may cause significant problems during the self survey. Dynamic techniques perform a batch estimation using the collected data for a given period of time while the integer ambiguities remain constant over the collection period. Since these techniques require that a certain amount of motion has occurred, several minutes of collection time may be required for convergence. Also, large matrix inversions need to be taken. This leads to numerical errors, however, dynamic techniques are more robust than instantaneous techniques because dynamic techniques have numerous checks that can be implemented into the solution before it is accepted.<sup>71</sup>

Cohen developed an algorithm that uses a linearized iterative batch estimator.<sup>71</sup> By varying the sample rate and the data collection period, this algorithm can be applied for almost any vehicle motion. However, there are several disadvantages, including: 1) an a priori attitude should be given, 2) for large initial attitude errors it may converge to wrong estimates, and 3) depending on the amount of data large-order matrix inversions may be accomplished. Crassidis et al.<sup>61</sup> developed an algorithm

that has advantages over Cohen’s method, including: 1) it doesn’t require any a priori attitude information, 2) large matrix inversions are not required, and 3) it is non-iterative. Also, a covariance expression has been derived that can be used to check the integrity of the integer ambiguity. However, this algorithm assumes that at least three non-coplanar baselines exist. Also, a significant amount of vehicle motion is still required in order for the integers to be observable. Lightsey and Crassidis developed a real-time attitude independent ambiguity resolution algorithm based on UF which is more robust than EKF.<sup>42</sup>

In the self survey, however, the antenna set connected to the receiver is not moving generally. Therefore, motion based dynamic techniques cannot be used. Instead, a fast integer ambiguity resolution algorithm by Lightsey et al. can be used.<sup>63</sup> This algorithm uses the geometric inequality to reduce the integer search spaces. Also, it can be applied for coplanar baselines. Then, a batch-type loss function is used to resolve the integer ambiguity with the covariance integrity check. Therefore, even with a few data the integer ambiguities can be resolved successfully.

#### *5.2.1.1 Geometric Constraint*

Instantaneous algorithms have an advantage in that they provide integers directly at a specific time, although they are prone to noise errors, which can induce incorrect solutions. An integer search is performed to maximize the probability that a unique solution is the correct solution, while at the same time reducing the search space by using normality constraints as well as geometric constraints. First, it is assumed that either three non-coplanar baselines or three non-coplanar sightlines are available (if three non-coplanar baselines exist then they should be used). The first step involves reducing the integer search space by using a subset of only two baselines and two sightlines. With this subset, a significant reduction in the search space is possible (especially for long baselines). For example, with three baselines (assuming that  $\kappa$  is possible integers associated with each baseline) the search space required to determine the integers is on the order of  $\kappa^3$ ; however, with the reduced subset the search space is now on the order of  $3\kappa^2$ .

This test is used to significantly reduce the search space since only a few integers will pass the geometric constraint described in the following. First, at any instant of time, it is assumed that either three non-coplanar baselines or three non-coplanar sightlines are available. When three non-coplanar baselines are available, using two baselines  $\mathbf{b}_1$  and  $\mathbf{b}_2$ , the following inequality pertaining to the  $j$ -th sightline must be true:

$$\begin{aligned} \|\mathbf{b}_1\|^2\|\mathbf{b}_2\|^2 &> (\mathbf{b}_1 \cdot \mathbf{b}_2)^2 + \|\mathbf{b}_2\|^2(\Delta\tilde{\phi}_{1j} - n_{1j})^2 \\ &\quad - 2(\Delta\tilde{\phi}_{1j} - n_{1j})(\Delta\tilde{\phi}_{2j} - n_{2j})(\mathbf{b}_1 \cdot \mathbf{b}_2) + \|\mathbf{b}_1\|^2(\Delta\tilde{\phi}_{2j} - n_{2j})^2 \end{aligned} \quad (5.2)$$

If three non-coplanar sightlines are available, the same inequality relative to the  $i$ -th baseline can be expressed using sightlines  $\mathbf{s}_1$  and  $\mathbf{s}_2$  by

$$\begin{aligned} \|\mathbf{b}_i\|^2 \left[ 1 - (\mathbf{s}_1 \cdot \mathbf{s}_2)^2 \right] &> (\Delta\tilde{\phi}_{i1} - n_{i1})^2 \\ &\quad - 2(\Delta\tilde{\phi}_{i1} - n_{i1})(\Delta\tilde{\phi}_{i2} - n_{i2})(\mathbf{s}_1 \cdot \mathbf{s}_2) + (\Delta\tilde{\phi}_{i2} - n_{i2})^2 \end{aligned} \quad (5.3)$$

If the integers have been properly resolved, then it can be shown that Eq. (5.2) reduces down to (in the noise free case)

$$\left[ (\mathbf{A}\mathbf{s}_j) \cdot (\mathbf{b}_1 \times \mathbf{b}_2) \right]^2 > 0 \quad (5.4)$$

This means that  $\mathbf{A}\mathbf{s}_j$ ,  $\mathbf{b}_1$  and  $\mathbf{b}_2$  must not lie in the same plane. This condition is required to be able to extract attitude information outside of the  $\mathbf{b}_1$  and  $\mathbf{b}_2$  plane. Equation (5.4) is almost always satisfied if the integers pass the test using Eq. (5.2).

### 5.2.1.2 Cost Minimization

The next step involves converting the sightlines into the body frame,  $\mathbf{A}\mathbf{s}_j$ , as the sum of two components. This is accomplished by minimizing the following loss function:

$$J(\mathbf{A}\mathbf{s}_j) = \frac{1}{2} \sum_{i=1}^M \frac{1}{\tilde{w}_{ij}^2} (\Delta\tilde{\phi}_{ij} - n_{ij} - \mathbf{b}_i^T \mathbf{A}\mathbf{s}_j)^2 \quad \text{for } j = 1, 2, \dots, N \quad (5.5)$$

where  $M$  is the number of baselines and  $N$  is the number of available sightlines. If at least three non-coplanar baselines exist, the minimization of Eq. (5.5) leads to

$$\mathbf{A}\mathbf{s}_j = \hat{\mathbf{s}}_j - \mathbf{c}_j \quad (5.6)$$

where  $\hat{\mathbf{s}}_j$  and  $\mathbf{c}_j$  are given by

$$\hat{\mathbf{s}}_j = \mathbf{B}_j^{-1} \left[ \sum_{i=1}^M \frac{1}{\bar{w}_{ij}^2} \Delta \tilde{\phi}_{ij} \mathbf{b}_i \right] \quad (5.7a)$$

$$\mathbf{c}_j = \mathbf{B}_j^{-1} \left[ \sum_{i=1}^M \frac{1}{\bar{w}_{ij}^2} n_{ij} \mathbf{b}_i \right] \quad (5.7b)$$

$$\mathbf{B}_j = \sum_{i=1}^M \frac{1}{\bar{w}_{ij}^2} \mathbf{b}_i \mathbf{b}_i^\top \quad (5.7c)$$

Since the measurements are not perfect, Eq. (5.6) is replaced by the following measurement model

$$\hat{\mathbf{s}}_j = \mathbf{A} \mathbf{s}_j + \mathbf{c}_j + \boldsymbol{\epsilon}_j \quad (5.8)$$

where  $\boldsymbol{\epsilon}_j$  is a zero-mean Gaussian process with covariance  $\mathbf{R}_j = \mathbf{B}_j^{-1}$ .

The next step is to use an attitude-independent method to find the phase-bias vector  $\mathbf{c}_j$ . To eliminate the dependence on the attitude, the orthogonality of  $\mathbf{A}$  and Eq. (5.8) are used to give

$$\begin{aligned} \|\mathbf{s}_j\|^2 &= \|\mathbf{A} \mathbf{s}_j\|^2 = \|\hat{\mathbf{s}}_j - \mathbf{c}_j - \boldsymbol{\epsilon}_j\|^2 \\ &= \|\hat{\mathbf{s}}_j\|^2 - 2\hat{\mathbf{s}}_j \cdot \mathbf{c}_j + \|\mathbf{c}_j\|^2 - 2(\hat{\mathbf{s}}_j - \mathbf{c}_j) \cdot \boldsymbol{\epsilon}_j + \|\boldsymbol{\epsilon}_j\|^2 \end{aligned} \quad (5.9)$$

Next, following Alonso and Shuster,<sup>72</sup> an effective measurement and noise are defined as

$$z_j \equiv \|\hat{\mathbf{s}}_j\|^2 - \|\mathbf{s}_j\|^2 \quad (5.10a)$$

$$v_j \equiv 2(\hat{\mathbf{s}}_j - \mathbf{c}_j) \cdot \boldsymbol{\epsilon}_j - \|\boldsymbol{\epsilon}_j\|^2 \quad (5.10b)$$

The effective measurement model can be shown to be equivalent to

$$z_j = 2\hat{\mathbf{s}}_j \cdot \mathbf{c}_j - \|\mathbf{c}_j\|^2 + v_j \quad (5.11)$$

where  $v_j$  is approximately Gaussian for small  $\boldsymbol{\epsilon}_j$  having mean and variance given by

$$\mu_j \equiv E\{v_j\} = -\text{trace}\{\mathbf{R}_j\} \quad (5.12a)$$

$$\sigma_j^2 \equiv E\{v_j^2\} - \mu_j^2 = 4(\hat{\mathbf{s}}_j - \mathbf{c}_j)^\top \mathbf{R}_j (\hat{\mathbf{s}}_j - \mathbf{c}_j) - \mu_j^2 \quad (5.12b)$$

Equations (5.10) to (5.12) define an attitude-independent set of conditions since they do not contain the attitude matrix  $\mathbf{A}$ . The negative-log-likelihood function for the bias is given by

$$J(\mathbf{c}_j) = \frac{1}{2} \sum_{k=1}^L \left\{ \frac{1}{\sigma_j^2(k)} [z_j(k) - 2\hat{\mathbf{s}}_j(k) \cdot \mathbf{c}_j + \|\mathbf{c}_j\|^2 - \mu_j(k)]^2 + \log \sigma_j^2(k) + \log 2\pi \right\} \quad (5.13)$$

where  $L$  is the total number of measurement epochs, and the symbol  $k$  denotes the variable at time  $t_k$ . The maximum-likelihood estimate for  $\mathbf{c}_j$ , denoted by  $\mathbf{c}_j^*$ , minimizes the negative-log-likelihood function, and satisfies

$$\left. \frac{\partial J(\mathbf{c}_j)}{\partial \mathbf{c}_j} \right|_{\mathbf{c}_j^*} = \mathbf{0} \quad (5.14)$$

The minimization of Eq. (5.13) is not straightforward since the likelihood function is quartic in  $\mathbf{c}_j$ . A number of algorithms have been proposed for estimating the bias. A new approach is to consider the case for  $M = 3$ , so that Eq. (5.7b) and Eq. (5.7a) are rewritten as

$$\hat{\mathbf{s}}_j = \mathbf{B}_j^{-1} \mathbf{\Gamma}_j \mathbf{\Phi}_j \quad (5.15a)$$

$$\mathbf{c}_j = \mathbf{B}_j^{-1} \mathbf{\Gamma}_j \mathbf{n}_j \quad (5.15b)$$

where

$$\mathbf{\Gamma}_j = [\bar{w}_{1j}^{-2} \mathbf{b}_1 \quad \bar{w}_{2j}^{-2} \mathbf{b}_2 \quad \bar{w}_{3j}^{-2} \mathbf{b}_3]$$

$$\mathbf{n}_j \equiv \begin{bmatrix} n_{1j} \\ n_{2j} \\ n_{3j} \end{bmatrix}, \quad \mathbf{\Phi}_j \equiv \begin{bmatrix} \Delta \tilde{\Phi}_{1j} \\ \Delta \tilde{\Phi}_{2j} \\ \Delta \tilde{\Phi}_{3j} \end{bmatrix} \quad (5.16)$$

The loss function in Eq. (5.13) can be re-written as

$$J(\mathbf{n}_j) = \frac{1}{2} \sum_{k=1}^L \left\{ \frac{1}{\sigma_j^2(k)} \left[ \|\mathbf{B}_j^{-1} \mathbf{\Gamma}_j (\mathbf{\Phi}_j(k) - \mathbf{n}_j)\|^2 - \|\mathbf{s}_j(k)\|^2 + \text{trace}\{\mathbf{B}_j^{-1}\} \right]^2 + \log \sigma_j^2(k) \right\} \quad (5.17)$$

Equation (5.17) can now be used to directly determine the integers without pre-computing the sightline vector in the body frame.

The integer  $n_{ij}$  for all sightlines and baselines should be determined instantaneously or using small number of data. The number of possible integers for a baseline is obtained by taking the floor value of the length of the baseline. For example, if  $\mathbf{b}_1 = [2 \ 1 \ 1]^T$ , then its length is 2.45, and  $n_{1j}$  can be among -2, -1, 0, 1, 2. If we have 6 sightlines and 3 baselines and their lengths are 2.45, 2.62, 1.34 respectively, then the total number of integers to be searched is  $6 \times 5 \times 5 \times 3 = 450$ . In other words, the cost function in Eq. (5.17) needs to be calculated 450 times to find the minimum value. However, the required search space can be significantly reduced when the constraint in Eq. (5.2) is tested. The number of integers that pass the geometric constraint test is approximately 5%~40% of the total number. Once the integers have been resolved, the attitude can be obtained.

### 5.2.2 Survey Window

Since the GPS satellites are not always in view, the estimation accuracy will be affected by the number of available sightlines and their relative positions as well as their duration of connectivity. To investigate these effects a concept of survey window is introduced. The survey window denotes the duration of time that a certain number of sightlines are available without cycle slips in the measurements. An example of a survey window is shown in Fig. 5.2 of which the longitudinal-axis denotes GPS time in hours and the vertical-axis denotes the Pseudo-Random Number (PRN) of each GPS satellite.

If the duration is increased, the number of available sightlines is decreased. Conversely, if the duration is decreased, the number of available sightlines is increased. Also, the location of the receiver dictates the sightlines availability. By using both a MATLAB based GPS simulator and Satellite Tool Kit (STK)<sup>98</sup> the GPS constellation is simulated for 48 hours worth of data. Then, a covariance analysis of the self survey error can be accomplished. Since the receiver is not moving during the self survey, the sightlines can be pre-computed. Therefore, if the self survey should be done in space, the prediction of the self survey time can be made in the mission design because the covariance analysis can be performed beforehand.

### GPS Receiver Access

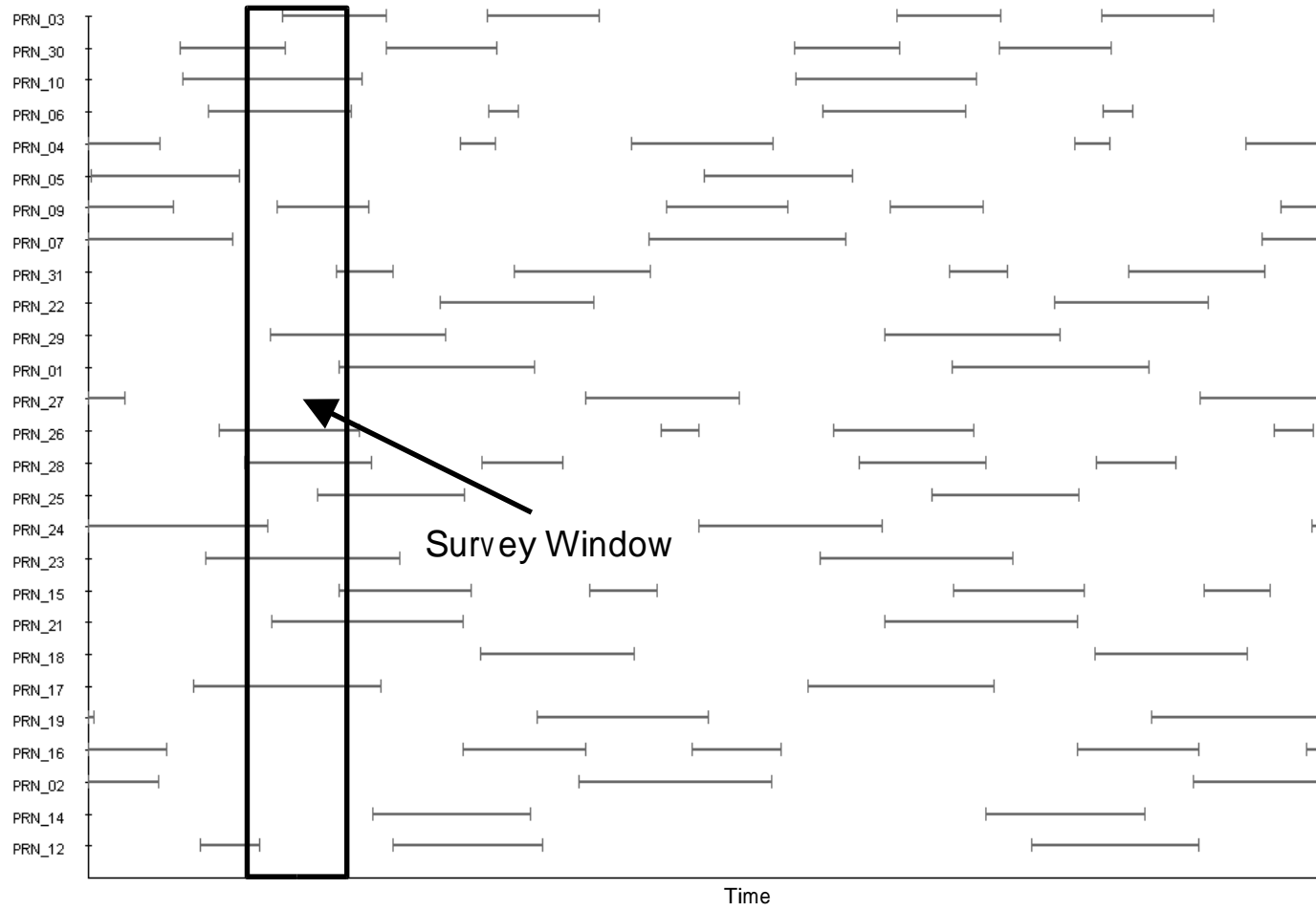


Fig. 5.2. An Example of Survey Window



Table 5.1. Survey Window Types

Types	Description
Type 1	the same 6 or more sightlines are in view for 1 hour
Type 2	the same 6 or more sightlines are in view for 2 hours
Type 3	the same 5 or more sightlines are in view for 3 hours

To investigate the effects of the number of the sightlines and duration of access, three types of survey windows are devised and compared. These three survey windows are shown in Table 5.1.

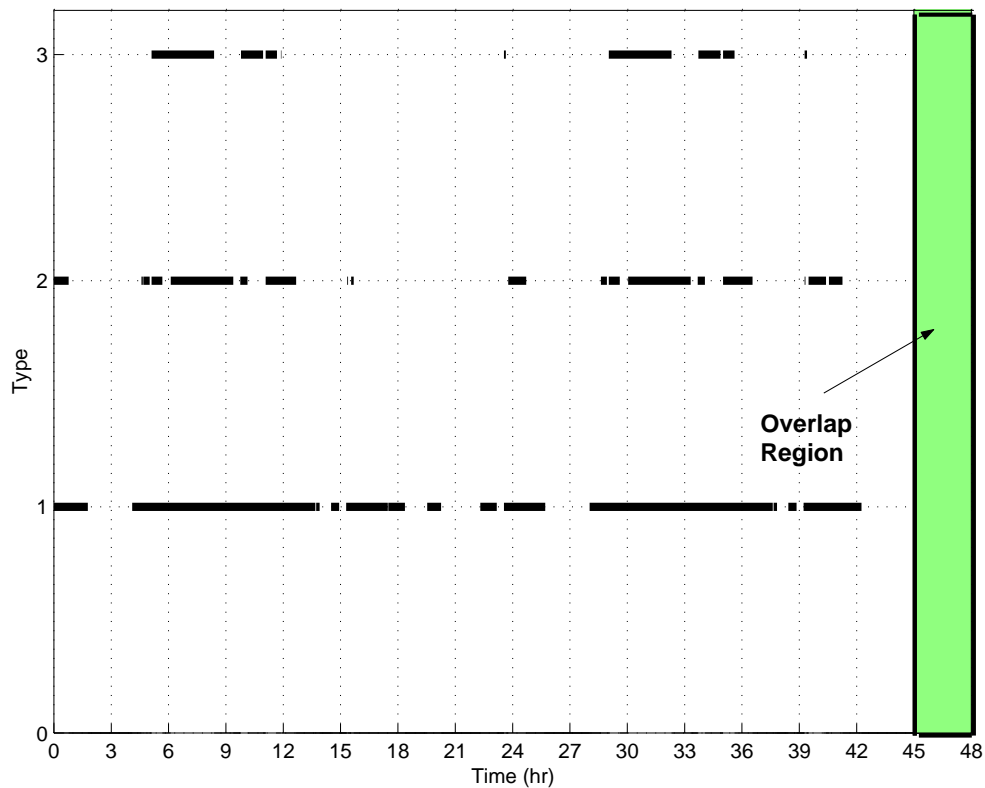


Fig. 5.3. Availability of Survey Window

We cannot conclude the self survey performance with a few hours simulation because the sightlines are moving slowly. The sightlines are moving because the orbits of the GPS satellites have 12 hour period circular orbits and their ground tracks are varying due to a perturbation effect. Since the sightlines are moving, these three

survey windows are not always available. The availabilities of survey windows are shown in Fig. 5.3 of which the longitudinal axis denotes the GPS time in hours and the perpendicular axis represents the type of the survey window.

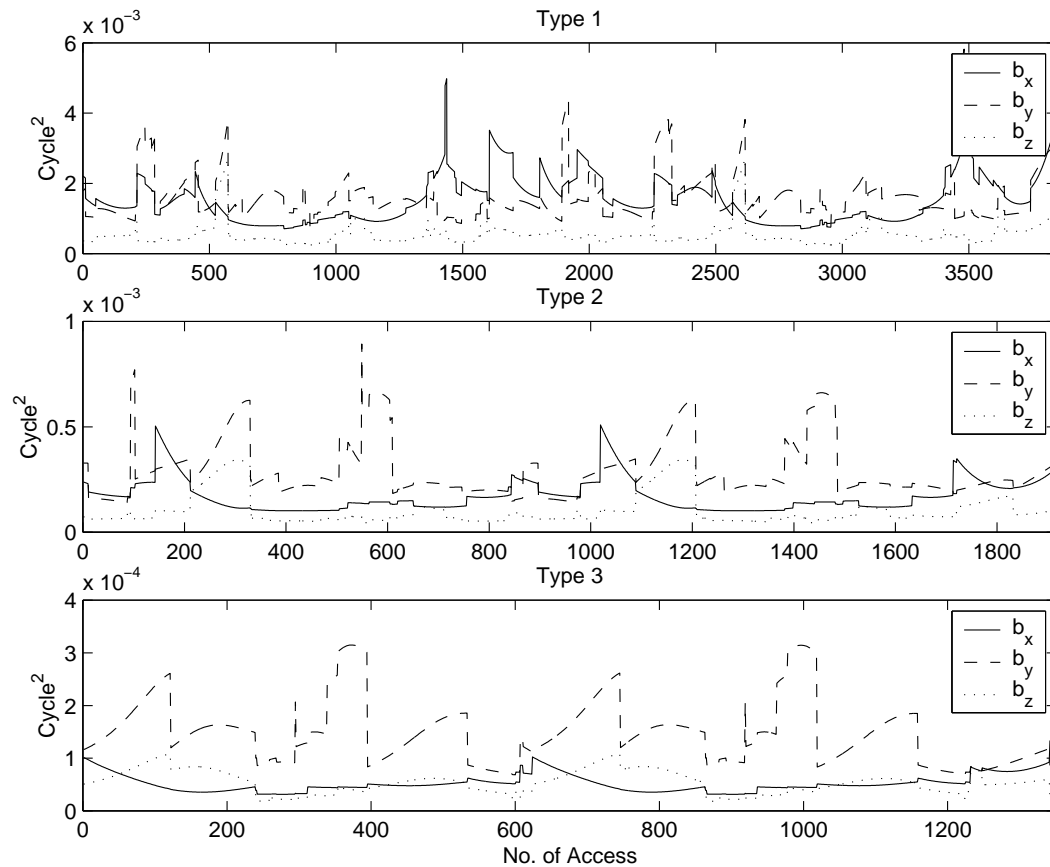


Fig. 5.4. Covariance of Baseline Estimation Error for Each Type

The ephemerides of the satellites in the GPS constellation as well as their connectivity to the ground receiver are simulated by using STK and its Chains module. Since the connection between the GPS satellites and the receiver can be conveniently simulated by STK, two days of sightlines and their availability are generated with an interval of 30 seconds. Figure 5.3 shows the availability of each type of survey window. The overlap region is neglected because the simulated sightlines are not available after 48 hours. It is clear that the Type 1 survey window has the longest availability, while Type 3 has the shortest availability. This means that sometimes we cannot use a

Type 2 survey window for 8 hours or a Type 3 survey window more than 10 hours, while a Type 1 survey window can be used within approximately 2 hours.

Although the survey window availability of each type is different, the self survey result of each type is compared. The covariance of a baseline estimation error for each type is shown in Fig. 5.4 where the number of access in the longitudinal axis means the count of time when that type of survey window is available. The perpendicular axis denotes the covariance values of the error in cycles<sup>2</sup>. The estimation error of the Type 3 survey window is the smallest while the number of access is the smallest. Also, the covariance in the  $z$ -axis is the smallest and those of the other axes show some fluctuation.

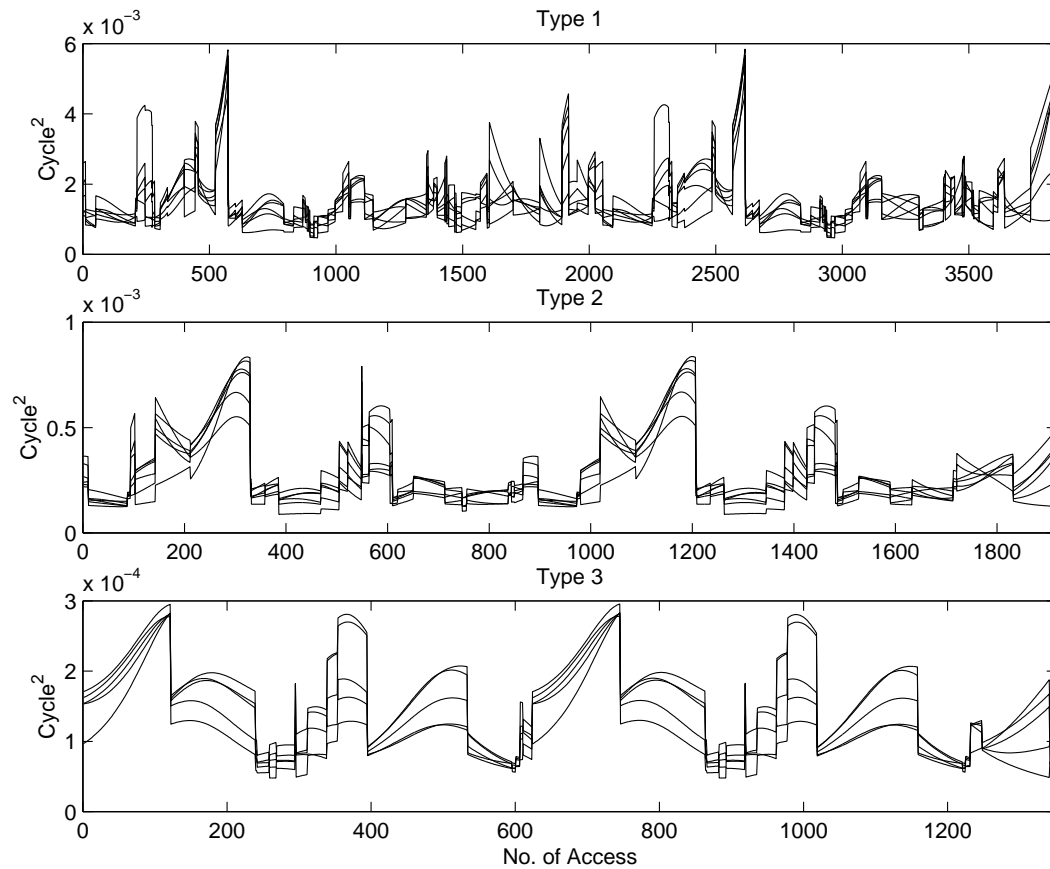


Fig. 5.5. Covariance of Line Bias Estimation Error for Each Type

Figure 5.5 shows the covariance of the estimation error of the summation of a line bias and the integer ambiguities. Similar to the baseline result, the Type 3 survey window results in the best estimate. Although the estimation errors depend on the sightlines, the covariance values of the Type 3 survey windows are the smallest. Therefore, a longer connection is the better for the self survey which intuitively makes sense, however, a longer connection might not be achieved for an extended time as shown in Fig. 5.3. Therefore, the commercial receivers such as TANS Vector receiver take at least 8 hours for the self survey in general.

### 5.3 New Approach

The assumptions applied in the previous approaches do not allow for changes of the baseline length. However, the lengths of the baselines might be changed since the phase centers are different from the geometric centers. Furthermore, the integer ambiguity resolution algorithm does not work if line biases errors are contained in the phase measurements. In the new approach, these two problems are solved using a double difference technique with nonlinear least squares. Also, the cycle slip detection and repair problem is analyzed. The flow chart of new approach is shown in Fig. 5.6.

#### 5.3.1 Cycle Slip Detection and Repair

When a GPS receiver is turned on, the fractional part of the phase difference between the satellite transmitted carrier and a receiver generated replica signal is observed and an integer counter is initialized. During the tracking, the counter is incremented by one cycle whenever the fractional phase changes from 1 to 0. The initial integer number,  $n$ , of cycles between the satellite and the receiver remains constant as long as no loss of signal lock occurs. When the signal lock is lost, the integer counter is restarted. Therefore, a cycle jump, called cycle slip, may occur. Sources of cycle slips are: 1) obstruction of GPS signal due to trees, buildings, mountains, etc., 2) a low SNR due to bad ionospheric conditions, multipath, high receiver dynamics, or low GPS satellite elevation, or 3) a failure in the receiver software.<sup>67</sup> A single difference

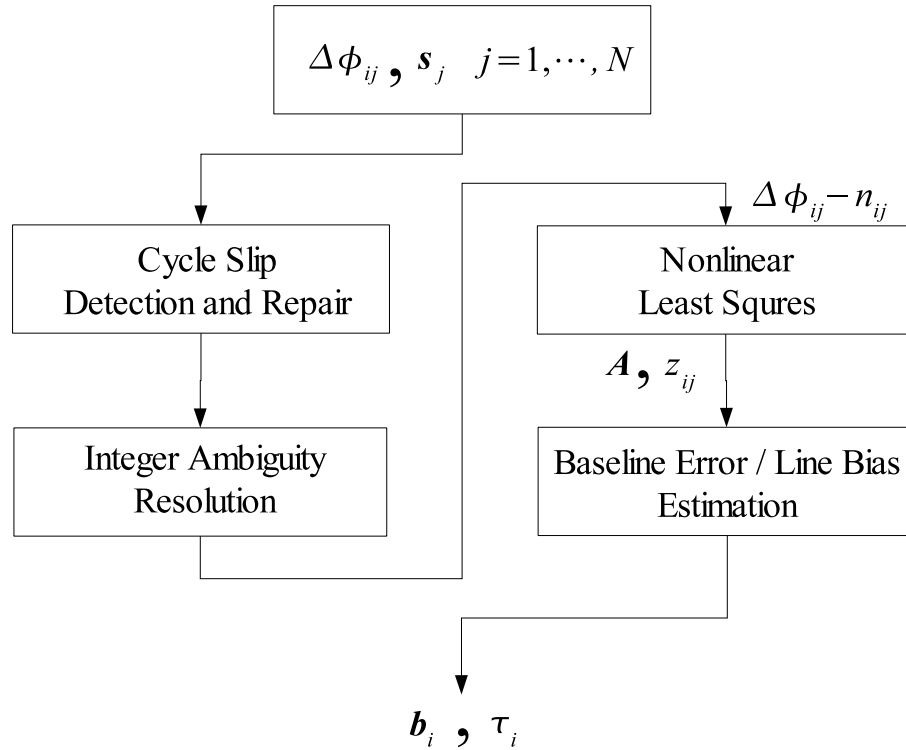


Fig. 5.6. Flow Chart of Self Survey

of the phase measurements and its cycle slip repaired counterpart is shown in Fig. 5.7. As seen from Fig. 5.7, initial and end raw measurements contain numerous cycle slips and signal lock loss because the TANS Vector receiver collects only 6-channels of data. Also, the duration of signal lock loss lasts several minutes for some reason, such as signal jamming. Therefore, the determination of cycle slip size becomes complex. However, by monitoring its time derivative, large signal lock loss cases are compensated successfully. An example of the time derivative comparison between the measurements and the estimates is shown in Fig. 5.8.

A first order polynomial fit works successfully for the early 30 to 50 minutes data because the sightlines are moving slowly in static case. After then, a real-time sequential estimator is used for the cycle slip detection and repair since the slope of the time derivatives is changing. Since a higher-order polynomial fitting is required, at least 30 minutes of data are needed for the initialization of the estimator. In real data applications an 8-th order polynomial is sometimes required for the correct

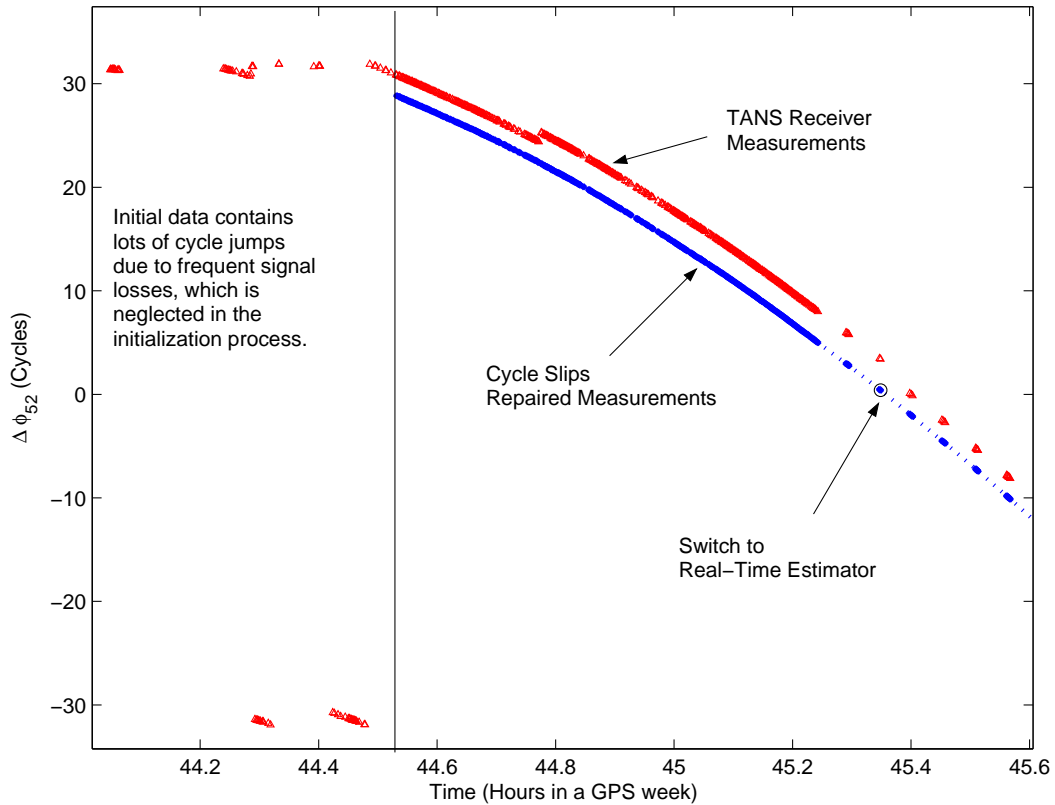


Fig. 5.7. Measured and Cycle Slips Repaired  $\Delta\phi$  Example

result. The reason is that, for example, the TANS receiver has only 6-channels so that the connection between a satellite and a receiver could be unstable for the early part and the end of the connection. A block diagram of cycle slip detection and repair algorithm is shown in Fig. 5.9.

### 5.3.2 Integer Ambiguity Resolution

The integer ambiguities need to be resolved before the attitude problem is solved. However, existing integer ambiguity algorithms cannot be applied due to the line biases errors contained in the measurements. This problem can be resolved by taking double differences, because the line biases errors are cancelled.<sup>69</sup> However, the double differenced integer ambiguity should still be resolved. It can be resolved by using the modified fast integer ambiguity resolution algorithm. Since double differ-

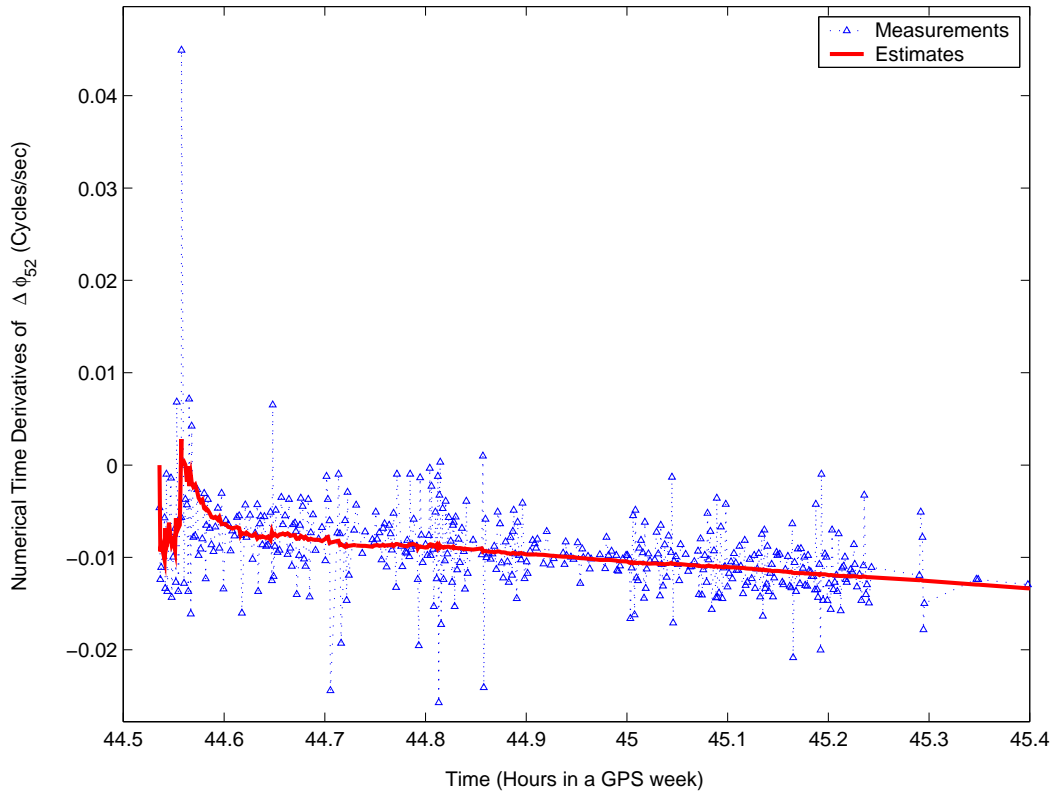


Fig. 5.8. Measured and Estimated  $\Delta\dot{\phi}$  Example

ences between sightlines are applied, the cost function and the geometric constraint are reconstructed. Then, the baselines in the reference frame and line biases can be determined. Finally, the integer ambiguities of the single differential phase measurements can be obtained by taking the integer part of the residual between the measurement and the dot product of the baseline estimates and the sightlines.

### 5.3.2.1 Double Differences

For a single difference carrier phase measurements, line biases between receivers are troublesome. This problem can be resolved by taking between-receiver, between-sightlines double difference measurements. Using Eq. (5.1), the single difference measurement model is expressed by

$$\Delta\phi_{ij} = \mathbf{b}_i^T \mathbf{A} \mathbf{s}_j + n_{ij} + \tau_i + \epsilon_{ij} \quad (5.18)$$

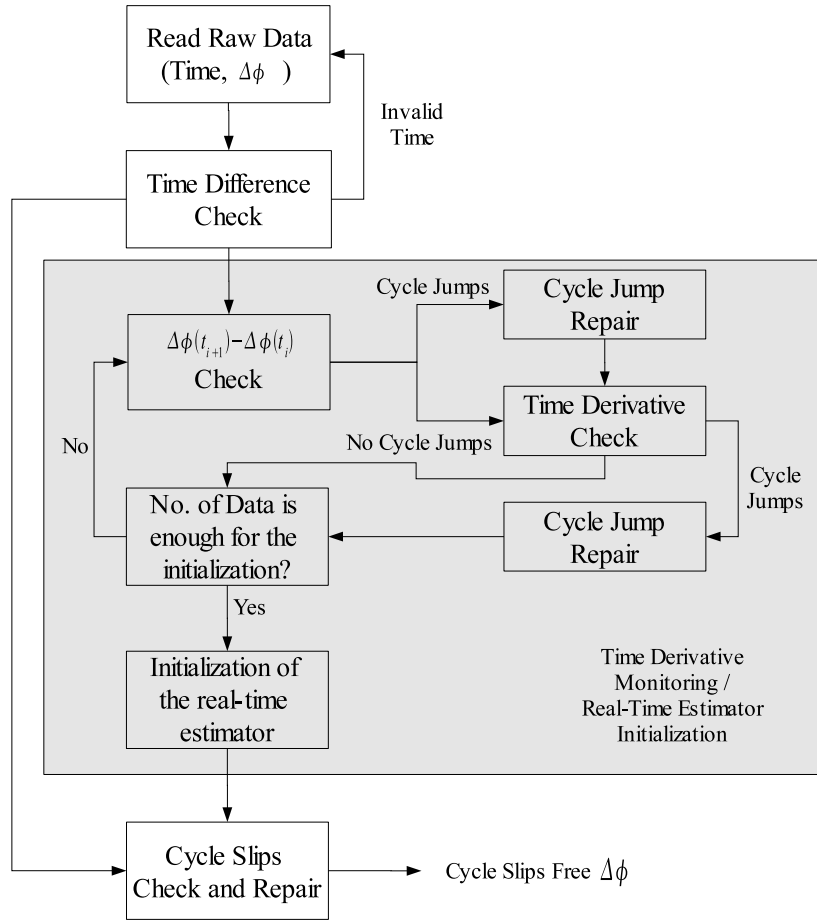


Fig. 5.9. Cycle Slips Detection and Repair Block Diagram

where  $\epsilon_{ij}$  denotes the phase measurement error. If we take the differences of the single differences in the sightlines  $j$  and  $k$ , we would get rid of the line bias on the  $i$ -th baseline,  $\tau_i$ . Therefore, the double differenced phase measurements can be written by

$${}^2\Delta\phi_i^{jk} = \mathbf{b}_i^T \mathbf{A}(\mathbf{s}_j - \mathbf{s}_k) - (n_{ij} - n_{ik}) + (\epsilon_{ij} - \epsilon_{ik}) \quad (5.19)$$

where  ${}^2\Delta\phi_i^{jk}$  denotes the double differenced phase between single differenced phases  $\Delta\phi_{ij}$  and  $\Delta\phi_{ik}$ . However, measurement noise is increased by a factor of  $\sqrt{2}$  times that of the single differences. Still, double differenced phase measurements are useful since line biases do not need to be determined.



### 5.3.2.2 Geometric Constraint for Double Differences

From the identity of three dimensional vectors,  $\mathbf{A}\mathbf{s}_{jk}$ ,  $\mathbf{b}_1$ ,  $\mathbf{b}_2$ , the geometric constraint for double differences is now rewritten by

$$\begin{aligned}
[(\mathbf{A}\mathbf{s}_{jk}) \cdot (\mathbf{b}_1 \times \mathbf{b}_2)]^2 &= (\mathbf{A}\mathbf{s}_{jk} \times \mathbf{b}_1) \cdot [(\mathbf{b}_1 \times \mathbf{b}_2) \cdot (\mathbf{b}_2 \times \mathbf{A}\mathbf{s}_{jk})] \\
&= (\mathbf{A}\mathbf{s}_{jk})^2 (\mathbf{b}_1)^2 (\mathbf{b}_2)^2 - (\mathbf{A}\mathbf{s}_{jk})^2 (\mathbf{b}_1 \cdot \mathbf{b}_2)^2 \\
&\quad - (\mathbf{b}_1)^2 (\mathbf{A}\mathbf{s}_{jk} \cdot \mathbf{b}_2)^2 - (\mathbf{b}_2)^2 (\mathbf{A}\mathbf{s}_{jk} \cdot \mathbf{b}_1)^2 \\
&\quad + 2 (\mathbf{A}\mathbf{s}_{jk} \cdot \mathbf{b}_2) (\mathbf{A}\mathbf{s}_{jk} \cdot \mathbf{b}_1) (\mathbf{b}_1 \cdot \mathbf{b}_2) \\
&= \|\mathbf{s}_{jk}\|^2 \|\mathbf{b}_1\|^2 \|\mathbf{b}_2\|^2 - \|\mathbf{s}_{jk}\|^2 (\mathbf{b}_1 \cdot \mathbf{b}_2)^2 \\
&\quad - \|\mathbf{b}_1\|^2 \left( {}^2\Delta\phi_2^{jk} + n_2^{jk} \right)^2 - \|\mathbf{b}_2\|^2 \left( {}^2\Delta\phi_1^{jk} + n_1^{jk} \right)^2 \\
&\quad + 2 \left( {}^2\Delta\phi_1^{jk} + n_1^{jk} \right) \left( {}^2\Delta\phi_2^{jk} + n_2^{jk} \right) (\mathbf{b}_1 \cdot \mathbf{b}_2) \\
&> 0
\end{aligned} \tag{5.20}$$

where  $\mathbf{s}_{jk} = \mathbf{s}_j - \mathbf{s}_k$ ,  ${}^2\Delta\phi_1^{jk} = \Delta\phi_{1j} - \Delta\phi_{1k}$ , and  ${}^2\Delta\phi_2^{jk} = \Delta\phi_{2j} - \Delta\phi_{2k}$ . Although double differences may increase the search space twice as much as using single differences, a reduction of search space is achieved by using the constraint in Eq. (5.20).

### 5.3.2.3 Integer Ambiguity Resolution

The double differenced integer ambiguities in Eq. (5.19) can now be resolved using the cost function defined in Eq. (5.21):

$$J(\mathbf{n}_i^{jk}) = \frac{1}{2} \sum_{m=1}^L \left\{ \frac{1}{\sigma_{jk}^2(m)} \left[ \|\mathbf{S}_{jk}^{-1}(m) \mathbf{\Gamma}_{jk}(m) \left( \mathbf{\Phi}_i^{jk}(m) - \mathbf{n}_i^{jk} \right)\|^2 - \|\mathbf{b}_i\|^2 + \text{trace}\{\mathbf{S}_{jk}^{-1}(m)\} \right]^2 + \log \sigma_{jk}^2(m) \right\} \tag{5.21}$$

where

$$\begin{aligned}
\sigma_{jk}^2(m) &= -\text{trace}^2\{\mathbf{S}_{jk}^{-1}(m)\} \\
&\quad + \left( \mathbf{\Phi}_i^{jk}(m) - \mathbf{n}_i^{jk} \right)^\top \mathbf{\Gamma}_{jk}^\top(m) \mathbf{S}_{jk}^{-3}(m) \mathbf{\Gamma}_{jk}(m) \left( \mathbf{\Phi}_i^{jk}(m) - \mathbf{n}_i^{jk} \right)
\end{aligned} \tag{5.22a}$$

$$\mathbf{\Gamma}_{jk}(m) \equiv [\varpi_{i1}^{-2} \mathbf{s}_{12}(m), \varpi_{i2}^{-2} \mathbf{s}_{13}(m), \varpi_{i3}^{-2} \mathbf{s}_{14}(m)] \tag{5.22b}$$

$$\Phi_i^{jk}(m) \equiv \begin{bmatrix} {}^2\Delta\phi_{i1}^{jk} \\ {}^2\Delta\phi_{i2}^{jk} \\ {}^2\Delta\phi_{i3}^{jk} \end{bmatrix} \quad (5.22c)$$

$$\begin{aligned} \mathbf{S}_{jk}(m) &= \left(\varpi_{i1}^{jk}\right)^{-2} \mathbf{s}_{12}(m) \mathbf{s}_{12}^\top(m) + \left(\varpi_{i2}^{jk}\right)^{-2} \mathbf{s}_{13}(m) \mathbf{s}_{13}^\top(m) \\ &+ \left(\varpi_{i3}^{jk}\right)^{-2} \mathbf{s}_{14}(m) \mathbf{s}_{14}^\top(m) \end{aligned} \quad (5.22d)$$

For further application, however, the integer ambiguities contained in the single differenced phase measurements should be resolved. Therefore, the baselines in the reference frame can be estimated using linear least squares. The loss function to be minimized is given by

$$J(\tilde{\mathbf{b}}_i) = \frac{1}{2} \sum_{\text{all } jk} \left(\varpi_i^{jk}\right)^{-2} \left({}^2\Delta\tilde{\phi}_i^{jk} - \tilde{\mathbf{b}}_i^\top \mathbf{s}_{jk}\right)^2 \quad (5.23)$$

Then, the baselines in the reference frame are given by

$$\tilde{\mathbf{b}}_i = \mathbf{N}_i^{-1} \mathbf{y}_i \quad (5.24)$$

where

$$\mathbf{N}_i = \sum_{\text{all } jk} \left(\varpi_i^{jk}\right)^{-2} \mathbf{s}_{jk} \mathbf{s}_{jk}^\top \quad (5.25a)$$

$$\mathbf{y}_i = \sum_{\text{all } jk} \left(\varpi_i^{jk}\right)^{-2} {}^2\Delta\tilde{\phi}_i^{jk} \mathbf{s}_{jk} \quad (5.25b)$$

After determining the baselines in the reference frame, the integer ambiguities of the single differential phase measurements are resolved by taking the integer part of the residual given by

$$n_{ij} = \text{floor} \left( \Delta\phi_{ij} - \tilde{\mathbf{b}}_i^\top \mathbf{s}_j \right) \quad (5.26)$$

where floor is the MATLAB command which rounds the residual to the nearest integer towards minus infinity. This approach may not resolve the integers if the line bias errors are close to 0 or 1, however, it means that the line bias errors can be considered as the integer ambiguities.

### 5.3.3 Nonlinear Least Squares

Since the integer ambiguities are resolved, Eq. (5.1) can be rewritten as

$$\Delta\phi_{ij} = {}^g\mathbf{b}_i^\top \mathbf{A}\mathbf{s}_j + z_{ij} \quad (5.27)$$

where  ${}^g\mathbf{b}$  represents the geometric baseline vector in the body frame that connects the geometric center of two antennas and  $z_{ij}$  is the dummy parameter used in the baseline estimation, given by

$$z_{ij} = \Delta\mathbf{b}_i^\top \mathbf{A}\mathbf{s}_j + \tau_i \quad (5.28)$$

where  $\Delta\mathbf{b}_i \in \mathbb{R}^3$  is the additive error of baselines in the body frame. To estimate attitude parameters and  $z_{ij}$  in Eq. (5.27), nonlinear least squares can be used. By using the Modified Rodriguez Parameters (MRPs) as attitude parameters, the optimal estimates are obtained to minimize the loss function, given by

$$J(\hat{\mathbf{p}}, \mathbf{z}) = \sum_{i=1}^N \sum_{j=1}^M \left[ \widetilde{\Delta\phi}_{ij} - \Delta\phi_{ij}(\hat{\mathbf{p}}, \mathbf{z}) \right]^2 \quad (5.29)$$

where  $\hat{\mathbf{p}} \in \mathbb{R}^3$  denotes MRP estimates and  $\mathbf{z}$  represents a row vector of which element is  $z_{ij}$ . To express the solution of Eq. (5.29), we assume the nominal states as

$$\mathbf{x}_c = \begin{bmatrix} \mathbf{p}_c \\ \mathbf{z}_c \end{bmatrix}$$

Then, Eq. (5.27) can be written as

$$\Delta\phi_i(\hat{\mathbf{x}}) \approx \Delta\phi_i(\mathbf{x}_c) + \mathbf{H}\delta\mathbf{x} \quad (5.30)$$

where  $\delta\mathbf{x} = [\delta\mathbf{p}^\top \Delta\mathbf{z}^\top]^\top$  and the Jacobian matrix  $\mathbf{H}$  is given by

$$\begin{aligned}
\mathbf{H} &= \frac{\partial}{\partial \delta \mathbf{x}} [{}^g \mathbf{b}_i^\top \mathbf{A}(\mathbf{p}) \mathbf{s}_j + \mathbf{z}] \\
&= \frac{\partial}{\partial \delta \mathbf{x}} [{}^g \mathbf{b}_i^\top \mathbf{A}(\delta \mathbf{p}) \mathbf{A}(\mathbf{p}_c) \mathbf{s}_j + \mathbf{z}_c + \Delta \mathbf{z}] \\
&= \frac{\partial}{\partial \delta \mathbf{x}} [{}^g \mathbf{b}_i^\top (\mathbf{I} - 4[\delta \mathbf{p} \times]) \mathbf{A}(\mathbf{p}_c) \mathbf{s}_j + \mathbf{z}_c + \Delta \mathbf{z}] \\
&= \begin{bmatrix} \text{total M sightlines} \\ 4{}^g \mathbf{b}_i^\top [\mathbf{A}(\mathbf{p}_c) \mathbf{s}_j \times] \underbrace{, 0, 0, \dots, 0, 1, 0, \dots, 0}_{(j-1) \text{ zeros before 1}} \\ \vdots \end{bmatrix} \quad \text{for } i = 1, 2, 3
\end{aligned} \tag{5.31}$$

where

$$[\mathbf{a} \times] = \begin{bmatrix} 0 & -a_3 & a_2 \\ a_3 & 0 & -a_1 \\ -a_2 & a_1 & 0 \end{bmatrix} \tag{5.32}$$

Then, the measurement residual can be written as

$$\begin{aligned}
\widetilde{\Delta \phi} - \Delta \phi(\hat{\mathbf{x}}) &\approx \widetilde{\Delta \phi} - \Delta \phi(\hat{\mathbf{x}}_c) - \mathbf{H} \delta \mathbf{x} \\
&= \Delta \mathbf{y} - \mathbf{H} \delta \mathbf{x}
\end{aligned} \tag{5.33}$$

Using the residual, the new cost  $\Delta J$  can be defined as

$$\Delta J = \frac{1}{2} [\Delta \mathbf{y} - \mathbf{H} \delta \mathbf{x}]^\top \mathbf{W} [\Delta \mathbf{y} - \mathbf{H} \delta \mathbf{x}] \tag{5.34}$$

The minimization of  $\Delta J$  is equivalent to the minimization of  $J$ . If the process is convergent, then  $\delta \mathbf{x}$  determined by minimizing  $\Delta J$  would be expected to decrease on successive iterations until the linearization is an extremely good approximation.

A stopping condition with an accuracy dependent tolerance for the minimization of  $J$  is given by

$$\frac{\Delta J}{J} = \frac{\epsilon}{\|\mathbf{W}\|} \tag{5.35}$$

Then, the  $\delta \mathbf{x}$  is given by

$$\delta \mathbf{x} = (\mathbf{H}^\top \mathbf{W} \mathbf{H})^{-1} \mathbf{H}^\top \mathbf{W} \Delta \mathbf{y} \tag{5.36}$$

By using the obtained  $\delta \mathbf{x}$ , the updates are given by

$$\hat{\mathbf{p}} = \frac{(1 - \mathbf{p}_c^T \mathbf{p}_c) \delta \mathbf{p} + (1 - \delta \mathbf{p}^T \delta \mathbf{p}) \mathbf{p}_c - 2 [\delta \mathbf{p} \times] \mathbf{p}_c}{1 + \delta \mathbf{p}^T \delta \mathbf{p} \mathbf{p}_c^T \mathbf{p}_c - 2 \delta \mathbf{p}^T \mathbf{p}} \quad (5.37a)$$

$$\hat{\mathbf{z}} = \mathbf{z}_c + \Delta \mathbf{z} \quad (5.37b)$$

Since the problem itself is a nonlinear, the convergence to a correct estimate is not guaranteed. Therefore, for robustness, the Levenberg-Marquardt (LM) method is also used and compared with nonlinear least squares in the simulations.

#### 5.3.4 Baseline Estimation

By using the estimation results of the nonlinear least squares, the differences in the baselines in the body reference frame and the line biases errors are determined. Referring to Eq. (5.28), linear least squares is sufficient to estimate the baselines differences and line biases errors. It is given by

$$\mathbf{z} = \begin{bmatrix} \mathbf{s}_1^T \mathbf{A}^T, 1 \\ \vdots \\ \mathbf{s}_M^T \mathbf{A}^T, 1 \end{bmatrix} \begin{bmatrix} \Delta \mathbf{b}_i \\ \tau_i \end{bmatrix} \quad (5.38)$$

Then, the baselines in the body frame are determined by

$$\mathbf{b}_i = {}^g \mathbf{b}_i + \Delta \mathbf{b}_i \quad (5.39)$$

Since the antenna phase errors can easily be as much as 2cm, baseline estimation is important in the self survey if the baselines are short.

#### 5.3.5 Covariance Study

The covariance study of the self survey needs to be performed in three part. First, the covariance of integer ambiguity resolution should be computed to monitor the integrity of cycle ambiguity. Then, nonlinear least squares is investigated. Finally, the covariance of the baselines and the line biases is derived.

### 5.3.5.1 Integer Ambiguity Resolution

By using the double differences technique, the baselines in the reference frame are determined first. Then, the integer ambiguities are obtained by taking the integer part of the residual between the measurements and the dot product between the baseline estimates and the sightlines. By the nature of the integers, therefore, the integer ambiguity estimates contain no error if those estimates are correct.

### 5.3.5.2 Nonlinear Least Squares

The loss function consisting of the residual error is written as

$$J = \frac{1}{2} (\Delta \mathbf{y} - \mathbf{H} \delta \mathbf{x})^\top \mathbf{W} (\Delta \mathbf{y} - \mathbf{H} \delta \mathbf{x}) \quad (5.40)$$

The Jacobian is

$$\frac{\partial J}{\partial \delta \mathbf{x}} = -\mathbf{H}^\top \mathbf{W} (\Delta \mathbf{y} - \mathbf{H} \delta \mathbf{x}) \quad (5.41)$$

The Fisher information matrix is given by

$$\begin{aligned} \mathbf{F}_{\delta \mathbf{x}} &= E \left\{ \frac{\partial J}{\partial \delta \mathbf{x}} \frac{\partial J}{\partial \delta \mathbf{x}}^\top \right\} \\ &= E \left\{ \mathbf{H}^\top \mathbf{W} (\Delta \mathbf{y} - \mathbf{H} \delta \mathbf{x}) (\Delta \mathbf{y} - \mathbf{H} \delta \mathbf{x})^\top \mathbf{W} \mathbf{H} \right\} \\ &\approx \mathbf{H}^\top \mathbf{W} \mathbf{H} \end{aligned} \quad (5.42)$$

where the matrix  $\mathbf{W}$  denotes the measurement error covariance matrix. Then, the covariance matrix is given by

$$\mathbf{P}_{\delta \mathbf{x}} = [\mathbf{H}^\top \mathbf{W} \mathbf{H}]^{-1} \quad (5.43)$$

### 5.3.5.3 Baseline/Line Biases Estimation

The estimation of the baselines and line biases is the linear least squares. Therefore, the covariance matrix can be obtained by

$$\mathbf{P}_{\mathbf{z}} = [\mathbf{H}_{\mathbf{z}}^\top \mathbf{W} E \{ \Delta \mathbf{z} \Delta \mathbf{z}^\top \} \mathbf{W} \mathbf{H}_{\mathbf{z}}]^{-1} \quad (5.44)$$

where the Jacobian matrix is given by

$$\mathbf{H}_z = \begin{bmatrix} \mathbf{s}_1^T \mathbf{A}^T, 1 \\ \vdots \\ \mathbf{s}_M^T \mathbf{A}^T, 1 \end{bmatrix} \quad (5.45)$$

## 5.4 Implementation

The simulation of the GPS constellation is obtained by STK with Chains module and GPS almanac data.

### 5.4.1 STK/Chains

The STK contains all the active 28 GPS satellites data. Also, the receiver can be added as a sensor object. Therefore, the  $15^\circ$  mask angle of the receiver can be applied. By using the Chains module all the GPS satellites can be accessed from the receiver. The STK main window used in the simulation is shown in Fig. 5.10. The positions of the available GPS satellites can be generated in the ECEF coordinate system with a specified time interval of 48 hours. For a given ground location, the simulated ground tracks of the GPS satellites are shown in Fig. 5.11. As can be seen, the access times of the satellites to the receiver are not the same because the the ground tracks of the GPS satellites are different.

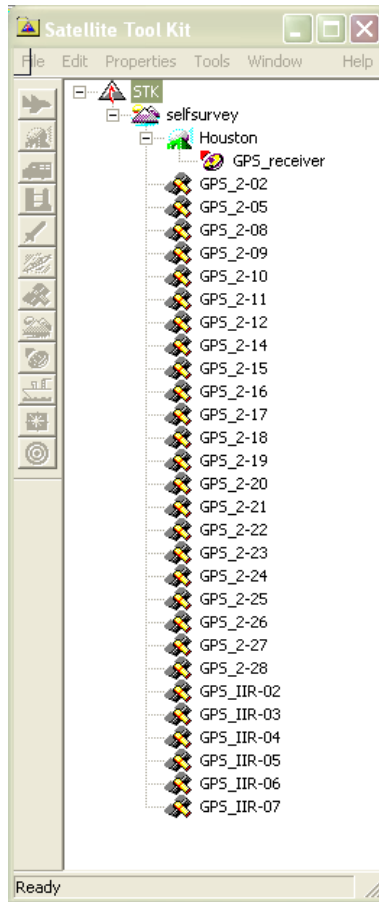


Fig. 5.10. STK Main Window for GPS Constellation

#### 5.4.2 GPS Almanac

The almanac data are available to determine position and velocity vectors of the satellites in a terrestrial reference frame at any instant. Both YUMA and SEM GPS almanac by Navigation Center (<http://www.navcen.uscg.gov/gps/almanacs.htm>) contain every GPS satellite information.<sup>90</sup> By using these almanac data, the GPS constellation can be simulated by using the formulas

$$n = \sqrt{\frac{\mu}{a^3}} \quad (5.46a)$$

$$M = M_o + n(t - t_o) \quad (5.46b)$$

$$i = 54^\circ + \delta i \quad (5.46c)$$

$$\Omega = \Omega_o + \dot{\Omega}(t - t_o) - \dot{\Omega}_E t \quad (5.46d)$$



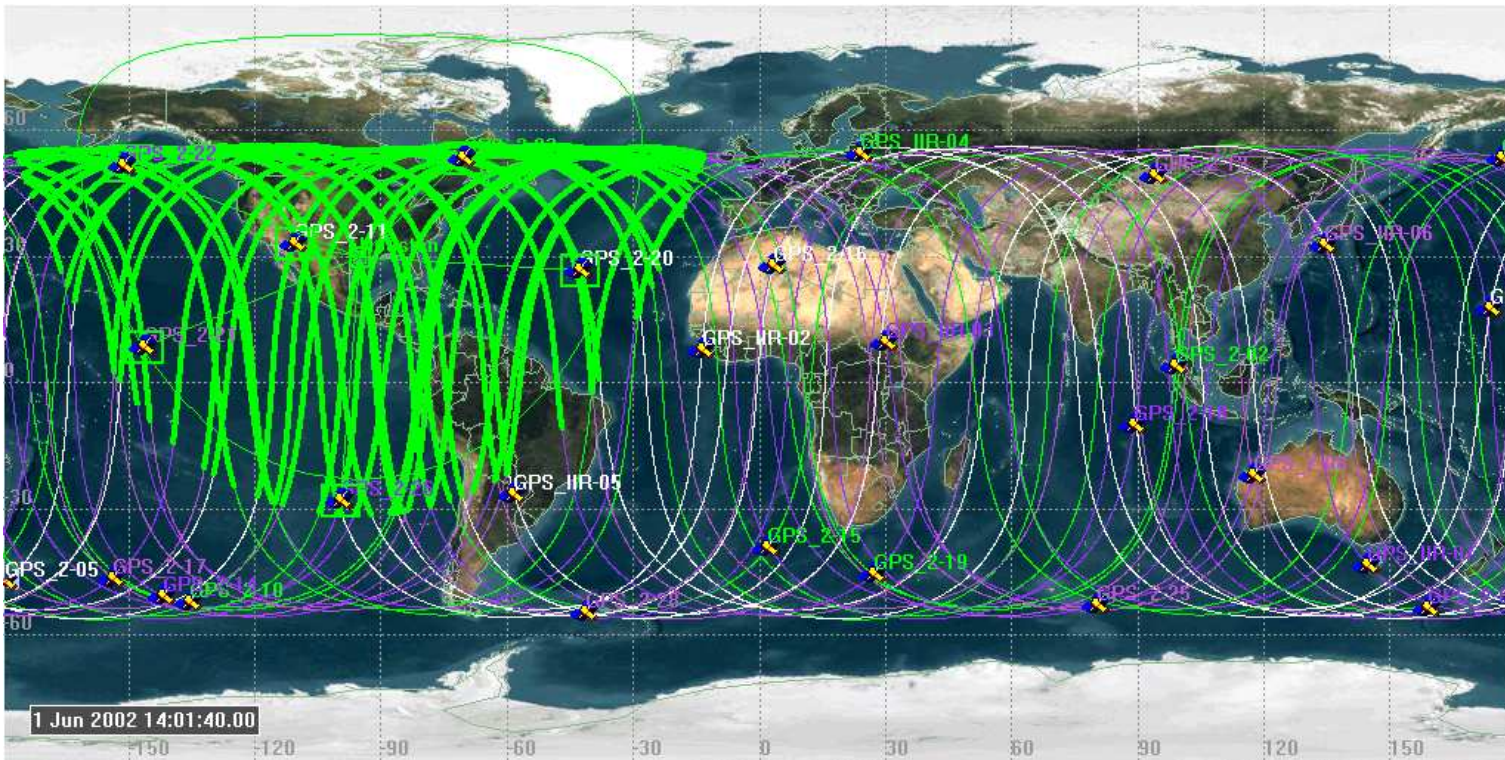


Fig. 5.11. GPS Constellation Simulation Using STK (2-D Map)

where  $n$  denotes the mean motion,  $\mu$  is the earth's gravitational constant,  $a$  is the semi-major axis,  $\dot{\Omega}_E$  is the angular velocity of the earth,  $M$  is the mean anomaly,  $i$  is the inclination,  $\delta i$  is the inclination offset,  $\Omega$  is the right ascension of ascending node, and the subscript  $o$  denotes the value at epoch time  $t_o$ . The WGS84 system values in Table 5.2 are used for the simulation. However, the prediction using almanac data

Table 5.2. WGS84 System Values

Parameters	Values
$\mu$	$3.986005 \times 10^{14} (m^3/s^2)$
$\dot{\Omega}_E$	$7.2921151467 \times 10^{-6} (rad/s)$

provides the GPS satellite positions with less precise data that has the following User Range Error (URE) in Table 5.3 during the operation interval due to perturbation effect. In Table 5.3, the normal and short-term extended operations URE are some

Table 5.3. GPS Almanac Ephemeris URE

Operation Interval	Ephemeris URE STD (m)
Normal	900
Short-term Extended	900 - 3,600
Long-term Extended	3,600 - 300,000

kilometers within approximately 70 hours after the first valid transmission time for this almanac data set. In the following, an example of SEM GPS almanac data is shown. The format of the data is shown in Fig. 5.12 and Table 5.4.

Table 5.4. SEM GPS Almanac Data Format

Number of Records	Title	
GPS Week Number	GPS Time of Applicability	
PRN Number		
SVN Number		
Average URA Number		
Eccentricity	Inclination Offset	Rate of Right Ascension
Square Root of Semi-Major Axis	Longitude of Orbital Plane	Argument of Perigee
Mean Anomaly	Zeroth-Order Clock Correction	First-Order Clock Correction
Satellite Health		
Satellite Configuration		

28 CURRENT.ALM 71 503808

```

1 32 1
0.50687789916992E-0002  0.66165924072266E-0002  -0.24738255888224E-0008
0.51535776367188E+0004  0.18455862998962E-0001  -0.55291974544525E+0000
-0.99051356315613E-0001  0.15926361083984E-0003  0.00000000000000E+0000
0
9

```

Fig. 5.12. SEM GPS Almanac Data

By using these almanac data and Eq. (5.46), the positions of the GPS satellites in the ECEF coordinate system can be computed by the equations given by

$$M = E - e \sin E \quad (5.47a)$$

$$\nu = \tan^{-1} \left\{ \frac{\sqrt{1-e^2} \sin E}{1-e \cos E} \bigg/ \frac{\cos E - e}{1-e \cos E} \right\} \quad (5.47b)$$

$$\Psi = \nu + \omega \quad (5.47c)$$

$$r = a(1 - e \cos E) \quad (5.47d)$$

$$x' = r \cos \Psi \quad (5.47e)$$

$$y' = r \sin \Psi \quad (5.47f)$$

$$x = x' \cos \Omega - y' \cos i \sin \Omega \quad (5.47g)$$

$$y = y' \sin \Omega + y' \cos i \cos \Omega \quad (5.47h)$$

$$z = y' \sin i \quad (5.47i)$$

where the eccentric anomaly  $E$  is obtained by solving the Kepler's equation in Eq. (5.47a),  $\nu$  is the true anomaly,  $\Psi$  is the argument of latitude,  $r$  is the radius,  $x'$  and  $y'$  are the positions in the orbit plane, and  $x$ ,  $y$ , and  $z$  are the positions in the ECEF frame.

## 5.5 Simulation and Result

The 8 hours phase measurement data are generated by using '351.al3' SEM GPS almanac data, three baselines shown in section 5.6, and the phase measurement model is shown in Fig. 5.1. Then, 100 different random attitude matrices and line biases are generated to simulate the phase measurements. Multipath errors are not considered in

the measurement data because the effect of the nearby structure can be compensated before the self survey. The integers are resolved first using the double differences technique. Then, the data to solve the nonlinear least squares are constructed using the available sightlines information. To consider large initial errors, initial Euler angle errors are generated using MATLAB command given by

$$\begin{bmatrix} \delta\phi \\ \delta\theta \\ \delta\psi \end{bmatrix} = 60 \text{ randn}(3, 1) \text{ (Deg)}$$

Both the NLS and LM algorithm are applied for the simulation and compared. Then, the baselines in the body frame and the line biases are determined.

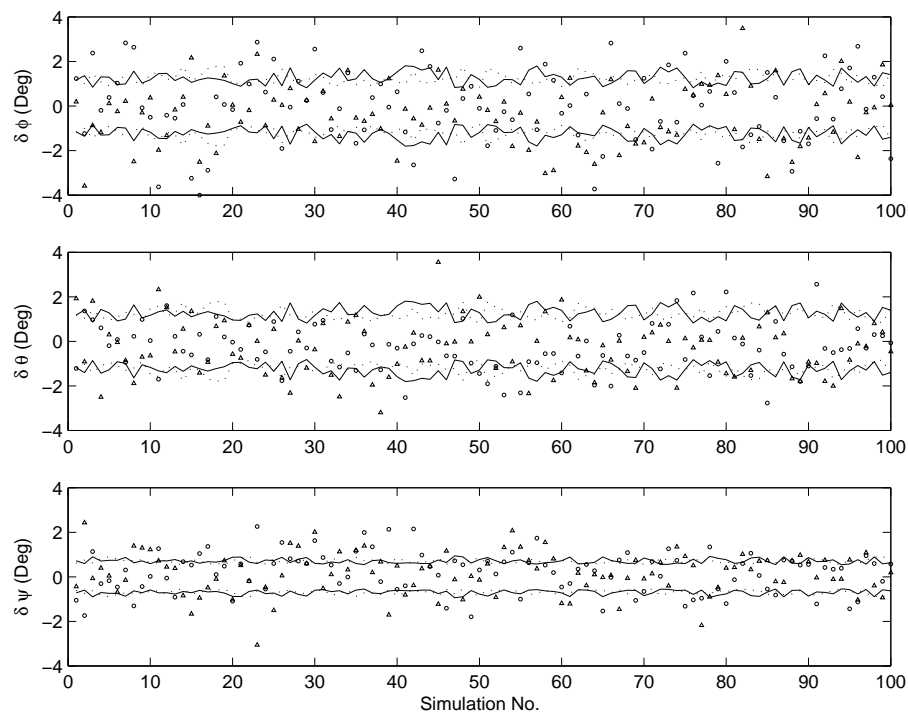


Fig. 5.13. Attitude Error Comparison Between NLS and LM

Figure 5.13 shows the Euler angles errors and their  $3\text{-}\sigma$  boundary layers. The triangle marker represents the NLS Euler angles errors and the circle marker denotes the LM Euler angles errors. As can be seen, both NLS and LM show the same level of estimation errors. For the pitch axis, the errors are well inside the  $3\text{-}\sigma$  boundary layers, however, for other axes some errors are outside the  $3\text{-}\sigma$  bounds. This is because the baselines are nearly coplanar which is aligned with body  $x\text{-}y$  axes. Also, the geometry of the sightlines affects the covariance. Figure 5.14 shows the line bias errors comparison between NLS and LM. As for the errors in the baselines 2 and 3,

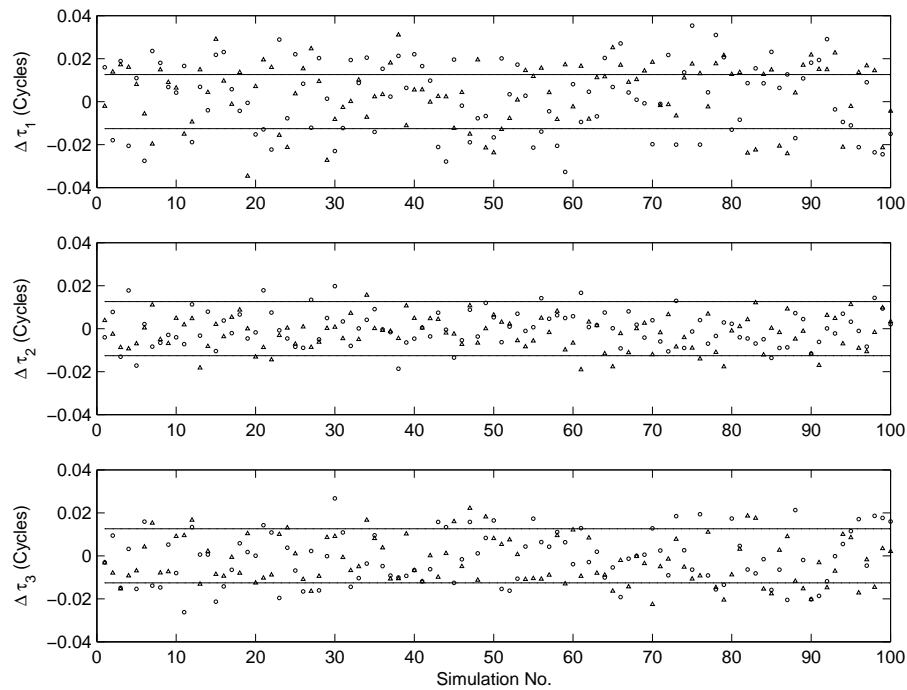


Fig. 5.14. Line Bias Error Comparison Between NLS and LM

the line biases are well below the  $3\text{-}\sigma$  layers. The line bias in the baseline 1 is not, however, it is still below the standard deviation of the phase measurement errors. Also, the baseline 3 estimation errors are shown in Fig. 5.15. As can be seen, all estimation errors are well inside the  $3\text{-}\sigma$  bounds.

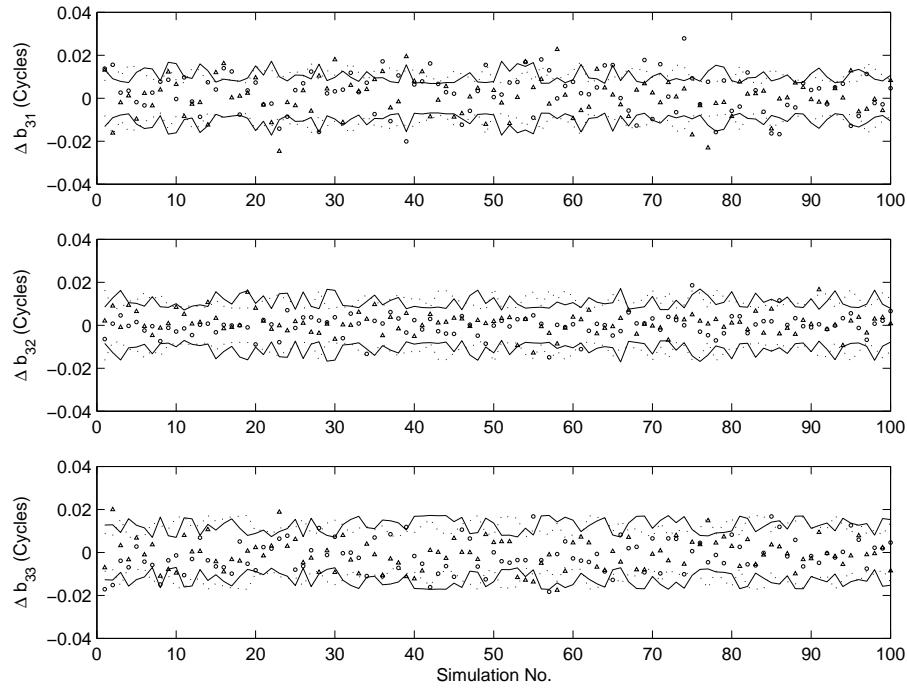


Fig. 5.15. Baseline Error Comparison Between NLS and LM

In the comparison of nonlinear estimation errors, there is no difference between NLS and LM for small initial errors. The NLS converges faster than LM, however, the convergence to the correct estimate is not guaranteed. In the comparison using large initial attitude error, the NLS fails two times out of 100 simulations while the LM method works successfully. A comparison of the number of iterations is shown in Fig. 5.16. In general, the number of iterations of the LM algorithm is larger than that of NLS, however, it guarantees the correct convergence. Also, the convergence speed of the LM method can be enhanced by taking smaller  $\eta$  values.

In the simulation study, the convergence performance of LM for relatively larger initial errors seems to be improved over NLS. To compare the convergence behaviour of LM and NLS, large initial errors are considered as

$$\begin{bmatrix} \delta\phi \\ \delta\theta \\ \delta\psi \end{bmatrix} = \begin{bmatrix} -106.07^\circ \\ 73.247^\circ \\ 153.15^\circ \end{bmatrix}, \quad \begin{bmatrix} \Delta\tau_1 \\ \Delta\tau_2 \\ \Delta\tau_3 \end{bmatrix} = \begin{bmatrix} .0547 \\ 0.9129 \\ 0.5019 \end{bmatrix} \quad (\text{Cycles})$$

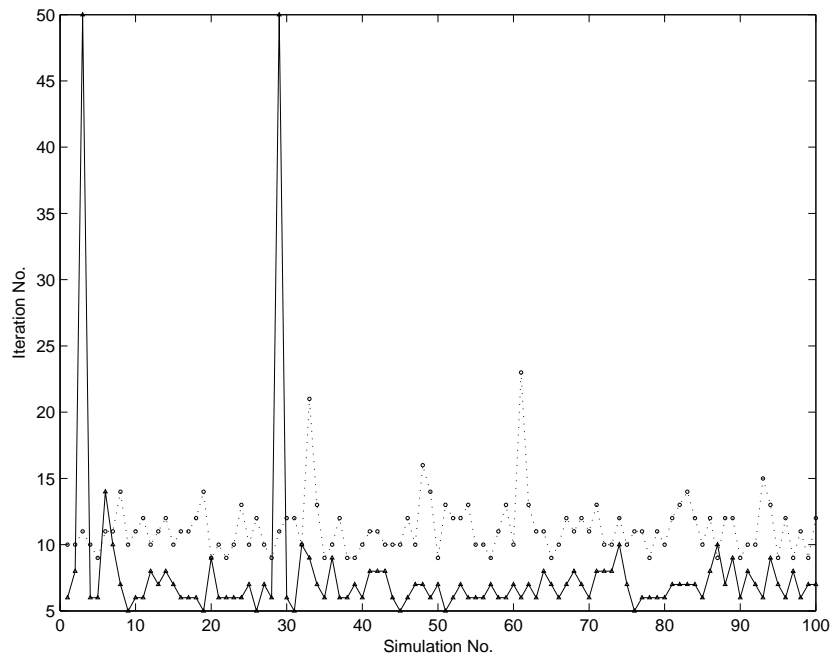


Fig. 5.16. Iteration Number Comparison Between NLS and LM

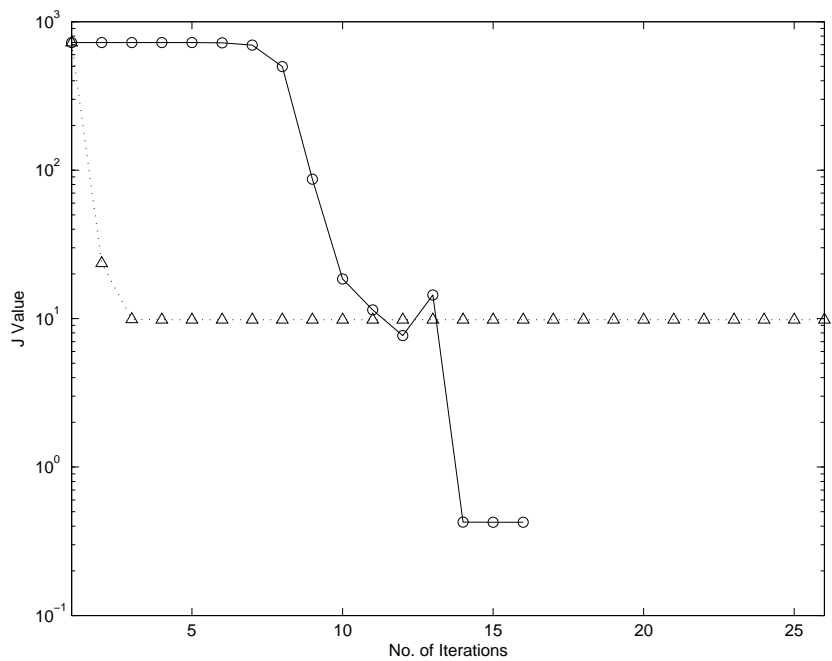


Fig. 5.17. Convergence Comparison Between NLS and LM

Then, the convergence of NLS and LM is compared in Fig. 5.17. As can be seen, the NLS converges faster but leads to wrong estimates. However, the LM algorithm converges to the correct estimates after 16 iterations.

## 5.6 Real Data Application

The self survey algorithm is applied with real data collected by Navigation Systems and Technology Laboratory (NSTL) at NASA's Johnson Space Center (JSC) in Houston, Texas. The Trimble Advanced Navigation System (TANS) Vector receiver with a four antenna set is used for the test. To mitigate the multipath error, the antennas are installed on the roof of a building. Since the Vector receiver provides an internal self survey result, the estimates of the baselines and line biases are also compared.

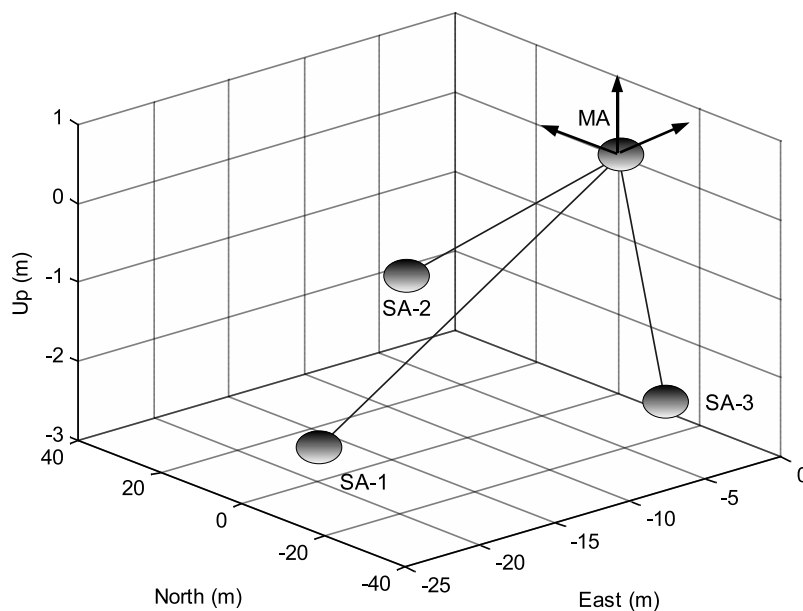


Fig. 5.18. Baselines in the ENU Coordinate System



The baselines in the East-North-Up (ENU) coordinate system shown in Fig. 5.18 are given by

$$[{}^g\mathbf{b}_1 \ {}^g\mathbf{b}_2 \ {}^g\mathbf{b}_3] = \begin{bmatrix} -115.91775 & -42.66246 & -20.74898 \\ -45.57186 & 114.46932 & -135.93129 \\ -11.68865 & -7.79448 & -12.01909 \end{bmatrix} \quad (\text{Cycles})$$

Although the baselines between geometric centers are not known, the TANS Vector receiver baselines output can be used as  ${}^g\mathbf{b}$ . The phase measurements of TANS Vector receiver have a range of  $-32 \sim 32$  cycles. Since the lengths of baselines are longer than 32 cycles, the phase measurement jumps to  $-32$  cycles when it reaches 32 cycles or vice versa. Thus, jumps of 64 cycles need to be compensated. Also, the cycle slips are detected and repaired by the algorithm described in subsection 5.3.1. Nonlinear least squares converges after 9 iterations. The value of  $\Delta J$  after each iteration is shown in Table 5.5.

Table 5.5. Convergence of Nonlinear Least Squares

Iteration	$J$	$\Delta J$
1	2.6512e+007	2.6512e+007
2	1.0413e+007	1.6098e+007
3	4.8126e+006	5.6007e+006
4	8.0795e+004	4.7318e+006
5	9.0319e+003	7.1763e+004
6	1.4622e+002	8.8857e+003
7	6.9967e-001	1.4552e+002
8	6.9942e-001	2.5235e-004
9	6.9942e-001	7.2299e-011

Figure 5.19 shows single differenced phase measurements data collected by the TANS Vector GPS receiver after integer ambiguity and cycle slip compensation. The re-

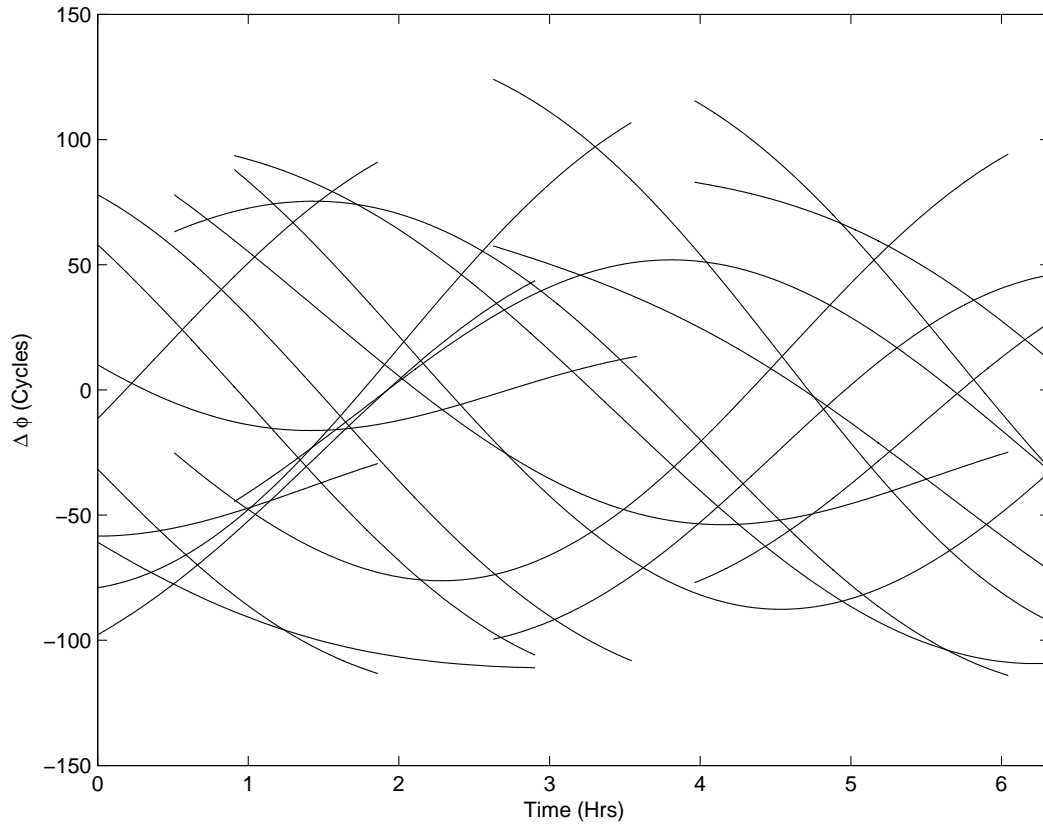


Fig. 5.19. TANS Vector GPS Receiver Phase Measurements

solved integer ambiguities are shown in Table 5.6 and the differences in the baseline estimates are determined as

$$[\Delta \mathbf{b}_1, \Delta \mathbf{b}_2, \Delta \mathbf{b}_3] = \begin{bmatrix} 0.0147 & -0.0059 & -0.0029 \\ -0.0005 & 0.0042 & 0.0098 \\ -0.0171 & -0.0125 & -0.0188 \end{bmatrix} \text{ (Cycles)}$$

The differences are well below the standard deviation of the phase measurements. The line bias estimates are compared with the TANS Vector receiver output in Table 5.7. The differences are less than 0.05 cycles.

Table 5.6. Integer Ambiguities

	$s_2$	$s_4$	$s_7$	$s_8$	$s_{11}$	$s_{19}$	$s_{24}$
$\mathbf{b}_1$	-73	-46	-114	-24	58	56	-81
$\mathbf{b}_2$	-80	88	70	-87	94	9	73
$\mathbf{b}_3$	46	-147	-118	80	-63	33	-116

Table 5.7. Line Biases (Unit: Cycles)

Line Biases	Self Survey	TANS Receiver
$\tau_1$	0.2637	0.2240
$\tau_2$	0.9367	0.8954
$\tau_3$	0.3056	0.3196

The attitude matrix is given by

$$\mathbf{A} = \begin{bmatrix} -0.0003 & -0.6662 & 0.7457 \\ -0.2844 & 0.7150 & 0.6387 \\ -0.9587 & -0.2119 & -0.1897 \end{bmatrix}$$

By using the estimated baselines, line biases, and attitude matrix the single differenced phases are computed and compared with the measurement data. Figures 5.20 through 5.26 show the residual error between the measured and the estimated phase. Since the multi-path errors exist in the measurement, oscillations are shown in the residual error. Also, the residual errors are increased both in the early part and in the end data. However, in the other regions the residual errors are below the measurement standard deviation.

Figure 5.20 shows the residual errors for the PRN 2 signal phase. The residuals between 100 and 300 minutes are well below than the standard deviation while the residuals before 80 minutes and after 300 minutes begin to increase. Similar trends are shown for the PRN 4, 7, 8, and 24 signal phases in Figs. 5.21, 5.22, 5.23, and 5.26. However, as can be seen in Figs. 5.24 and 5.25, the signal phases are different for PRN 11 and 19. There exist oscillations in the residual since the multipath errors are contained in the measurements.

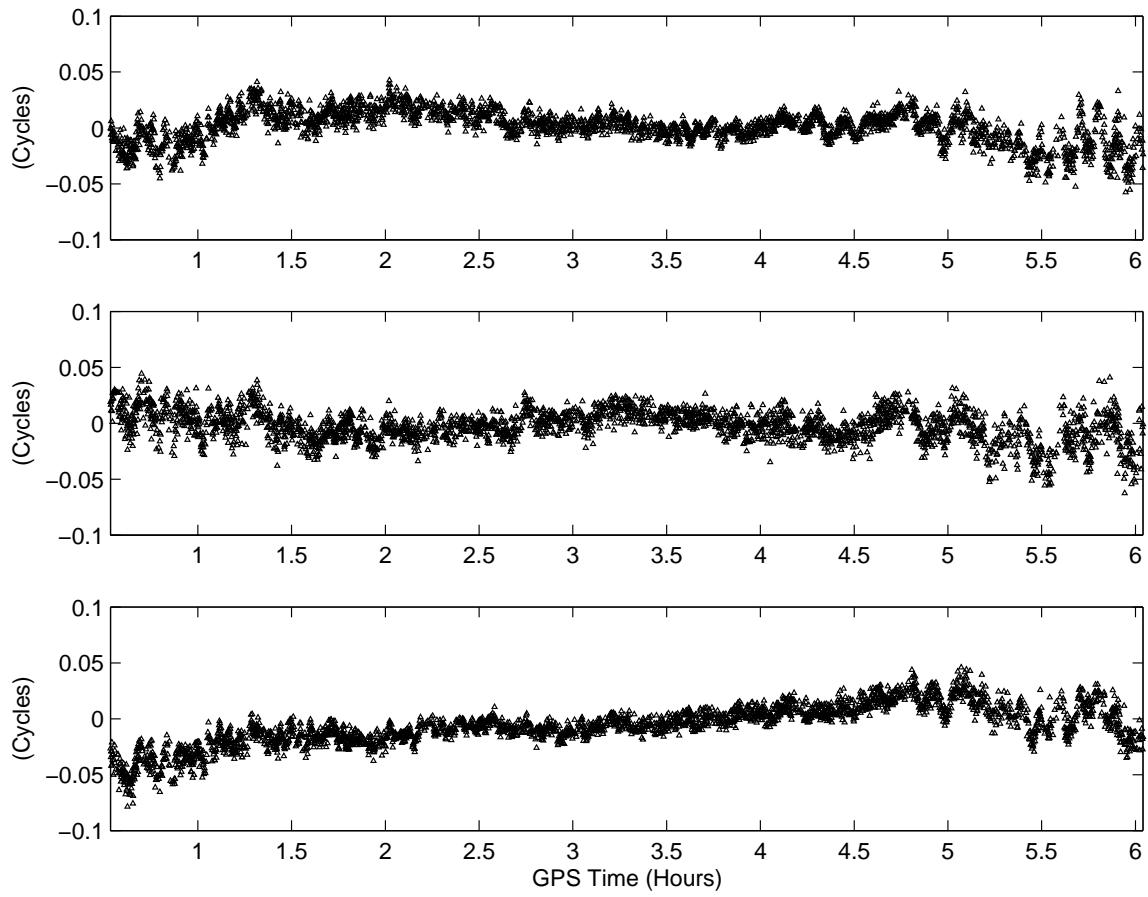


Fig. 5.20. The Residual Error of  $\widetilde{\Delta\phi}_{i2} - \Delta\phi_{i2}$  for  $i = 1, 2, 3$

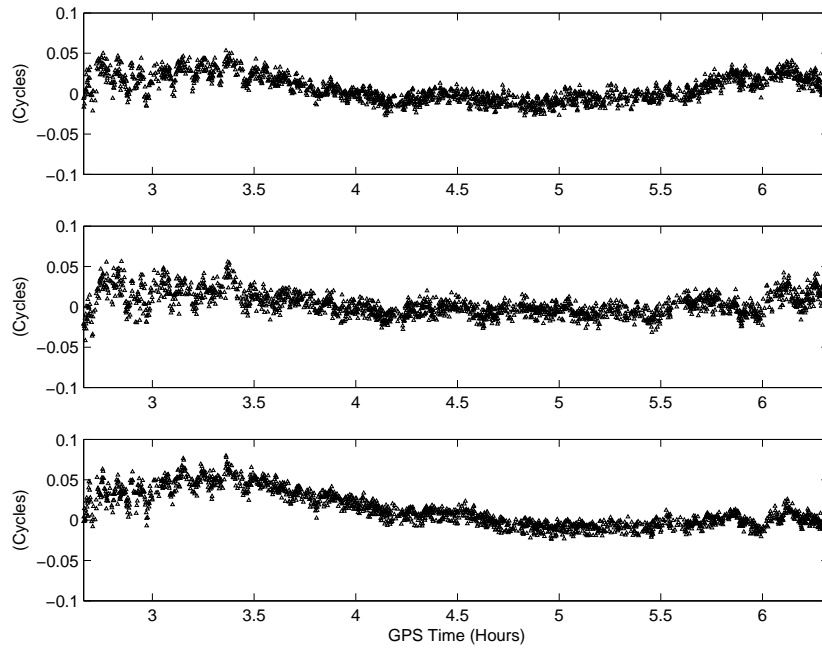


Fig. 5.21. The Residual Error of  $\widetilde{\Delta\phi}_{i4} - \Delta\phi_{i4}$  for  $i = 1, 2, 3$

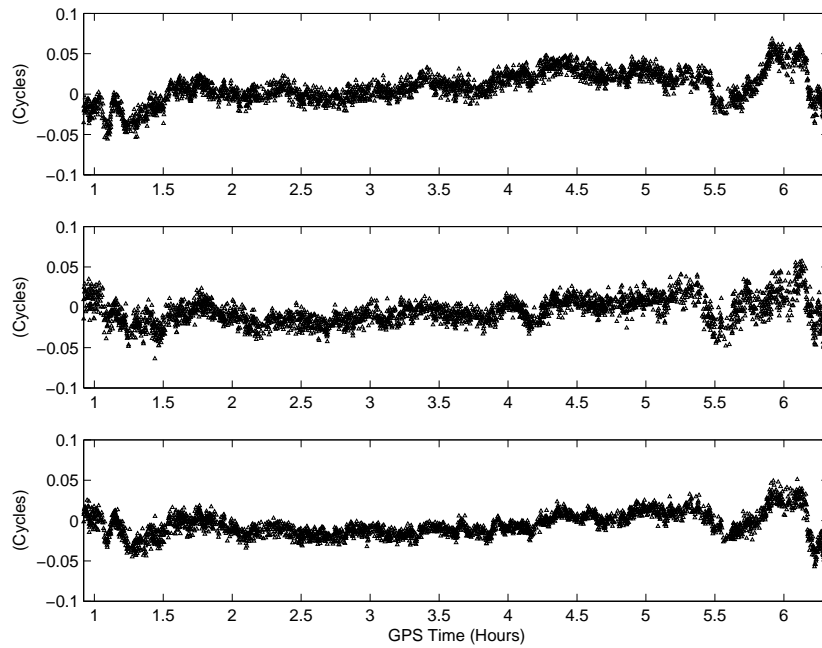


Fig. 5.22. The Residual Error of  $\widetilde{\Delta\phi}_{i7} - \Delta\phi_{i7}$  for  $i = 1, 2, 3$

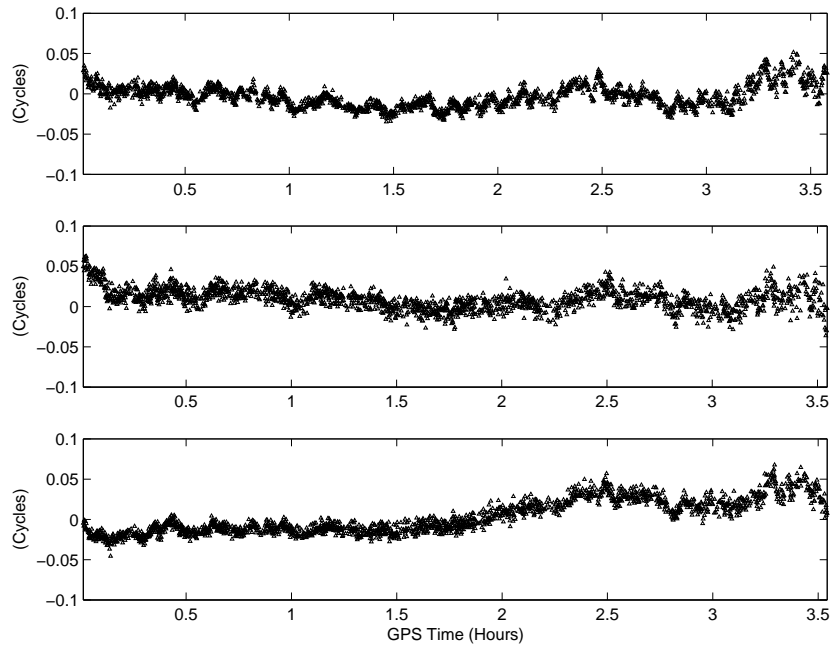


Fig. 5.23. The Residual Error of  $\widetilde{\Delta\phi}_{i8} - \Delta\phi_{i8}$  for  $i = 1, 2, 3$

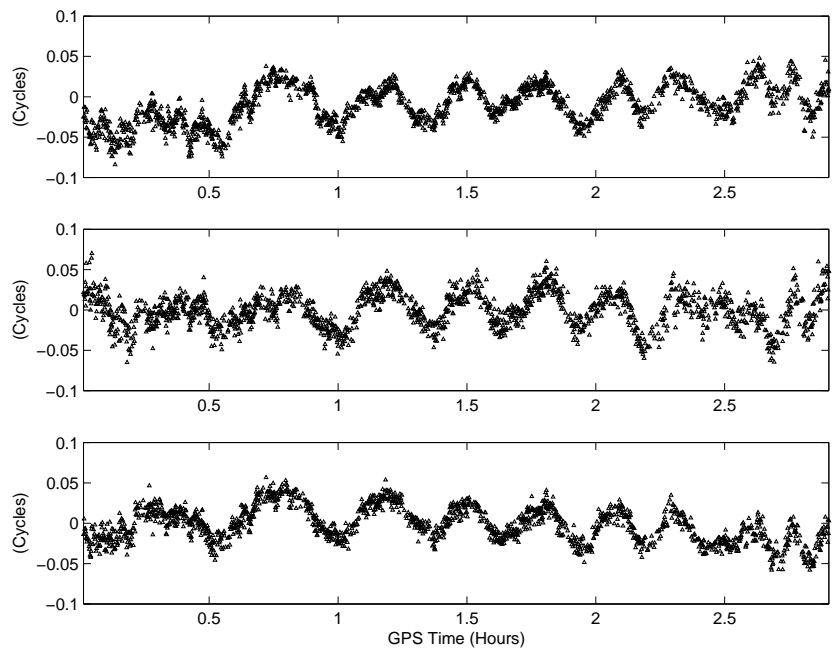


Fig. 5.24. The Residual Error of  $\widetilde{\Delta\phi}_{i11} - \Delta\phi_{i11}$  for  $i = 1, 2, 3$

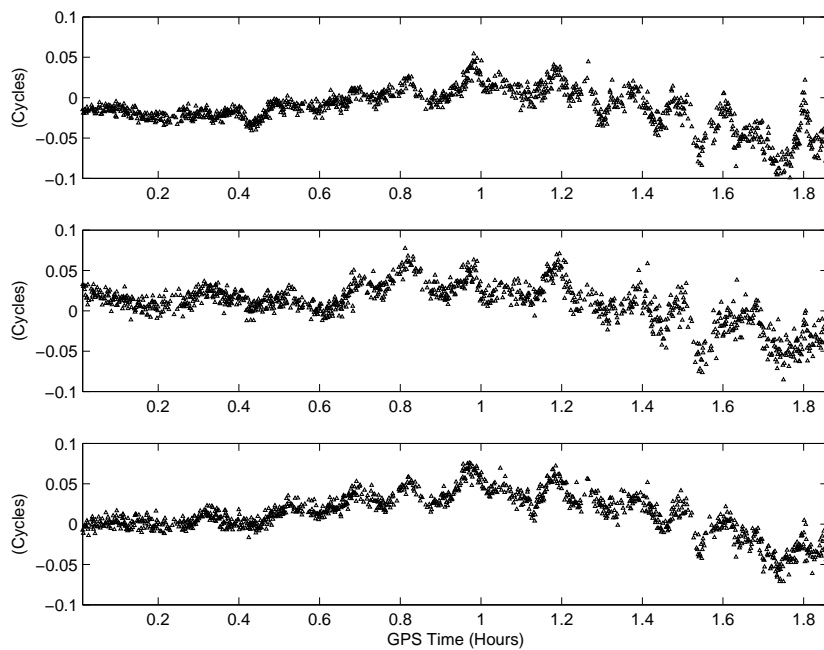


Fig. 5.25. The Residual Error of  $\widetilde{\Delta\phi}_{i19} - \Delta\phi_{i19}$  for  $i = 1, 2, 3$

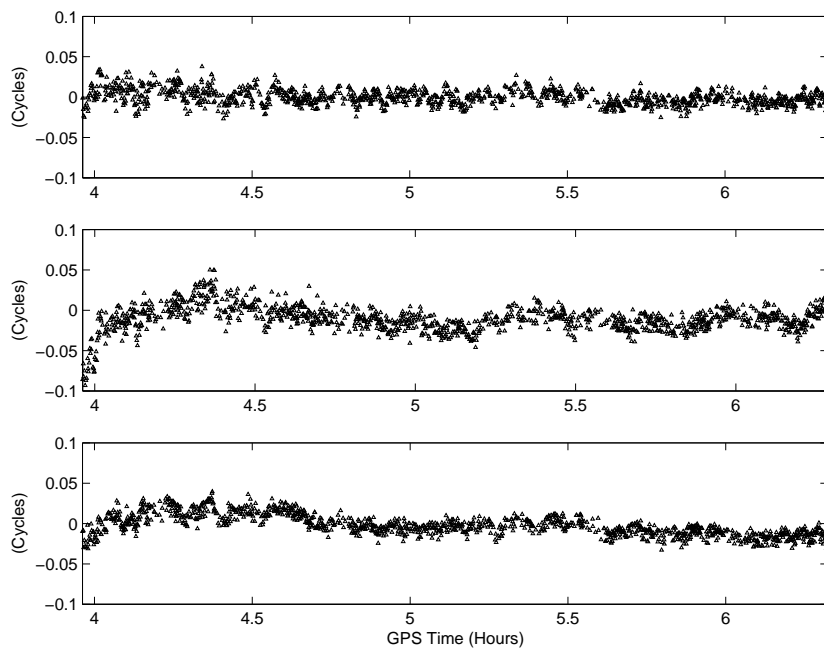


Fig. 5.26. The Residual Error of  $\widetilde{\Delta\phi}_{i24} - \Delta\phi_{i24}$  for  $i = 1, 2, 3$

## 5.7 Summary

A new self survey method has been developed and compared with a commercial GPS receiver self survey result. The new method includes cycle slip detection and a repair algorithm to compensate the cycle counter re-initialization problem when the GPS signal lock is lost. Also, it includes a double differences scheme to resolve integer ambiguities for the case that line biases errors are contained in the measurements.

For the cycle slip detection and repair, a first-order polynomial fit is used for the early data since frequent signal lock loss has occurred. Then, after 30 minutes an 8-th order polynomial replaces it because sightlines are moving. To verify algorithms, real data collected by TANS Vector GPS receiver is used for the cycle slip detection and repair algorithm. Integer ambiguity resolution using double differenced phase measurements was then accomplished. Then, nonlinear least squares and the Levenberg-Marquardt algorithm are used to determine attitude parameters. Finally, baselines in the body frame and line biases have been determined.

In the comparison of NLS and LM using 100 simulations with random initial conditions, the LM method shows more robust results for large initial errors, although the convergence speed of NLS is faster than that of LM. In the comparison with the TANS Vector receiver self survey output, the integer ambiguities matched exactly. Also, line biases and baselines differences were within  $3\text{-}\sigma$  error bounds.



## CHAPTER VI

## PSEUDOLITE SIGNALS APPLICATION

In this chapter the attitude determination algorithms using Pseudolite signals are developed and analyzed through various simulations.

## 6.1 Problem Statement

Pseudo-GPS-satellites, the Pseudolite (PL), signals are essentially the same as GPS signals.<sup>53,67,69,84,99-103</sup> The main purpose of using PL signals is to replace the GPS signals when the GPS signals are blocked by the nearby huge structures, or to enhance the positioning accuracy. Pseudolites are also used to determine relative attitude and positions. When the PL signals are used, the phase measurement model should be modified because the PL signal transceivers (TXs) are located too close to antennas so that the planar assumption does not hold. Since the relative distances between antennas and PL TXs are short, sightlines are no longer assumed as parallel. For PL signals, the wavefronts are spherical.<sup>53,79,80,104</sup> The new phase measurement model is shown in Fig. 6.1. Two coordinate systems, one is the reference coordinate system and the other is the body fixed coordinate system, are used to define the attitude. As can be seen in Fig. 6.1, the phase measurement contains the nonlinear spherical wavefront effect. This spherical phase difference measurement can be expressed by<sup>53,79,80,104</sup>

$$\Delta\phi = \frac{|\mathbf{r} + \mathbf{A}^T \mathbf{b}_m - \mathbf{t}| - |\mathbf{r} + \mathbf{A}^T \mathbf{b}_s - \mathbf{t}|}{\lambda} + n + \tau \quad (6.1)$$

where  $\mathbf{A}$  is the attitude matrix, which transforms coordinates from the reference frame to body frame,  $n$  is the integer ambiguity,  $\tau$  is the line bias error,  $\lambda$  is the wavelength,  $\mathbf{t}$  is the position vector of a PL TX in the reference frame,  $\mathbf{r}$  is the position vector of the body frame origin in the reference frame,  $\mathbf{b}_m$  is the position vector of the MA in the body frame, and  $\mathbf{b}_s$  is the position vector of the SA in the body fixed frame.

By using the self survey in Chapter V, it is assumed that the baselines, line

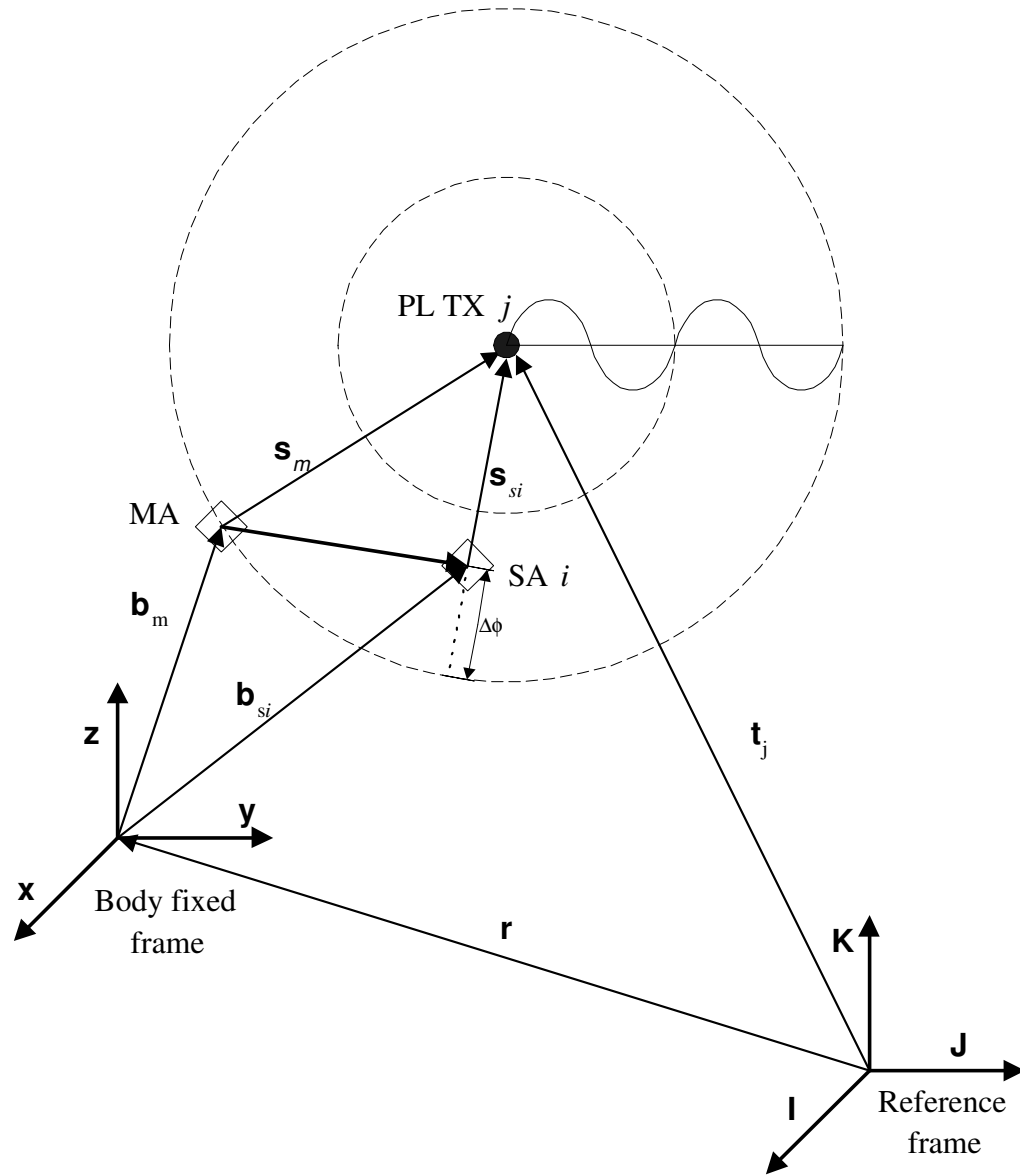


Fig. 6.1. Non-Planar Pseudolite Carrier Phase Measurement Model

biases, and integer ambiguities are already determined. Therefore, the attitude determination is a nonlinear estimation problem to estimate the attitude parameters of the attitude matrix  $\mathbf{A}$ . With the vector form implementation, Eq. (6.1) can be rewritten as

$$\Delta\phi_{ij} = \frac{|\mathbf{r} + \mathbf{A}^\top \mathbf{b}_m - \mathbf{t}_j| - |\mathbf{r} + \mathbf{A}^\top \mathbf{b}_{s_i} - \mathbf{t}_j|}{\lambda} + n_{ij} + \tau_i \quad (6.2)$$

where  $i$  denotes the  $i$ -th SA, and  $j$  denotes the  $j$ -th PL TX.

## 6.2 Previous Work

The most widely used attitude determination techniques using LOS vector measurements are methods to solve the Wahba's problem. Although the phase measurements are not a LOS vector, a modified Wahba's problem was posed by Crassidis et al. They also found a suboptimal attitude solution.<sup>6,50,51,53</sup> Nonlinear least squares or gradient-based search techniques can solve for the optimal attitude by minimizing a certain loss function. However, these methods are not computationally efficient because they are iterative. Also, convergence is not guaranteed if the initial errors are large. Thus, a predictive filter, called ALLEGRO, using standard GPS signals was developed by Crassidis,<sup>30,48,49,52</sup> which is non-iterative. Then, a new predictive filter using PL signals was developed by Park and Crassidis.<sup>53</sup>

## 6.3 New Approach

Since the Pseudolite signals are used, the sightlines are no longer parallel. Therefore, the ALLEGRO algorithm cannot be applied directly. However, only minor changes on a measurement model make ALLEGRO work for Pseudolite cases. Based on the new phase measurement model shown in Eq. (6.2) and Fig. 6.1, the new predictive filter is derived. To verify the new filter, two types of simulation cases are shown, since the implementation of the static and moving cases is different.

For the static case, a comparison with the result using nonlinear least squares as well as the LM method is presented. For moving cases, only the result of the new filter

is presented because it is impossible to apply iterative methods. A more enhanced attitude estimation can be obtained by combining the system dynamics with the PL signal measurements. The EKF and UF using Pseudolite signals are developed and compared with simulations.

## 6.4 Implementation

By using the Pseudolite signal measurement model, the attitude estimation algorithms are developed in this section.

### 6.4.1 Nonlinear Least Squares

A nonlinear least squares using the quaternion is developed. The estimated attitude matrix can be written by

$$\mathbf{A}(\hat{\mathbf{q}}) = \mathbf{A}(\delta\mathbf{q}) \mathbf{A}(\mathbf{q}) \quad (6.3)$$

where  $\hat{\mathbf{q}}$  represented the estimated quaternion,  $\delta\mathbf{q}$  is the error quaternion, and  $\mathbf{q}$  is the true quaternion. In the small angle approximation,  $\mathbf{A}(\delta\mathbf{q})$  can be rewritten as

$$\mathbf{A}(\delta\mathbf{q}) = \mathbf{I} - 2[\delta\mathbf{q}_{13}\times] \quad (6.4)$$

Then, the PL signal phase measurement model in Eq. (6.2) can be approximated as

$$\begin{aligned} \Delta\hat{\phi}_{ij} &= \frac{1}{\lambda} (|\mathbf{r} + \mathbf{A}^\top \mathbf{b}_m - \mathbf{t}_j| - |\mathbf{r} + \mathbf{A}^\top \mathbf{b}_{s_i} - \mathbf{t}_j|) + n_{ij} + \tau_i \\ &\approx \frac{1}{\lambda} \left[ |\mathbf{r} + \mathbf{A}^\top(\mathbf{q})(\mathbf{I} + 2[\delta\mathbf{q}\times])\mathbf{b}_m - \mathbf{t}_j| \right. \\ &\quad \left. - |\mathbf{r} + \mathbf{A}^\top(\mathbf{q})(\mathbf{I} + 2[\delta\mathbf{q}\times])\mathbf{b}_{s_i} - \mathbf{t}_j| \right] + n_{ij} + \tau_i \\ &\approx \frac{1}{\lambda} \left[ \sqrt{\ell_m - 4(\mathbf{r} + \mathbf{A}^\top(\mathbf{q})\mathbf{b}_m - \mathbf{t}_j)^\top \mathbf{A}^\top(\mathbf{q})[\mathbf{b}_m\times]\delta\mathbf{q}} \right. \\ &\quad \left. - \sqrt{\ell_{s_i} - 4(\mathbf{r} + \mathbf{A}^\top(\mathbf{q})\mathbf{b}_{s_i} - \mathbf{t}_j)^\top \mathbf{A}^\top(\mathbf{q})[\mathbf{b}_{s_i}\times]\delta\mathbf{q}} \right] + n_{ij} + \tau_i \\ &\approx \frac{1}{\lambda} \left[ \sqrt{\ell_m} \left\{ 1 - \frac{2(\mathbf{r} + \mathbf{A}^\top(\mathbf{q})\mathbf{b}_m - \mathbf{t}_j)^\top \mathbf{A}^\top(\mathbf{q})[\mathbf{b}_m\times]\delta\mathbf{q}}{\ell_m} \right\} \right. \\ &\quad \left. - \sqrt{\ell_{s_i}} \left\{ 1 - \frac{2(\mathbf{r} + \mathbf{A}^\top(\mathbf{q})\mathbf{b}_{s_i} - \mathbf{t}_j)^\top \mathbf{A}^\top(\mathbf{q})[\mathbf{b}_{s_i}\times]\delta\mathbf{q}}{\ell_{s_i}} \right\} \right] + n_{ij} + \tau_i \end{aligned} \quad (6.5)$$

where

$$\ell_m = (\mathbf{r} + \mathbf{A}^\top(\mathbf{q})\mathbf{b}_m - \mathbf{t}_j)^\top (\mathbf{r} + \mathbf{A}^\top(\mathbf{q})\mathbf{b}_m - \mathbf{t}_j) \quad (6.6a)$$

$$\ell_{s_i} = (\mathbf{r} + \mathbf{A}^\top(\mathbf{q}) \mathbf{b}_{s_i} - \mathbf{t}_j)^\top (\mathbf{r} + \mathbf{A}^\top(\mathbf{q}) \mathbf{b}_{s_i} - \mathbf{t}_j) \quad (6.6b)$$

Thus, the Jacobian matrix is given by

$$\begin{aligned} \mathbf{H}_{ij} &= \frac{\partial \Delta \hat{\phi}_{ij}}{\partial \delta \mathbf{q}_{13}} \\ &\approx -\frac{2}{\lambda} \left\{ \frac{(\mathbf{r} + \mathbf{A}^\top(\mathbf{q}) \mathbf{b}_m - \mathbf{t}_j)^\top \mathbf{A}^\top(\mathbf{q}) [\mathbf{b}_m \times]}{\sqrt{\ell_m}} - \frac{(\mathbf{r} + \mathbf{A}^\top(\mathbf{q}) \mathbf{b}_{s_i} - \mathbf{t}_j)^\top \mathbf{A}^\top(\mathbf{q}) [\mathbf{b}_{s_i} \times]}{\sqrt{\ell_{s_i}}} \right\} \end{aligned} \quad (6.7)$$

To compute the attitude covariance matrix, the Fisher information matrix is determined by

$$\begin{aligned} \mathbf{F} &\equiv \frac{1}{4} E \left\{ \frac{\partial J}{\partial \mathbf{q}_{13}} \frac{\partial J}{\partial \mathbf{q}_{13}}^\top \right\} \\ &= \frac{1}{4} \sum_{i=1}^m \sum_{j=1}^n \sigma_{ij}^{-2} \mathbf{H}_{ij}^\top \mathbf{H}_{ij} \end{aligned} \quad (6.8)$$

where the division by a factor of 4 is required because quaternion errors are two times the Euler angle errors and the loss function is defined by

$$J = \frac{1}{2} \sum_{i=1}^m \sum_{j=1}^n \sigma_{ij}^{-2} \left( \Delta \tilde{\phi}_{ij} - \Delta \phi_{ij} \right)^2 \quad (6.9)$$

where  $m$  represents the number of baselines,  $n$  represents the number of sightlines, and  $\sigma_{ij}$  denotes the standard deviation of the  $ij$ -th measurement error. Then, the attitude error covariance matrix is obtained by

$$\begin{aligned} \mathbf{P} &\equiv \mathbf{F}^{-1} \\ &= 4 \left[ \sum_{i=1}^m \sum_{j=1}^n \sigma_{ij}^{-2} \mathbf{H}_{ij}^\top \mathbf{H}_{ij} \right]^{-1} \end{aligned} \quad (6.10)$$

#### 6.4.2 Levenberg-Marquardt Method

As can be seen in section 5.5, the LM method is more robust than NLS for large initial errors. However, after the first estimation time the current estimates will be good guesses at the next estimation time. Therefore, the NLS algorithm is used after the first estimation time because it is faster than LM method.

#### 6.4.3 Nonlinear Predictive Filter

An algorithm using nonlinear predictive filtering from GPS signals was proposed by Crassidis et al.<sup>48,49,52</sup> This algorithm is called the Attitude Lean Loping Estimator

using GPS Recursive Operations (ALLEGRO). In the ALLEGRO algorithm, the model is assumed as the quaternion kinematics model. Also, the attitude rate is adequately modeled by a constant model error  $\mathbf{d}$  between measurements, so that the Eq. (2.37) can be written as

$$\dot{\hat{\mathbf{q}}} = \frac{1}{2} \Xi(\hat{\mathbf{q}}) \mathbf{d} \quad (6.11)$$

where  $\hat{\mathbf{q}}$  denotes the estimated quaternion. Then, the lowest order time derivative of  $\hat{\mathbf{q}}$  in Eq. (6.11) in which any component of  $\mathbf{d}$  first appears is one, so that  $p_i = 1$ . By using the model in Eq. (6.11) and the GPS signal phase measurement model in Eq. (5.1), the optimal model error is found. Therefore, the attitude parameter, i.e. the quaternion, is determined without using angular rate information.

In this section, a predictive filter using the Pseudolite signal observation model in Eq. (6.2) is developed. The only difference from ALLEGRO is that the Pseudolite signal observation model contains the nonplanar effect of the carrier wavefronts. To derive the  $\mathbf{S}(\hat{\mathbf{q}})$  matrix in Eq. (2.38), the following matrix is defined

$$\mathbf{\Gamma}(\mathbf{b}) \equiv \begin{bmatrix} -[\mathbf{b} \times] & \vdots & -\mathbf{b} \\ \cdots & \cdots & \cdots \\ \mathbf{b}^\top & \vdots & 0 \end{bmatrix} \quad (6.12)$$

where  $\mathbf{b}$  is a 3-dimensional vector. Another useful properties between quaternions and 3-dimensional vectors are given by

$$\mathbf{\Omega}(\mathbf{a}) \mathbf{q} = \Xi(\mathbf{q}) \mathbf{a} \quad (6.13a)$$

$$\mathbf{\Gamma}(\mathbf{b}) \mathbf{q} = \Psi(\mathbf{q}) \mathbf{b} \quad (6.13b)$$

where  $\mathbf{a}$  is a 3-dimensional vector,  $\mathbf{q}$  is a quaternion, and matrices  $\Xi$  and  $\Psi$  are defined in Eq. (3.7). Substituting Eqs. (6.12), (6.13), (3.6), and Eq. (3.14) into Eq. (6.2) yields

$$\begin{aligned} c_{ij}[\hat{\mathbf{x}}(t), t] &= \frac{\sqrt{(\mathbf{r} + \mathbf{A}^\top(\hat{\mathbf{q}})\mathbf{b}_m - \mathbf{t}_j)^\top (\mathbf{r} + \mathbf{A}^\top(\hat{\mathbf{q}})\mathbf{b}_m - \mathbf{t}_j)} - \sqrt{(\mathbf{r} + \mathbf{A}^\top(\hat{\mathbf{q}})\mathbf{b}_{s_i} - \mathbf{t}_j)^\top (\mathbf{r} + \mathbf{A}^\top(\hat{\mathbf{q}})\mathbf{b}_{s_i} - \mathbf{t}_j)}}{\lambda} \\ &= \frac{\sqrt{\ell + \mathbf{b}_m^\top \mathbf{b}_m - 2\hat{\mathbf{q}}^\top \mathbf{\Omega}(\mathbf{b}_m) \mathbf{\Gamma}(\mathbf{t}_j - \mathbf{r}) \hat{\mathbf{q}}} - \sqrt{\ell + \mathbf{b}_{s_i}^\top \mathbf{b}_{s_i} - 2\hat{\mathbf{q}}^\top \mathbf{\Omega}(\mathbf{b}_{s_i}) \mathbf{\Gamma}(\mathbf{t}_j - \mathbf{r}) \hat{\mathbf{q}}}}{\lambda} \end{aligned} \quad (6.14)$$

where  $\ell = \mathbf{r}^\top \mathbf{r} - 2\mathbf{r}^\top \mathbf{t}_j + \mathbf{t}_j^\top \mathbf{t}_j$ . The  $\mathbf{S}(\hat{\mathbf{q}})$  matrix is formed by taking the partial derivative of Eq. (6.14) with respect to  $\hat{\mathbf{q}}$  and right-multiplying by  $\frac{1}{2}\Xi(\hat{\mathbf{q}})$ . Therefore, we have

$$\mathbf{S}(\hat{\mathbf{q}}) = \frac{1}{2\lambda} \begin{bmatrix} \frac{\hat{\mathbf{q}}^\top [\Omega(\mathbf{b}_{s_1})\Gamma(\mathbf{t}_1 - \mathbf{r}) + \Gamma(\mathbf{t}_1 - \mathbf{r})\Omega(\mathbf{b}_{s_1})]}{\sqrt{\ell + \mathbf{b}_{s_1}^\top \mathbf{b}_{s_1} - 2\hat{\mathbf{q}}^\top \Omega(\mathbf{b}_{s_1})\Gamma(\mathbf{t}_1 - \mathbf{r})\hat{\mathbf{q}}}} & - \frac{\hat{\mathbf{q}}^\top [\Omega(\mathbf{b}_m)\Gamma(\mathbf{t}_1 - \mathbf{r}) + \Gamma(\mathbf{t}_1 - \mathbf{r})\Omega(\mathbf{b}_m)]}{\sqrt{\ell + \mathbf{b}_m^\top \mathbf{b}_m - 2\hat{\mathbf{q}}^\top \Omega(\mathbf{b}_m)\Gamma(\mathbf{t}_1 - \mathbf{r})\hat{\mathbf{q}}}} \\ \vdots & \vdots \\ \frac{\hat{\mathbf{q}}^\top [\Omega(\mathbf{b}_{s_m})\Gamma(\mathbf{t}_n - \mathbf{r}) + \Gamma(\mathbf{t}_n - \mathbf{r})\Omega(\mathbf{b}_{s_m})]}{\sqrt{\ell + \mathbf{b}_{s_m}^\top \mathbf{b}_{s_m} - 2\hat{\mathbf{q}}^\top \Omega(\mathbf{b}_{s_m})\Gamma(\mathbf{t}_n - \mathbf{r})\hat{\mathbf{q}}}} & - \frac{\hat{\mathbf{q}}^\top [\Omega(\mathbf{b}_m)\Gamma(\mathbf{t}_n - \mathbf{r}) + \Gamma(\mathbf{t}_n - \mathbf{r})\Omega(\mathbf{b}_m)]}{\sqrt{\ell + \mathbf{b}_m^\top \mathbf{b}_m - 2\hat{\mathbf{q}}^\top \Omega(\mathbf{b}_m)\Gamma(\mathbf{t}_n - \mathbf{r})\hat{\mathbf{q}}}} \end{bmatrix} \Xi(\hat{\mathbf{q}}) \quad (6.15)$$

The remaining quantities in Eq. (2.38) are given by

$$\mathbf{\Lambda} = \Delta t \mathbf{I}_{3 \times 3} \quad (6.16a)$$

$$\hat{\mathbf{y}} = \begin{bmatrix} \frac{\sqrt{\ell + \mathbf{b}_m^\top \mathbf{b}_m - 2\hat{\mathbf{q}}^\top \Omega(\mathbf{b}_m)\Gamma(\mathbf{t}_1 - \mathbf{r})\hat{\mathbf{q}}} - \sqrt{\ell + \mathbf{b}_{s_1}^\top \mathbf{b}_{s_1} - 2\hat{\mathbf{q}}^\top \Omega(\mathbf{b}_{s_1})\Gamma(\mathbf{t}_1 - \mathbf{r})\hat{\mathbf{q}}}}{\lambda} \\ \vdots \\ \frac{\sqrt{\ell + \mathbf{b}_m^\top \mathbf{b}_m - 2\hat{\mathbf{q}}^\top \Omega(\mathbf{b}_m)\Gamma(\mathbf{t}_n - \mathbf{r})\hat{\mathbf{q}}} - \sqrt{\ell + \mathbf{b}_{s_m}^\top \mathbf{b}_{s_m} - 2\hat{\mathbf{q}}^\top \Omega(\mathbf{b}_{s_m})\Gamma(\mathbf{t}_n - \mathbf{r})\hat{\mathbf{q}}}}{\lambda} \end{bmatrix} \quad (6.16b)$$

$$\mathbf{z}(\hat{\mathbf{x}}, \Delta t) = \mathbf{0} \quad (6.16c)$$

In order to derive an attitude error covariance from Eq. (6.11), a propagated expression must be derived. The attitude error equation is given by<sup>52</sup>

$$\delta \dot{\boldsymbol{\alpha}} = -[\mathbf{d} \times] \delta \boldsymbol{\alpha} + \delta \mathbf{d} \quad (6.17)$$

Since the model error  $\mathbf{d}(t)$  can be assumed constant over the time interval  $[t, t + \Delta t]$ , the propagation of the estimated quaternion is given by

$$\hat{\mathbf{q}}_{k+1} = \left[ \mathbf{I}_{4 \times 4} + \frac{1}{2} \Delta t \boldsymbol{\Omega}(\mathbf{d}_k) \right] \hat{\mathbf{q}}_k \quad (6.18)$$

Thus, the discrete propagation is given by

$$\delta \boldsymbol{\alpha}_{k+1} = e^{-[\mathbf{d}_k \times] \Delta t} \delta \boldsymbol{\alpha}_k + \int_0^{\Delta t} e^{-[\mathbf{d}_k \times] t} dt \delta \mathbf{d}_k \quad (6.19)$$

The true output is given by using a first-order expansion of the predictive filter output in Eq. (2.38),

$$\mathbf{y}_{k+1} = \mathbf{y}_k + \Delta t \bar{\mathbf{S}}_k \bar{\mathbf{d}}_k + \boldsymbol{\nu}_{k+1} \quad (6.20)$$

where  $\bar{\mathbf{S}}_k$  and  $\bar{\mathbf{d}}_k$  correspond to true quantities of  $\mathbf{S}_k$  and  $\mathbf{d}_k$ . Then, the model error is given by

$$\mathbf{d}_k = \frac{1}{\Delta t} \mathbf{K}_k (\mathbf{y}_k - \hat{\mathbf{y}}_k + \boldsymbol{\nu}_{k+1} + \Delta t \bar{\mathbf{S}}_k \bar{\mathbf{d}}_k) \quad (6.21)$$

where

$$\mathbf{K}_k = (\mathbf{S}_k^\top \mathbf{R}^{-1} \mathbf{S}_k)^{-1} \mathbf{S}_k^\top \mathbf{R}^{-1} \quad (6.22)$$

Using a small angle assumption leads to

$$\mathbf{y}_k - \hat{\mathbf{y}}_k \approx \mathbf{S}_k \delta \boldsymbol{\alpha}_k \quad (6.23)$$

Also, we can approximate

$$\bar{\mathbf{S}}_k \approx \mathbf{S}_k (\mathbf{I}_{3 \times 3} + [\delta \boldsymbol{\alpha}_k \times]) \quad (6.24)$$

Since  $\mathbf{K}_k \mathbf{S}_k = \mathbf{I}_{3 \times 3}$ , the model error is rewritten as

$$\mathbf{d}_k = \frac{\delta \boldsymbol{\alpha}_k}{\Delta t} + \frac{\mathbf{K}_k \boldsymbol{\nu}_{k+1}}{\Delta t} + (\mathbf{I}_{3 \times 3} + [\delta \boldsymbol{\alpha}_k \times]) \bar{\mathbf{d}}_k \quad (6.25)$$

Since  $\delta \mathbf{d}_k = \bar{\mathbf{d}}_k - \mathbf{d}_k$ , we have

$$\delta \mathbf{d}_k = -\frac{\delta \boldsymbol{\alpha}_k}{\Delta t} - \frac{\mathbf{K}_k \boldsymbol{\nu}_{k+1}}{\Delta t} + [\bar{\mathbf{d}}_k \times] \delta \boldsymbol{\alpha}_k \quad (6.26)$$

Substituting Eq. (6.26) into Eq. (6.19) leads to

$$\begin{aligned} \delta \boldsymbol{\alpha}_{k+1} &= e^{-[\bar{\mathbf{d}}_k \times] \Delta t} \delta \boldsymbol{\alpha}_k + \int_0^{\Delta t} e^{-[\bar{\mathbf{d}}_k \times] t} dt \left( -\frac{\delta \boldsymbol{\alpha}_k}{\Delta t} - \frac{\mathbf{K}_k \boldsymbol{\nu}_{k+1}}{\Delta t} + [\bar{\mathbf{d}}_k \times] \delta \boldsymbol{\alpha}_k \right) \\ &\approx (\mathbf{I}_{3 \times 3} - [\bar{\mathbf{d}}_k \times] \Delta t) \delta \boldsymbol{\alpha}_k + \Delta t \left( -\frac{\delta \boldsymbol{\alpha}_k}{\Delta t} - \frac{\mathbf{K}_k \boldsymbol{\nu}_{k+1}}{\Delta t} + [\bar{\mathbf{d}}_k \times] \delta \boldsymbol{\alpha}_k \right) \\ &= -\mathbf{K}_k \boldsymbol{\nu}_{k+1} \end{aligned} \quad (6.27)$$

Then, the attitude error covariance is given by

$$\begin{aligned} \mathbf{P}_{k+1} &\equiv E \{ \delta \boldsymbol{\alpha}_{k+1} \delta \boldsymbol{\alpha}_{k+1}^\top \} \\ &= \mathbf{K}_k \mathbf{R} \mathbf{K}_k^\top \end{aligned} \quad (6.28)$$

Since  $\mathbf{K}_k$  contains  $\hat{\mathbf{q}}_k$ , we use the approximation of Eq. (6.18)

$$\hat{\mathbf{q}}_k \approx \left[ \mathbf{I}_{4 \times 4} - \frac{1}{2} \Delta t \boldsymbol{\Omega}(\mathbf{d}_k) \right] \hat{\mathbf{q}}_{k+1} \quad (6.29)$$



The term that involves  $[\mathbf{d}_k \times]$  is typically three orders of magnitude less than the term that doesn't involve  $[\mathbf{d}_k \times]$ , and the term that is quadratic in  $[\mathbf{d}_k \times]$  is typically six orders of magnitude less than the term that doesn't involve  $[\mathbf{d}_k \times]$ . Then, after some manipulations we have the equivalent attitude covariance expression to the optimal covariance shown in Eq. (6.10). Although this is valid only for small  $\Delta t$ , the nonlinear predictive filter is essentially equivalent to solving the loss function in Eq. (6.9).

#### 6.4.4 Extended Kalman Filter

In this section, a quaternion based Extended Kalman Filter (EKF) using Pseudolite signals is developed for attitude estimation. The state error vector has seven components consisting of error quaternion  $\delta \mathbf{q}$  and gyro bias error  $\Delta \boldsymbol{\beta}$ . The multiplicative error quaternion is defined by

$$\delta \mathbf{q} = \mathbf{q} \otimes \hat{\mathbf{q}}^{-1} \quad (6.30)$$

where  $\mathbf{q}$  is the true quaternion,  $\hat{\mathbf{q}}$  is the estimated quaternion, and the operator  $\otimes$  refers to quaternion multiplication in Eq. (3.12). The inverse quaternion is given by  $\mathbf{q}^{-1} = [-\mathbf{q}_{13}^\top \ q_4]^\top$ . However, the covariance matrix of the error quaternion is nearly singular since it has four components. Lefferts et al. solved this problem by reducing the covariance into a three-component representation.<sup>18</sup> The dimension of the covariance matrix is then 6 by 6. For a small rotation, the error quaternion in Eq. (6.30) can be approximated by

$$\delta \mathbf{q} \approx \begin{bmatrix} \delta \mathbf{q}_{13} \\ 1 \end{bmatrix} \quad (6.31)$$

The vector part of the error quaternion,  $\delta \mathbf{q}_{13}$ , corresponds to half Euler angle errors for a small angle approximation. By using the quaternion kinematics model in Eq. (3.13) and the gyro model in Eq. (3.25), the state model equation can be written by

$$\dot{\mathbf{q}} = \frac{1}{2} \boldsymbol{\Omega} (\tilde{\boldsymbol{\omega}} - \boldsymbol{\beta} - \boldsymbol{\eta}_v) \mathbf{q} \quad (6.32a)$$

$$\dot{\boldsymbol{\beta}} = \boldsymbol{\eta}_u \quad (6.32b)$$

where  $\boldsymbol{\eta}_v$  and  $\boldsymbol{\eta}_u$  are zero-mean Gaussian white-noise processes with the properties:

$$E [\boldsymbol{\eta}_v(s)\boldsymbol{\eta}_v(\tau)] = \sigma_v^2\delta(s - \tau)\mathbf{I}_{3\times 3} \quad (6.33a)$$

$$E [\boldsymbol{\eta}_u(s)\boldsymbol{\eta}_u(\tau)] = \sigma_u^2\delta(s - \tau)\mathbf{I}_{3\times 3} \quad (6.33b)$$

$$E [\boldsymbol{\eta}_v(s)\boldsymbol{\eta}_u(\tau)] = \mathbf{0}_{3\times 3} \quad (6.33c)$$

where  $\delta(t)$  is the Dirac delta function. By using the vector part of the error quaternion in Eq. (6.31) and the additive gyro drift error  $\Delta\boldsymbol{\beta}$ , the state error equation of the EKF is written as

$$\Delta\dot{\boldsymbol{x}} = \mathbf{f}_x\Delta\boldsymbol{x} + \mathbf{g}_x\boldsymbol{w} \quad (6.34)$$

where the state error is given by

$$\Delta\boldsymbol{x} = \begin{bmatrix} \delta\mathbf{q}_{13} \\ \Delta\boldsymbol{\beta} \end{bmatrix} \quad (6.35)$$

The Jacobian matrices are given by

$$\mathbf{f}_x = \begin{bmatrix} -[\hat{\boldsymbol{\omega}}\times] & -\frac{1}{2}\mathbf{I}_{3\times 3} \\ \mathbf{0}_{3\times 3} & \mathbf{0}_{3\times 3} \end{bmatrix} \quad (6.36a)$$

$$\mathbf{g}_x = \begin{bmatrix} -\frac{1}{2}\mathbf{I}_{3\times 3} & \mathbf{0}_{3\times 3} \\ \mathbf{0}_{3\times 3} & \mathbf{I}_{3\times 3} \end{bmatrix} \quad (6.36b)$$

where the angular velocity estimate is given by

$$\hat{\boldsymbol{\omega}} = \tilde{\boldsymbol{\omega}} - \hat{\boldsymbol{\beta}} \quad (6.37)$$

For the state-observable discrete measurements model of Pseudolite signals shown in Eq. (6.2), the corresponding  $\mathbf{H}_k$  matrix is given by

$$\mathbf{H}_k = \begin{bmatrix} \vdots \\ \mathbf{L}_k^{ij} \mathbf{0}_{1\times 3} \\ \vdots \end{bmatrix} \quad (6.38)$$

where

$$\begin{aligned} \mathbf{L}_k^{ij} &= \frac{\partial \Delta \phi_{ij}}{\partial \delta \mathbf{q}_{13}} \\ &\approx -\frac{2}{\lambda} \left\{ \frac{(\mathbf{r} + \mathbf{A}^\top(\hat{\mathbf{q}}_k^-) \mathbf{b}_m - \mathbf{t}_j)^\top \mathbf{A}^\top(\hat{\mathbf{q}}_k^-) [\mathbf{b}_m \times]}{\sqrt{\ell_m}} - \frac{(\mathbf{r} + \mathbf{A}^\top(\hat{\mathbf{q}}_k^-) \mathbf{b}_{s_i} - \mathbf{t}_j)^\top \mathbf{A}^\top(\hat{\mathbf{q}}_k^-) [\mathbf{b}_{s_i} \times]}{\sqrt{\ell_{s_i}}} \right\} \end{aligned} \quad (6.39)$$

The prediction of the covariance matrix is obtained by

$$\dot{\mathbf{P}} = \mathbf{f}_x \mathbf{P} + \mathbf{P} \mathbf{f}_x^\top + \mathbf{g}_x \mathbf{Q} \mathbf{g}_x^\top \quad (6.40)$$

Then, the continuous-discrete EKF update equations are summarized by

$$\Delta \hat{\mathbf{x}}_k^+ = \mathbf{K}_k [\tilde{\mathbf{y}}_k - \mathbf{h}_k(\hat{\mathbf{q}}_k^-)] \quad (6.41a)$$

$$\mathbf{P}_k^+ = [\mathbf{I}_{6 \times 6} - \mathbf{K}_k \mathbf{H}_k] \mathbf{P}_k^- \quad (6.41b)$$

$$\hat{\mathbf{q}}_k^+ = \delta \hat{\mathbf{q}}_k^+ \otimes \hat{\mathbf{q}}_k^- \quad (6.41c)$$

$$\hat{\boldsymbol{\beta}}_k^+ = \hat{\boldsymbol{\beta}}_k^- + \Delta \hat{\boldsymbol{\beta}}_k^+ \quad (6.41d)$$

where the Kalman gain matrix is obtained by

$$\mathbf{K}_k = \mathbf{P}_k^- \mathbf{H}_k^\top [\mathbf{H}_k \mathbf{P}_k^- \mathbf{H}_k^\top + \mathbf{R}_k]^{-1} \quad (6.42)$$

#### 6.4.5 Unscented Filter

In this section, an Unscented Filter (UF) is developed using Pseudolite signal measurements. The quaternion is used as the attitude parameter because it is singularity free and the kinematics equation is bilinear. However, since quaternions are not independent parameters, the normalization constraint in Eq. (3.5) should be satisfied. The sigma points generated by using quaternions will violate the constraint. To solve this problem the MRPs are used to generate the sigma points, which are converted into quaternions. Although the MRPs have singularity at a  $360^\circ$ , the error MRPs related with the error quaternions should not have singularity in practice. Also, the exact form of quaternion propagation solution in Eq. (3.15) can still be used. This technique is first introduced by Crassidis et al.<sup>34</sup> and called the unscented quaternion estimator (USQUE). Let the state vector be

$$\hat{\mathbf{x}}_k^+ = \begin{bmatrix} \delta \hat{\mathbf{P}}_k^+ \\ \hat{\boldsymbol{\beta}}_k^+ \end{bmatrix} \quad (6.43)$$

where  $\delta\hat{\mathbf{p}}_k$  is the error MRP and  $\hat{\boldsymbol{\beta}}_k$  is the bias error. Then, the sigma points are generated by using Eq. (2.47) where the process covariance matrix is given by Eq. (3.28). By using those sigma points the corresponding error quaternions can be generated by

$$\delta q_4^+(k, i) = \frac{1 - \|\boldsymbol{\chi}_k^{\delta\mathbf{p}}(i)\|^2}{1 + \|\boldsymbol{\chi}_k^{\delta\mathbf{p}}(i)\|^2} \quad (6.44a)$$

$$\delta \mathbf{q}_{13}^+(k, i) = [1 + \delta q_4^+(k, i)] \boldsymbol{\chi}_k^{\delta\mathbf{p}}(i) \quad (6.44b)$$

where  $\boldsymbol{\chi}^{\delta\mathbf{p}}$  represents the sigma points pertaining to error MRPs. Then, the propagation of the error quaternions are given by

$$\hat{\mathbf{q}}_{k+1}^-(i) = \Omega [\hat{\boldsymbol{\omega}}_k^+(i)] \hat{\mathbf{q}}_k^+ \quad (6.45a)$$

$$\delta \mathbf{q}_{k+1}^-(i) = \hat{\mathbf{q}}_{k+1}^-(i) \otimes [\hat{\mathbf{q}}_{k+1}^-(0)]^{-1} \quad (6.45b)$$

where

$$\hat{\mathbf{q}}_k^+(0) = \hat{\mathbf{q}}_k^+ \quad , \quad \hat{\mathbf{q}}_k^+(i) = \delta \mathbf{q}_k^+(i) \otimes \hat{\mathbf{q}}_k^+ \quad (6.46)$$

Then, the propagated sigma points are given by

$$\boldsymbol{\chi}_{k+1}(0) \equiv \begin{bmatrix} \boldsymbol{\chi}_{k+1}^{\delta\mathbf{p}}(0) \\ \boldsymbol{\chi}_{k+1}^{\beta}(0) \end{bmatrix} = \begin{bmatrix} \mathbf{0} \\ \boldsymbol{\chi}_k^{\beta}(0) \end{bmatrix} \quad (6.47a)$$

$$\boldsymbol{\chi}_{k+1}(i) \equiv \begin{bmatrix} \boldsymbol{\chi}_{k+1}^{\delta\mathbf{p}}(i) \\ \boldsymbol{\chi}_{k+1}^{\beta}(i) \end{bmatrix} = \begin{bmatrix} \frac{\delta \mathbf{q}_{13}^-(k+1, i)}{1 + \delta q_4^-(k+1, i)} \\ \boldsymbol{\chi}_k^{\beta}(i) \end{bmatrix} \quad (6.47b)$$

Also, the predicted mean and covariances are computed using Eq. (2.49) and Eq. (2.50). The observation in Eq. (2.52) can now be written as

$$\begin{aligned} \boldsymbol{\gamma}_{k+1}(i) &= \mathbf{h} [\hat{\mathbf{q}}_{k+1}^-(i)] \\ &= \begin{bmatrix} \vdots \\ \frac{|\mathbf{r} + \mathbf{A}^T [\hat{\mathbf{q}}_{k+1}^-(i)] \mathbf{b}_m - \mathbf{t}_j| - |\mathbf{r} + \mathbf{A}^T [\hat{\mathbf{q}}_{k+1}^-(i)] \mathbf{b}_{s_i} - \mathbf{t}_j|}{\lambda} + n_{ij} + \tau_i \\ \vdots \end{bmatrix} \end{aligned} \quad (6.48)$$

The mean observation is obtained by using Eq. (2.51) and the output and cross covariance matrices are obtained using Eqs. (2.53) and (2.55). The updates of MRPs

and the biases are taken by using Eq. (2.44). Then, the quaternions are updated by

$$\hat{\mathbf{q}}_{k+1}^+ = \delta \hat{\mathbf{q}}_{k+1}^+ \otimes \hat{\mathbf{q}}_{k+1}^- (0) \quad (6.49)$$

where  $\delta \hat{\mathbf{q}}_{k+1}^+$  is given by

$$\delta q_4^+(k+1) = \frac{1 - \|\delta \hat{\mathbf{p}}_{k+1}^+\|^2}{1 + \|\delta \hat{\mathbf{p}}_{k+1}^+\|^2} \quad (6.50a)$$

$$\delta \mathbf{q}_{13}^+(k+1) = [1 + \delta q_4^+(k+1)] \delta \hat{\mathbf{p}}_{k+1}^+ \quad (6.50b)$$

For the next step the states should be set as

$$\hat{\mathbf{x}}_{k+1}^+ = \begin{bmatrix} \mathbf{0} \\ \Delta \boldsymbol{\beta}_{k+1}^+ \end{bmatrix} \quad (6.51)$$

The whole procedure flow of USQUE is shown in Fig. 6.2. First, the sigma points are generated by using some initial covariance. Then, they are transformed into error quaternions. The quaternions are propagated using Eq. (6.45) and the error quaternions are computed again. Then, the propagated sigma points and observations are obtained by using Eqs. (6.47) and (6.48). The predicted mean and covariance are then computed by using Eqs. (2.49), (2.51), (2.50), (2.53), and (2.55). Then, the update of covariance and error MRP are obtained by Eqs (2.44) and (2.46). Next, the update of the quaternion is accomplished by using the updated error MRP. Finally, the state is reset using Eq. (6.51) for the next propagation.

## 6.5 Simulation

To compare the attitude estimation algorithms described in section 6.4, the Pseudolite signals are simulated using the geometry shown in Fig. 6.3. The locations of the Pseudolite transceivers and receiver antennas are displayed as TX1, TX2, TX3, TX4, MA, SA1, SA2, and SA3, respectively. The unit vectors  $\{I, J, K\}$  are for the reference coordinate system and  $\{x, y, z\}$  are for the body fixed coordinate system. The coordinates of the transceivers in the reference frame and those of the antennas in the body fixed frame are shown in Table 6.1. The location of the origin of the body fixed frame is given by  $\mathbf{r} = [2.5, 2.5, 0]^T$ (m). It is assumed that the position of

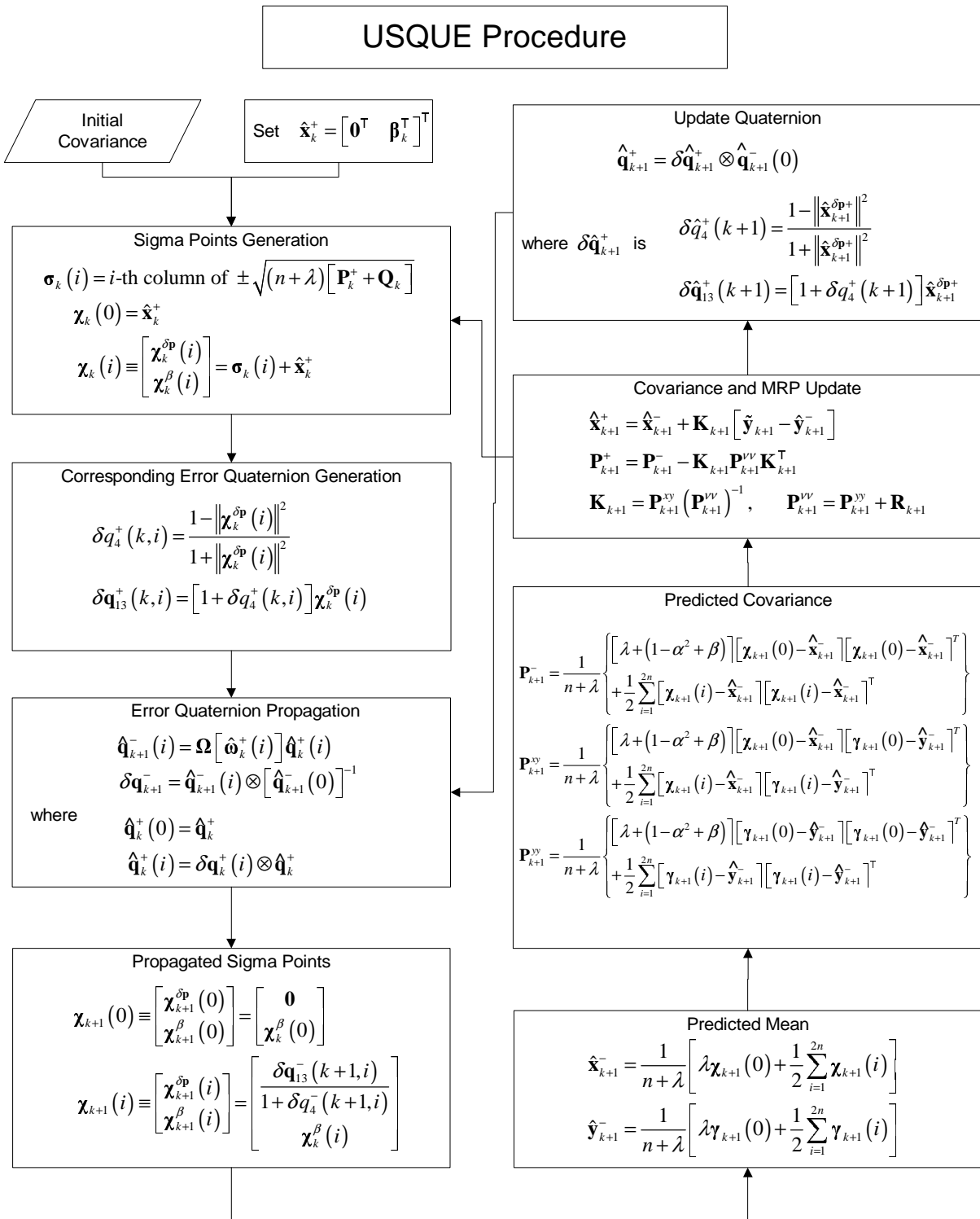


Fig. 6.2. USQUE Procedure

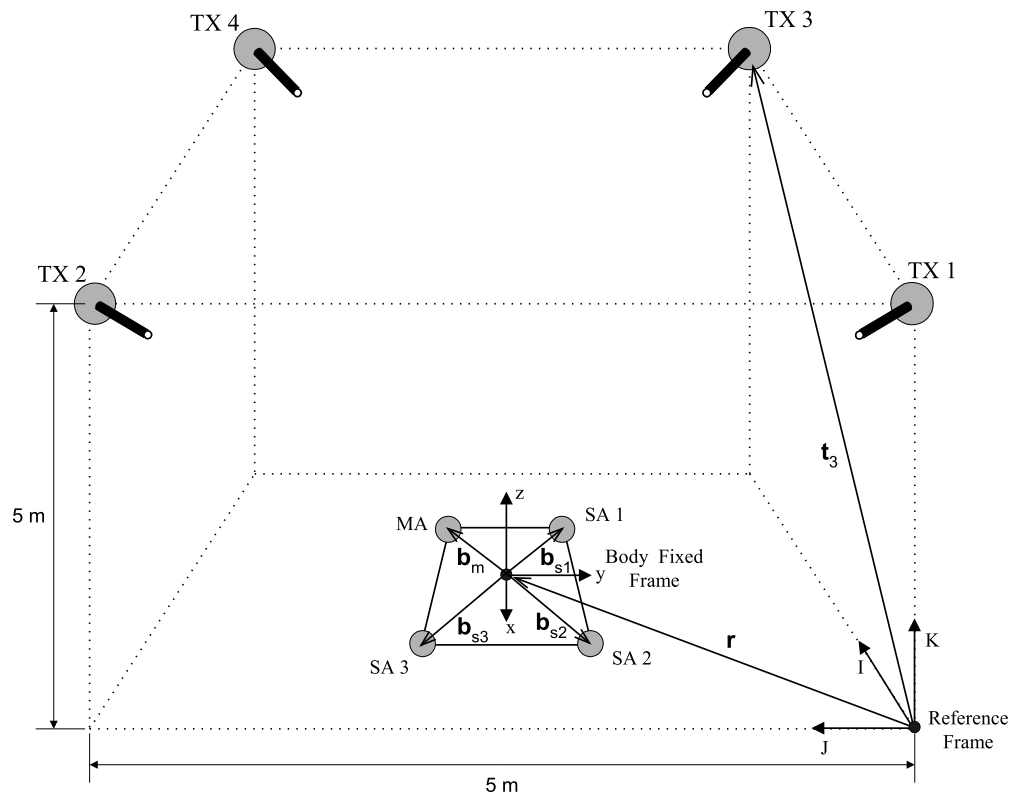


Fig. 6.3. Geometric Configuration of Simulation

the origin of the body fixed frame,  $\mathbf{r}$ , is given from another source such as navigation data. For several angular velocities, NLS, LM, nonlinear predictive filter, EKF, and UF are compared with intensive simulations.

Table 6.1. Locations of Transceivers and Antennas

Transceivers	Locations (m)	Antennas	Locations (m)
$\mathbf{t}_1$	$[0, 0, 5]^T$	$\mathbf{b}_m$	$[-0.05, -0.05, 0]^T$
$\mathbf{t}_2$	$[0, 5, 5]^T$	$\mathbf{b}_{s1}$	$[0.05, -0.05, 0]^T$
$\mathbf{t}_3$	$[5, 0, 5]^T$	$\mathbf{b}_{s2}$	$[0.05, 0.05, 0]^T$
$\mathbf{t}_4$	$[5, 5, 5]^T$	$\mathbf{b}_{s3}$	$[-0.05, 0.05, 0]^T$

### 6.5.1 NLS and LM

By using the same initial errors, the LM method is used to determine the quaternion estimate at the first step. Then, NLS is used to determine the quaternion since the previous estimate is a good guess for next estimation time. Figure 6.4 shows the Euler angle errors and their  $3\text{-}\sigma$  boundary layers of the NLS and LM estimation. As

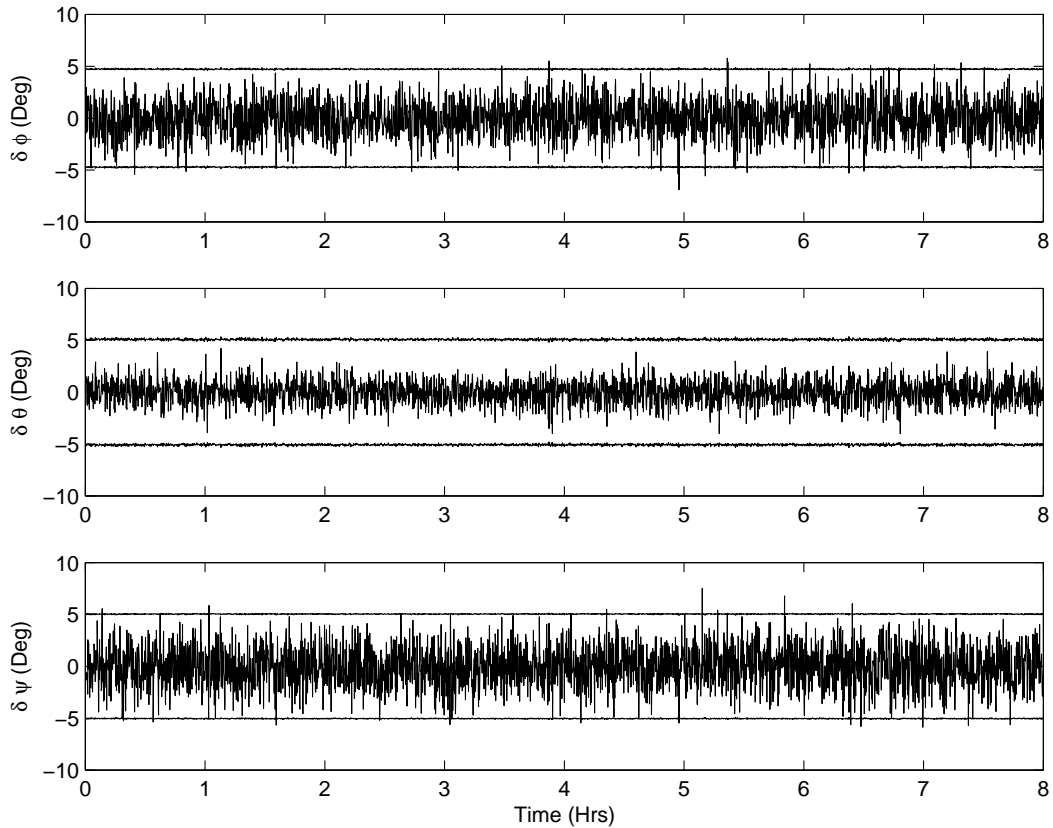


Fig. 6.4. Euler Angle Errors of NLS/LM Estimation (Static)

can be seen, the errors are well inside  $3\text{-}\sigma$  bounds. Also, we can notice that the errors in the pitch axis are smaller than those of the other axes when we use the sightline geometry shown in Fig. 6.3.



Table 6.2. Angular Velocities and Weighting Matrices for Each Case

Cases	Weighting Matrices	Angular Velocity (rad/s)
Static-1	$\mathbf{W} = \mathbf{0}$ $\mathbf{W} = 10^5 \mathbf{I}$ $\mathbf{W} = 10^6 \mathbf{I}$	$\boldsymbol{\omega} = \begin{bmatrix} 0 \\ 0 \\ 0 \end{bmatrix}$
Moving-1	$\mathbf{W} = \mathbf{0}$ $\mathbf{W} = 10^5 \mathbf{I}$ $\mathbf{W} = 5 \times 10^5 \mathbf{I}$	$\boldsymbol{\omega} = \begin{bmatrix} 0 \\ 0.0011 \\ 0 \end{bmatrix}$
Moving-2	$\mathbf{W} = \mathbf{0}$ $\mathbf{W} = 10^5 \mathbf{I}$ $\mathbf{W} = 5 \times 10^5 \mathbf{I}$	$\boldsymbol{\omega} = \begin{bmatrix} 5 \times 10^{-5} \sin(0.0011t) \\ 0.0011 \\ 5 \times 10^{-5} \cos(0.0011t) \end{bmatrix}$
Moving-3	$\mathbf{W} = \mathbf{0}$ $\mathbf{W} = 10^3 \mathbf{I}$ $\mathbf{W} = 10^4 \mathbf{I}$	$\boldsymbol{\omega} = \begin{bmatrix} 0 \\ 0.01 \\ 0 \end{bmatrix}$

### 6.5.2 Nonlinear Predictive Filter

To investigate the behaviour of the predictive filter, four different angular velocities are considered. First, the static case is compared with nonlinear least squares. Then, cases of a LEO spacecraft having an orbital period of 95 minutes are considered. Finally, relatively rapid angular motion is considered. The angular velocities and weighting matrices of all cases are shown in Table 6.2. As can be seen in section 2.6, both  $\Delta t$  and  $\mathbf{W}$  can affect the filter performance. The sampling interval,  $\Delta t$ , is set to 10 seconds for the first three cases and 2 seconds for the Moving-3 case.

#### 6.5.2.1 Static Case

To show the convergence behavior large initial errors are considered:

$$\begin{bmatrix} \delta\phi \\ \delta\theta \\ \delta\psi \end{bmatrix} = \begin{bmatrix} -43.086^\circ \\ -13.851^\circ \\ -55.382^\circ \end{bmatrix}$$

Three different weighting matrices shown in Table 6.2 are used in the 8 hour simulations. The attitude time histories are compared in Fig. 6.5 for two weighting

matrices,  $\mathbf{W} = 10^6 \mathbf{I}$  and  $\mathbf{W} = \mathbf{0}$ . The initial attitude is given by

$$\begin{bmatrix} \phi \\ \theta \\ \psi \end{bmatrix} = \begin{bmatrix} 27.962^\circ \\ -3.034^\circ \\ -54.706^\circ \end{bmatrix}$$

As can be seen, the convergence of the large weighting matrix is slower but the estimation errors are smaller after the convergence. A comparison of the Euler angle

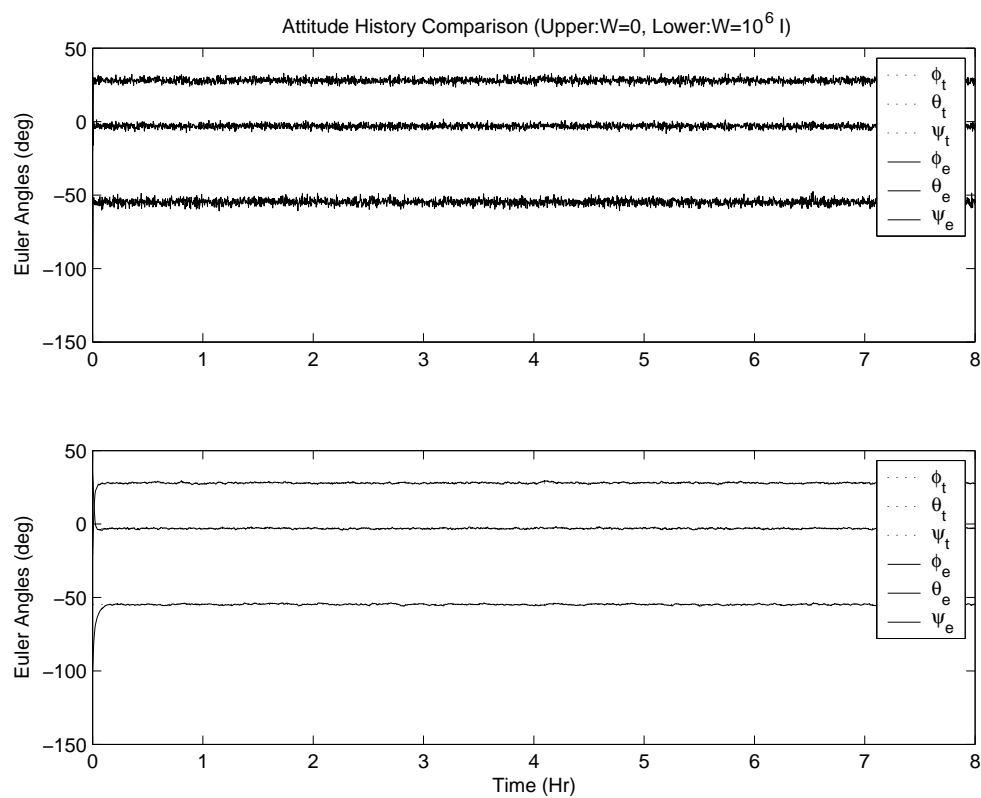


Fig. 6.5. Attitude History Comparison

errors is shown in Figs. 6.6 to 6.8. The horizontal axis of each figure represents the time in hours unit and the longitudinal axis is the Euler angle errors in degrees. The  $3\text{-}\sigma$  error bounds are also displayed in each figure. For all Euler angle comparisons, the differences among  $3\text{-}\sigma$  error bounds for each weighting matrix are not distinguishable.

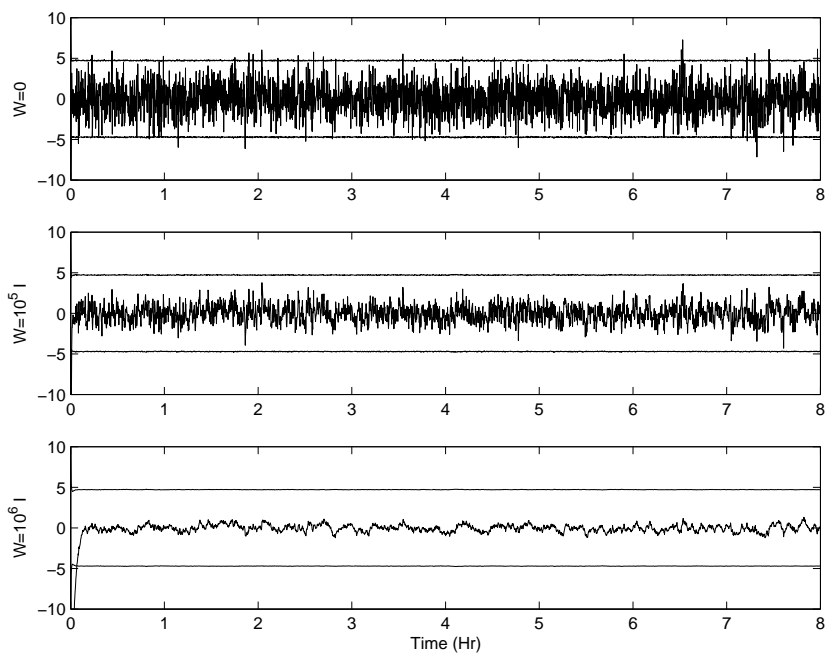


Fig. 6.6. Attitude Error Comparison in the Roll Axis

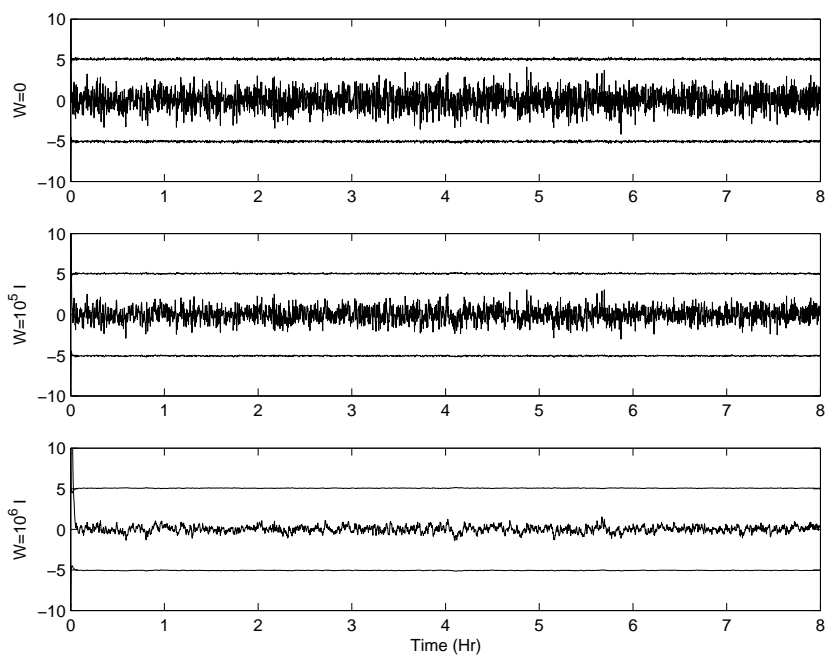


Fig. 6.7. Attitude Error Comparison in the Pitch Axis

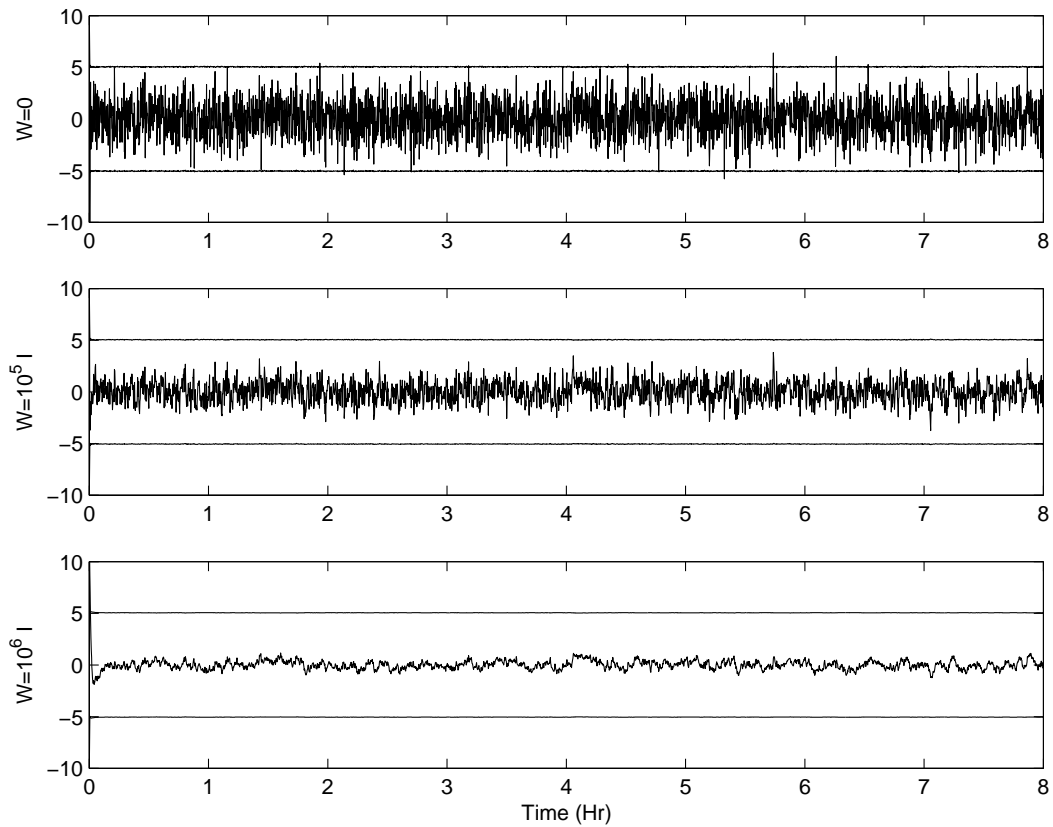


Fig. 6.8. Attitude Error Comparison in the Yaw Axis

As can be seen, the yaw angle error converges after 8 minutes for  $\mathbf{W} = 10^6\mathbf{I}$  and the others require several minutes. However, the Euler angle errors clearly decrease as the weighting increases.

To investigate the characteristics of the estimation errors, zero initial errors are considered with the weight matrices  $\mathbf{W} = 10^5\mathbf{I}$ ,  $\mathbf{W} = 10^4\mathbf{I}$ ,  $\mathbf{W} = 10^3\mathbf{I}$ , and  $\mathbf{W} = \mathbf{0}$ . Figure 6.9 shows the Euler angle estimates comparison between  $\mathbf{W} = 10^5\mathbf{I}$  and  $\mathbf{W} = \mathbf{0}$ . As can be seen, the estimation errors are smaller for the larger weighting. To investigate the statistical properties of the estimation errors, the Gaussian distribution of the Euler angle errors are compared in Figs. 6.10 through 6.12. As can be seen, the standard deviation decreases as the weighting increases.

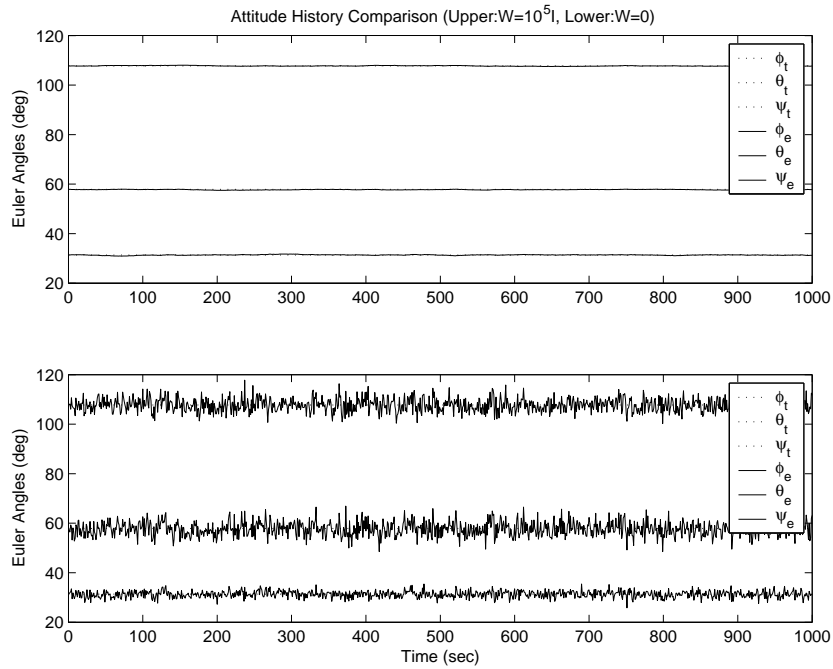


Fig. 6.9. Attitude History Comparison

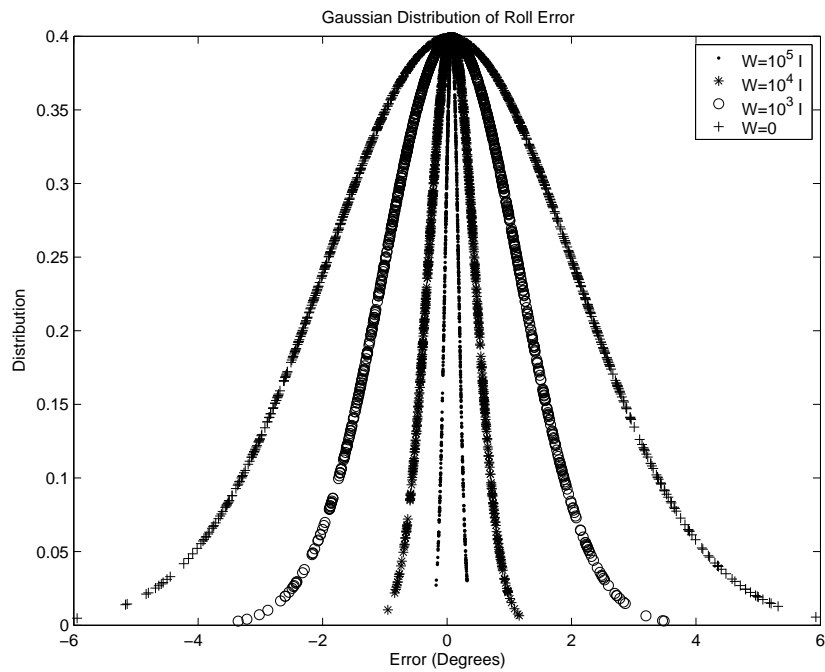


Fig. 6.10. Attitude Error Distribution in the Roll Axis

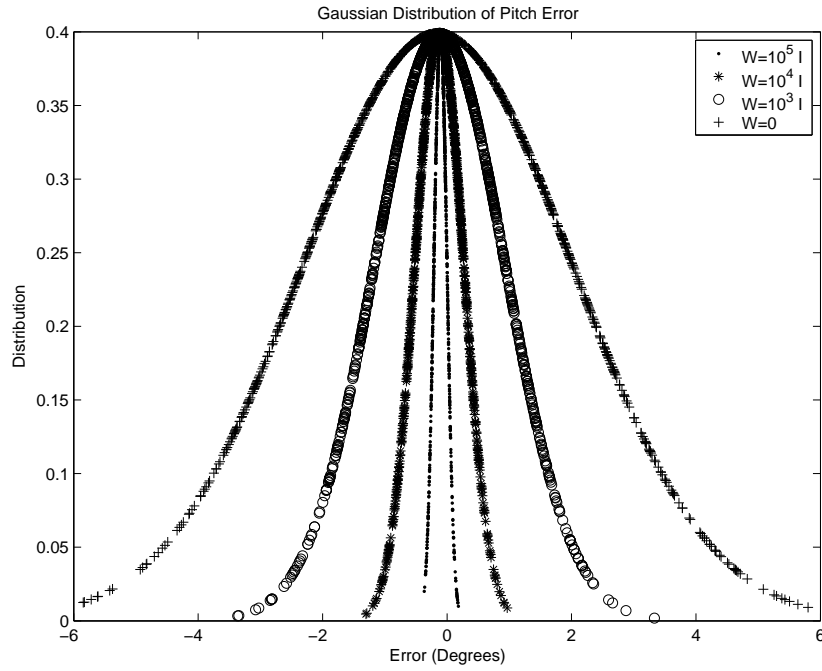


Fig. 6.11. Attitude Error Distribution in the Pitch Axis

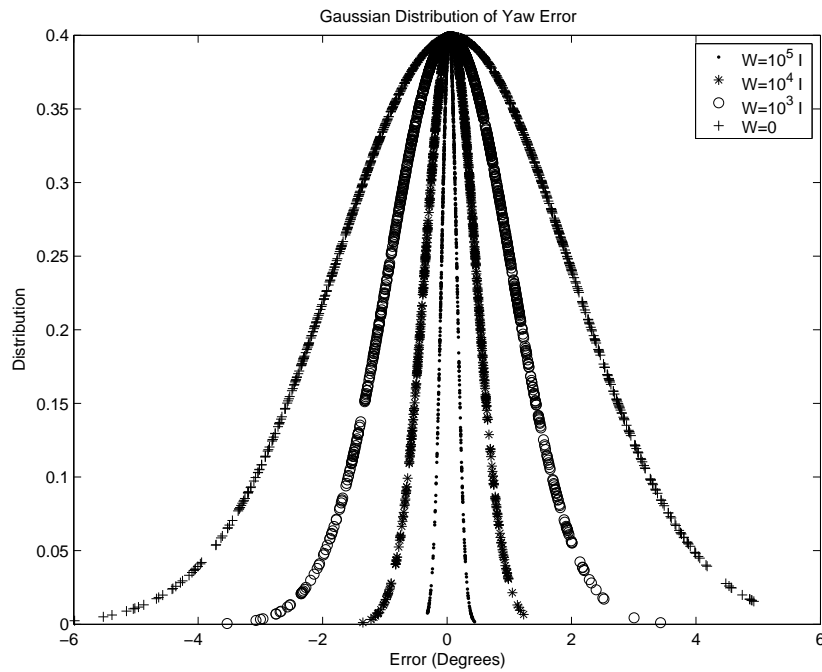


Fig. 6.12. Attitude Error Distribution in the Yaw Axis

Table 6.3. Mean and Standard Deviation Values

Weighting	Mean (Deg.)			Standard Deviation (Deg.)		
	Roll	Pitch	Yaw	Roll	Pitch	Yaw
$\mathbf{W} = 10^5 \mathbf{I}$	0.0755	-0.1059	0.0341	0.1085	0.1061	0.1237
$\mathbf{W} = 10^4 \mathbf{I}$	0.0708	-0.1248	0.0540	0.3787	0.3945	0.4120
$\mathbf{W} = 10^3 \mathbf{I}$	0.0690	-0.1170	0.0499	1.0880	1.0511	0.9850
$\mathbf{W} = \mathbf{0}$	0.0428	-0.1501	0.0891	2.0120	2.1646	1.9007

The mean and the standard deviation values are shown in Table 6.3. For  $\mathbf{W} = \mathbf{0}$ , which is the deterministic case, the  $3\text{-}\sigma$  values of Euler angle errors are over 6 degrees. However, for  $\mathbf{W} = 10^5 \mathbf{I}$ , the  $3\text{-}\sigma$  values of Euler angle errors are less than 0.4 degrees. From the static simulation survey, we conclude that the larger weighting introduces smaller attitude errors. However, the convergence to the correct attitude is the slower.

#### 6.5.2.2 Moving Cases

To investigate the attitude determination performance of the predictive filter in motion, various angular velocities shown in Table 6.2 are considered. For the spacecraft having an orbital period of 95 minutes, the attitude estimation results for  $\mathbf{W} = \mathbf{0}$  and  $\mathbf{W} = 5 \times 10^5 \mathbf{I}$  are compared in Fig. 6.13. Initial Euler angle errors are set to

$$\begin{bmatrix} \delta\phi \\ \delta\theta \\ \delta\psi \end{bmatrix} = \begin{bmatrix} -0.411^\circ \\ 7.106^\circ \\ -2.057^\circ \end{bmatrix}$$

Although the Euler angles for the roll and yaw axes seem to be changing rapidly, they represent the same orientation. Euler angle errors for each axis are compared in Figs. 6.14 to 6.16. At first as the weighting increases the Euler angle errors decrease. However, unlike the static case the errors seem to be biased for larger weightings. In Fig. 6.14 the Roll angle errors decrease as  $\mathbf{W}$  increases from  $\mathbf{W} = \mathbf{0}$  to  $\mathbf{W} = 10^5 \mathbf{I}$ . But, after that, the errors become large as  $\mathbf{W}$  increases.

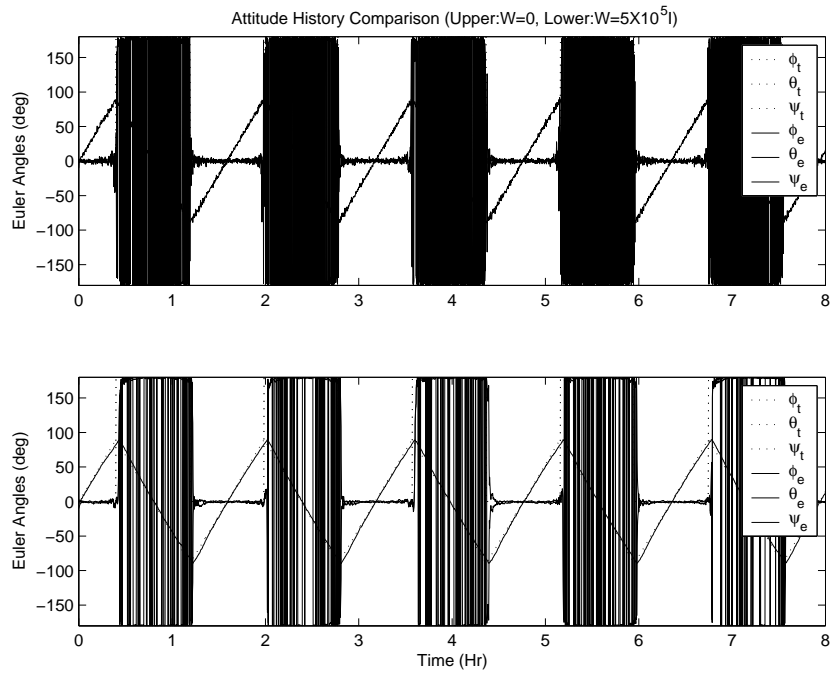


Fig. 6.13. Attitude History Comparison (Moving-1)

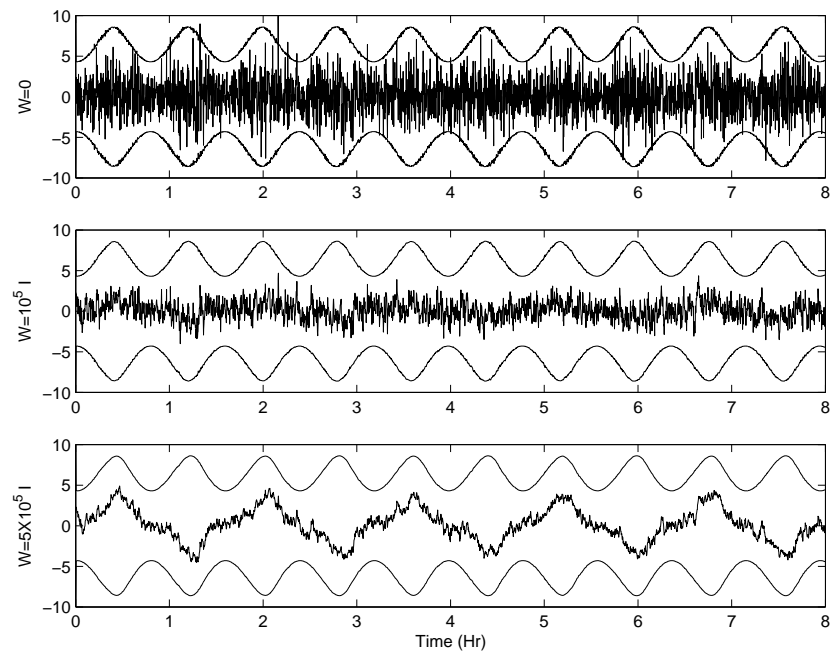


Fig. 6.14. Attitude Error Comparison in the Roll Axis (Moving-1)



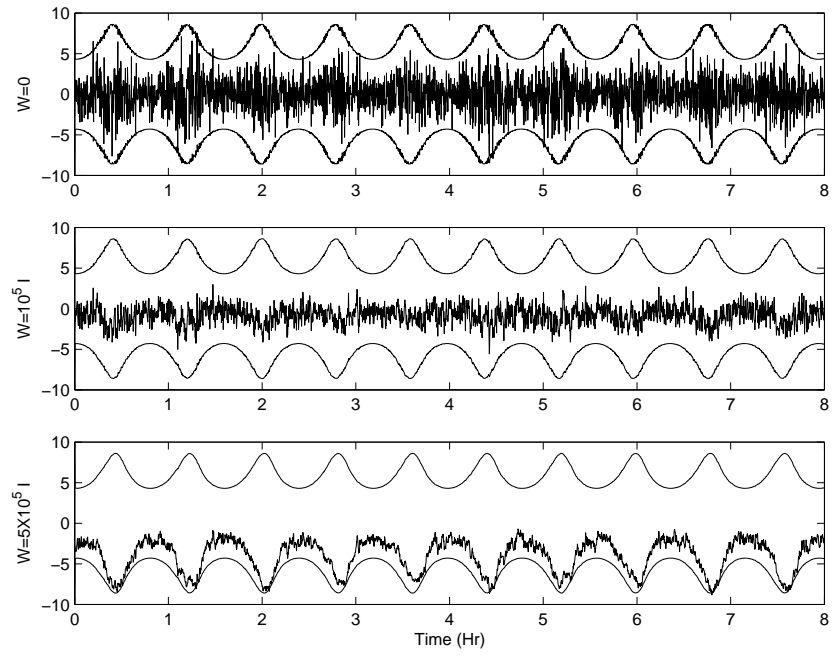


Fig. 6.15. Attitude Error Comparison in the Pitch Axis (Moving-1)

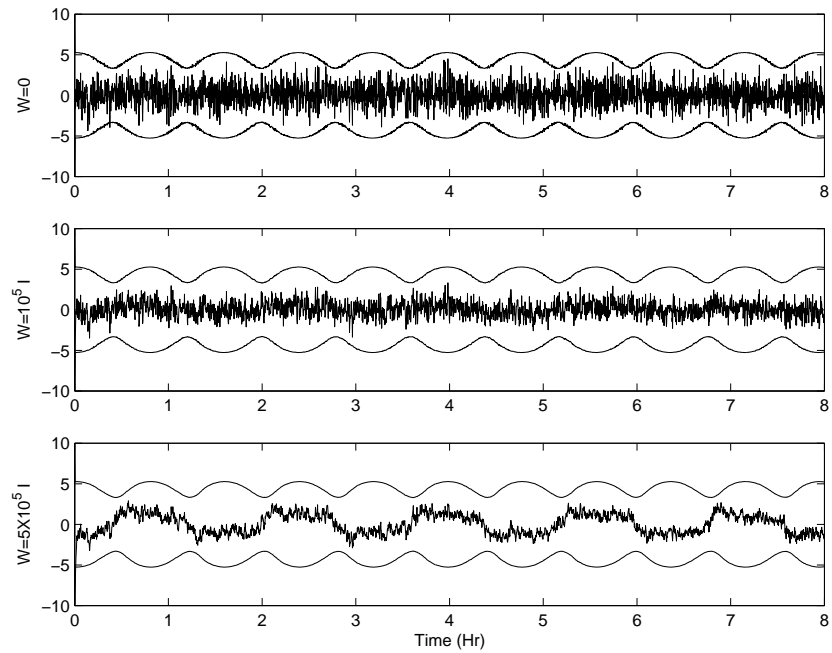


Fig. 6.16. Attitude Error Comparison in the Yaw Axis (Moving-1)

The same motion with small sinusoidal disturbances is considered in the Moving-2 case. The weighting matrices are the same as those of Moving-1 case. Also, the initial Euler angle errors are the same. The attitude estimation results for  $\mathbf{W} = \mathbf{0}$  and  $\mathbf{W} = 5 \times 10^5 \mathbf{I}$  are compared in Fig. 6.17.

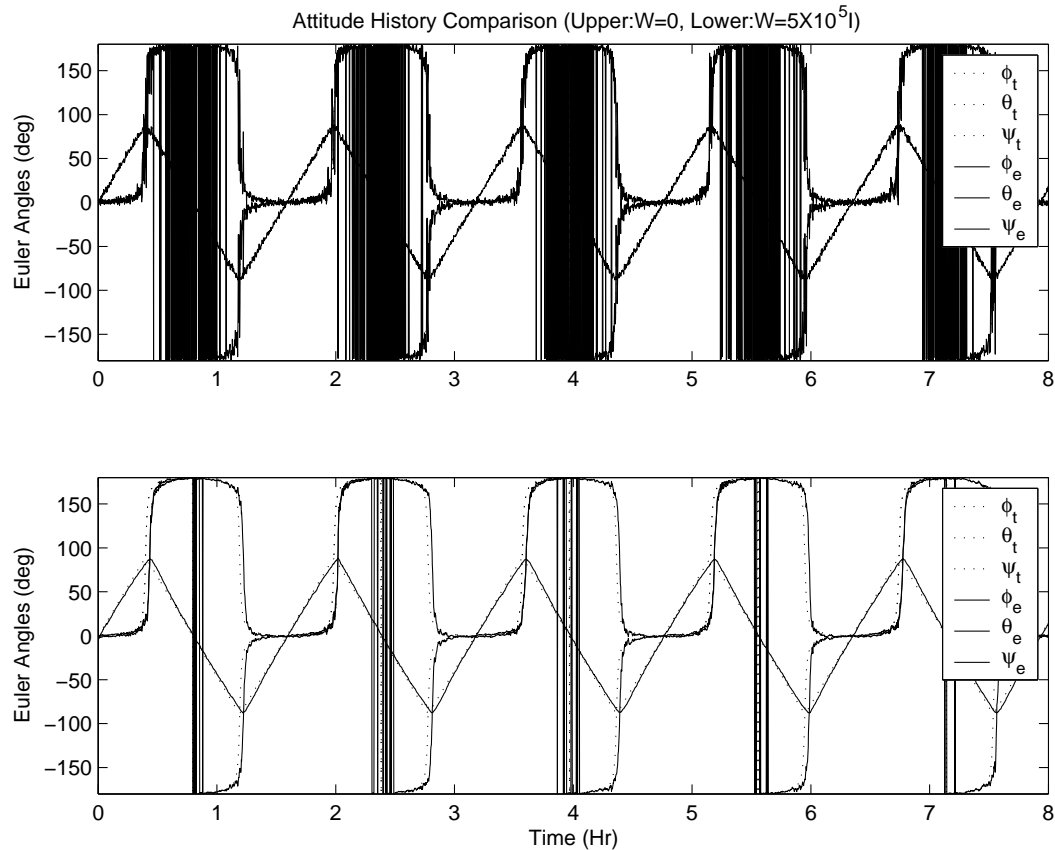


Fig. 6.17. Attitude History Comparison (Moving-2)

Figures 6.18 to 6.20 show the Euler angle errors of Moving-2 case. The behavior seems to be the same as that of Moving-1. The estimation errors are all within the  $3\text{-}\sigma$  bounds. As can be seen, the  $3\text{-}\sigma$  bounds for yaw axis is smaller than the other two axes due to the sightline geometry.

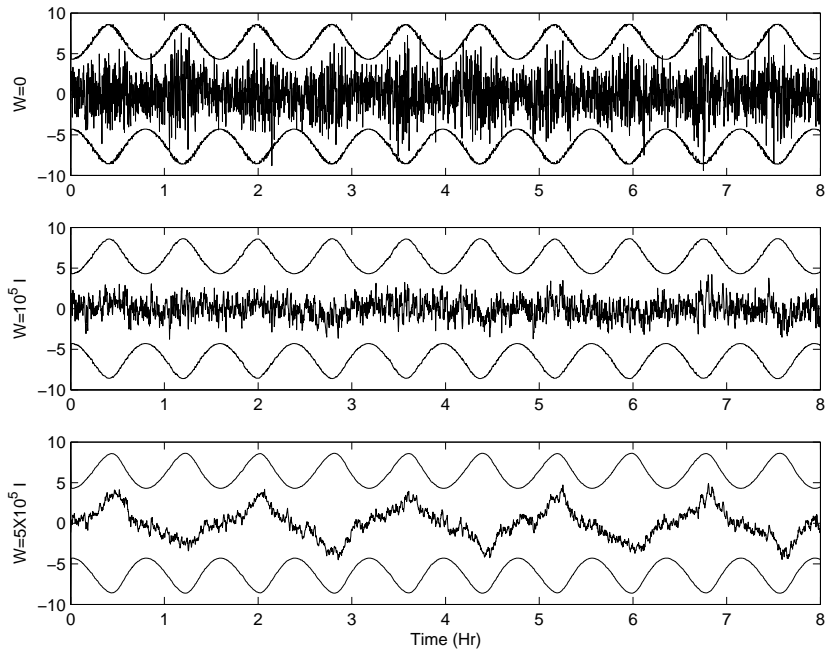


Fig. 6.18. Attitude Error Comparison in the Roll Axis (Moving-2)

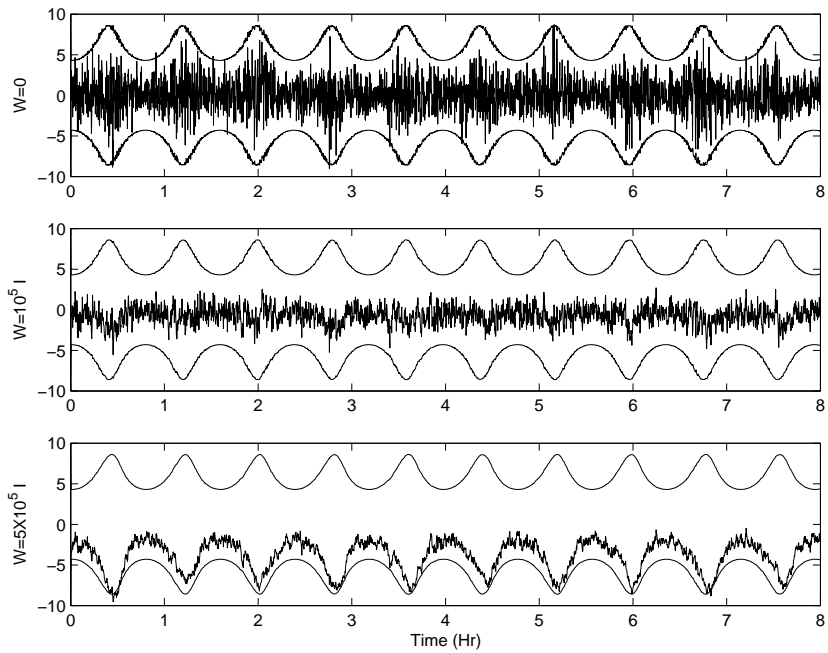


Fig. 6.19. Attitude Error Comparison in the Pitch Axis (Moving-2)

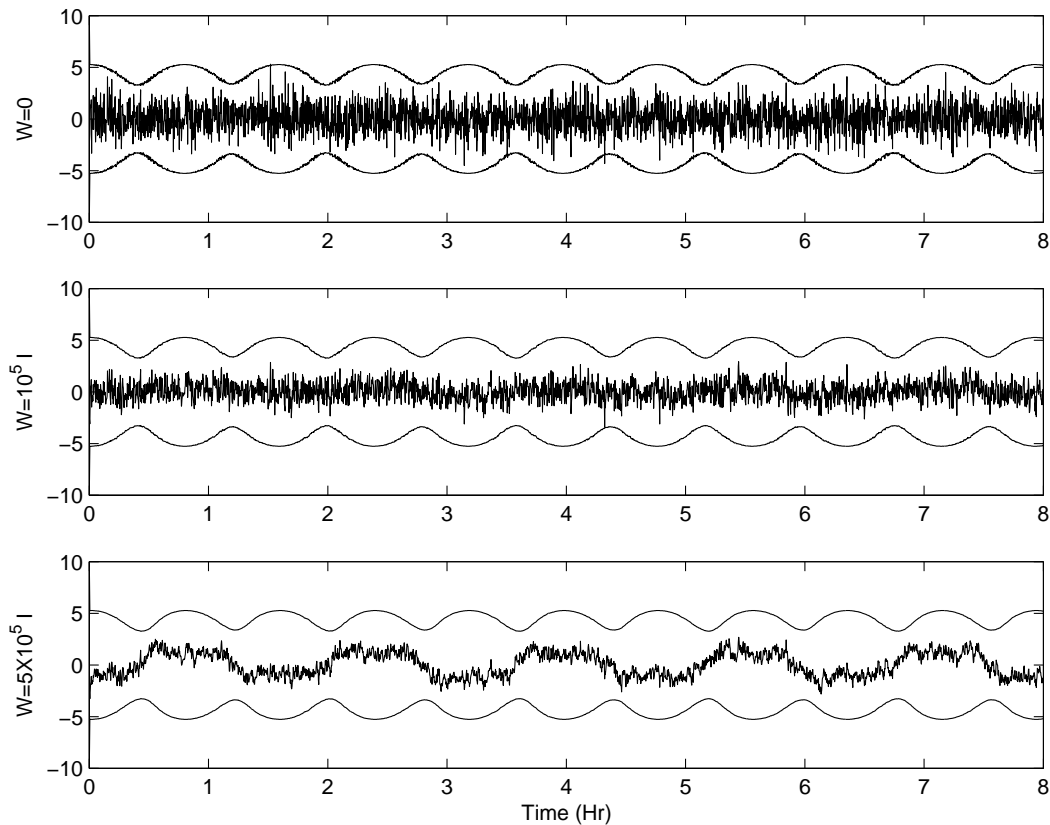


Fig. 6.20. Attitude Error Comparison in the Yaw Axis (Moving-2)

In the Moving-3 case relatively rapid angular motion is considered. Thus, only a one-hour simulation is used. Since  $\Delta t$  is now set by 2 seconds, the weightings are also changed. The attitude estimation results for  $\mathbf{W} = \mathbf{0}$  and  $\mathbf{W} = 10^4 \mathbf{I}$  are compared in Fig. 6.21. Figures 6.22 to 6.24 show the Euler angle errors for the Moving-3 case. The behavior of Euler angle errors is the same as that of the others. However, as  $\Delta t$  decreases the choice of weights should be reconsidered.

As a conclusion, for the static case the estimation error of the predictive filter decreases as the weight increases. However, for the moving cases if the weights exceed certain limits the estimation errors increase and can violate the  $3\text{-}\sigma$  bounds.

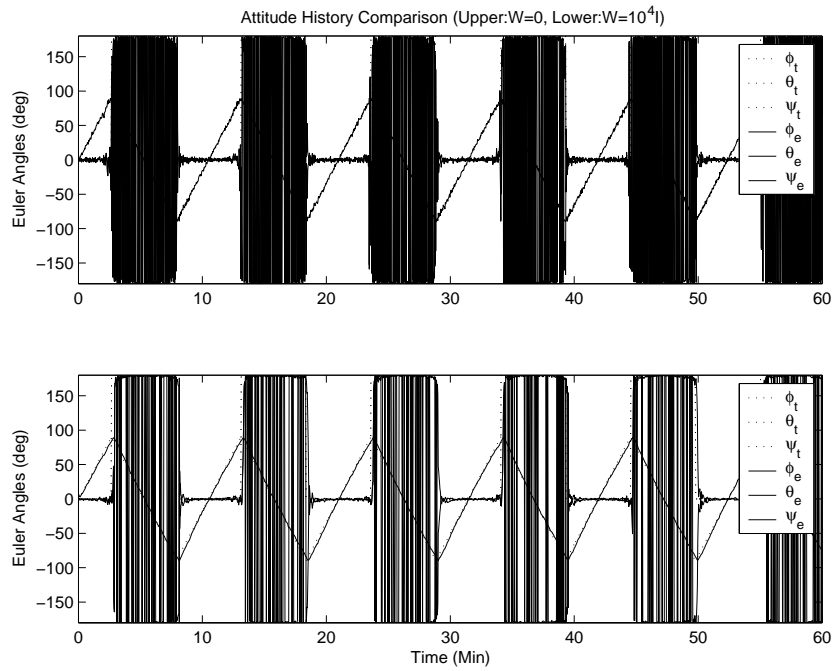


Fig. 6.21. Attitude History Comparison (Moving-3)

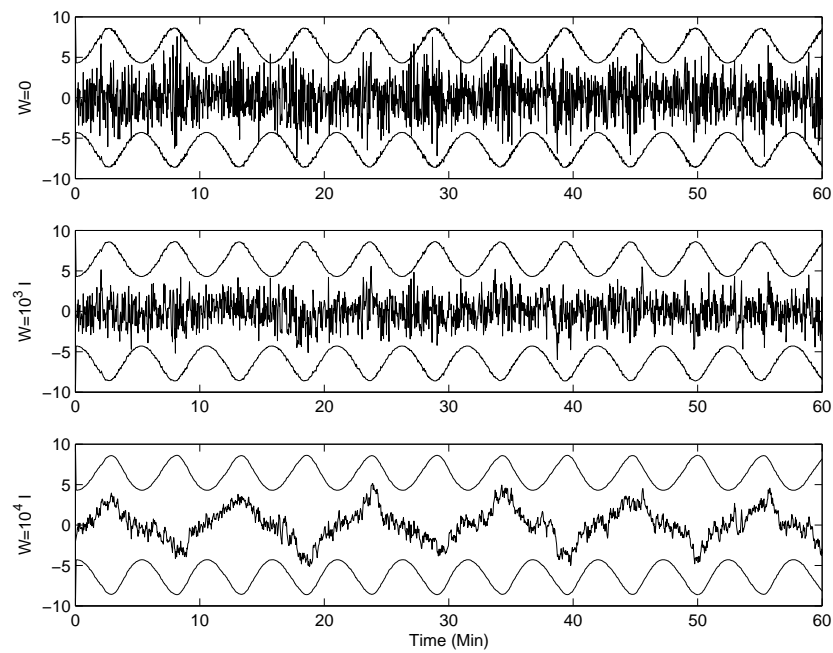


Fig. 6.22. Attitude Error Comparison in the Roll Axis (Moving-3)

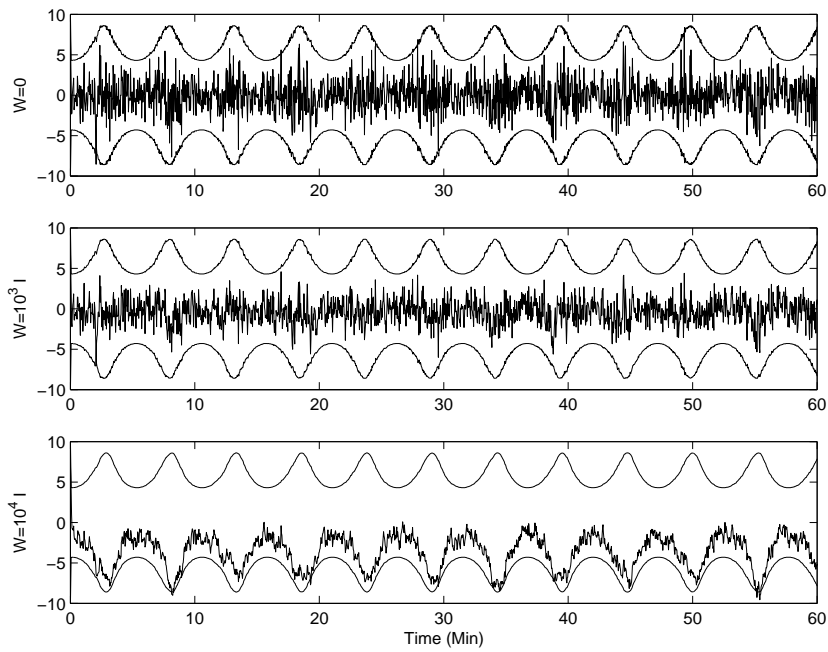


Fig. 6.23. Attitude Error Comparison in the Pitch Axis (Moving-3)

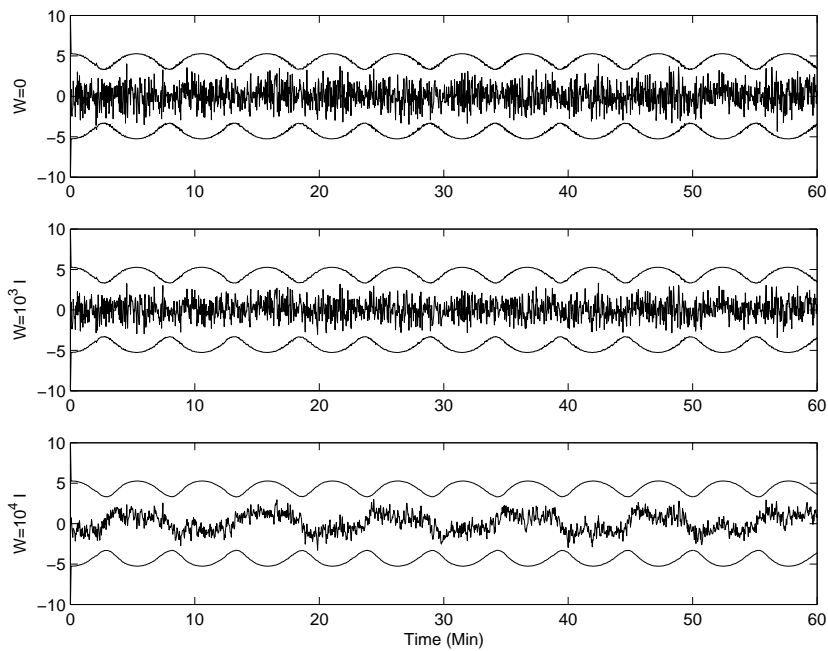


Fig. 6.24. Attitude Error Comparison in the Yaw Axis (Moving-3)

### 6.5.3 EKF and UF

The Pseudolite signal measurements as well as angular velocity measurements with gyros are used for the comparison of EKF and UF. The comparison is accomplished in two parts. The first compares the mean estimation error through Monte Carlo like simulations. By using this comparison, the statistical properties of the EKF and UF can be investigated. Then, by using large initial errors the convergence behaviors are investigated.

#### 6.5.3.1 Monte Carlo Simulation

To compare the EKF and UF, a Monte Carlo simulation is applied. The initial Euler angle errors and gyro drift errors are generated randomly by

$$\begin{aligned} \begin{bmatrix} \delta\phi \\ \delta\theta \\ \delta\psi \end{bmatrix} &= 30 \text{ randn}(3, 1) \text{ (Deg)} \\ \Delta\boldsymbol{\beta} &= .0001 \text{ randn}(3, 1) \text{ (rad/sec)} \end{aligned}$$

where the ‘randn’ is the MATLAB command used to generate a Gaussian normal random number whose standard deviation is 1. The initial covariance matrix is set to

$$\mathbf{P}_0 = \begin{bmatrix} 0.5\mathbf{I}_{3\times 3} & \mathbf{0}_{3\times 3} \\ \mathbf{0}_{3\times 3} & 10^{-5}\mathbf{I}_{3\times 3} \end{bmatrix}$$

The process covariance matrix is given by Eq. (3.28) where  $\Delta t = 10$  seconds,  $\sigma_v = 1.7222\text{e-}5$  (rad/sec<sup>3/2</sup>), and  $\sigma_u = 1.8133\text{e-}8$  (rad/sec<sup>3/2</sup>). The measurement covariance matrix is given by  $\mathbf{R} = \sigma_p^2\mathbf{I}_{12\times 12}$  where  $\sigma_p = 0.0263$ (cycles).

By using 100 random initial attitude errors, bias errors, and measurements, the mean values of Euler angle errors and biases errors are compared in the following figures. Figures 6.25 to 6.27 show the Euler angle errors comparison. As can be seen, the 3- $\sigma$  bounds of UF are slightly larger than those of the EKF. However, this does not mean that the EKF’s covariance is the smaller. Since the EKF uses

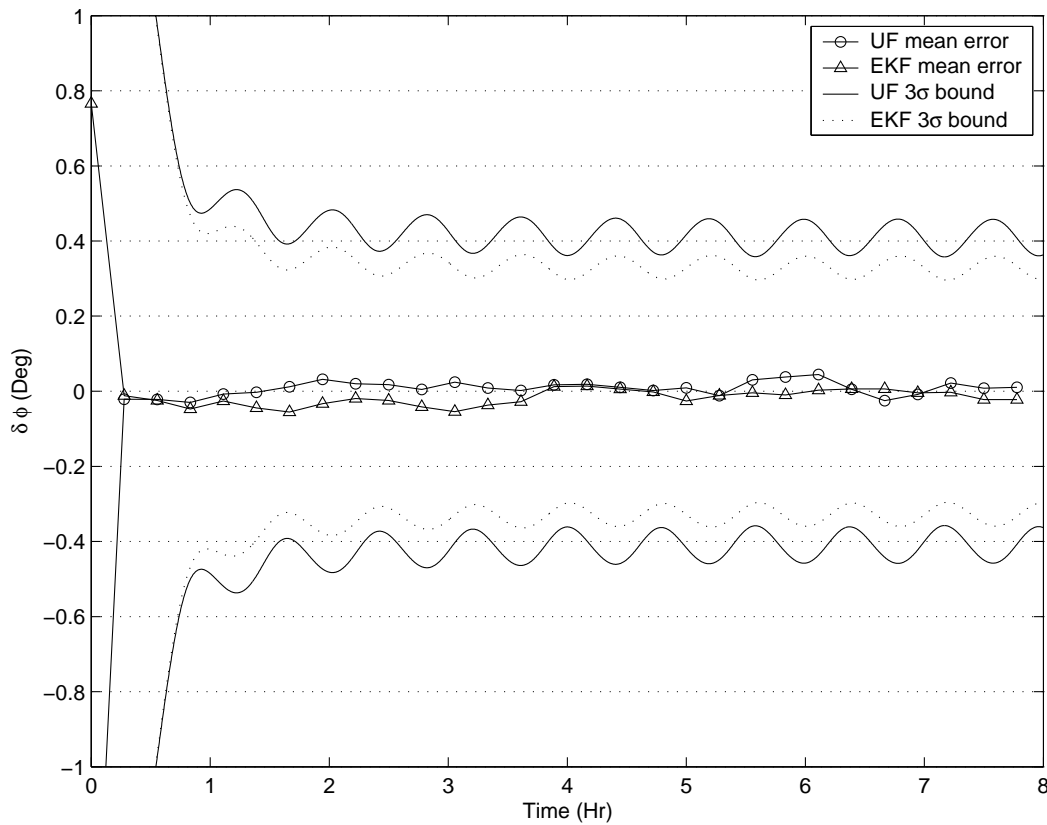


Fig. 6.25. EKF vs. UF Roll Error

a linearization approximation, the mean and covariance expression do have errors.<sup>35</sup> The covariance expression of UF is more correct than the EKF. In fact, the differences in the mean estimation errors cannot be distinguishable. Also, the differences of  $3\text{-}\sigma$  bounds between the UF and EKF are the smallest for the pitch axis while the values of  $3\text{-}\sigma$  bounds are the largest due to the sightline geometry.

Figures 6.28 to 6.30 show the gyro drift errors comparison. Now, the  $3\text{-}\sigma$  bounds of the UF are slightly smaller than those of the EKF. For the same reason in the Euler angle errors, the covariance of the UF is more reliable than that of the EKF. The magnitudes of the  $3\text{-}\sigma$  bounds are largest for  $\beta_3$  and smallest for  $\beta_2$ . Similar to the Euler angles error, the differences in the mean value of the gyro drift error are not distinguishable while the differences in the  $3\sigma$  bounds are slightly different.



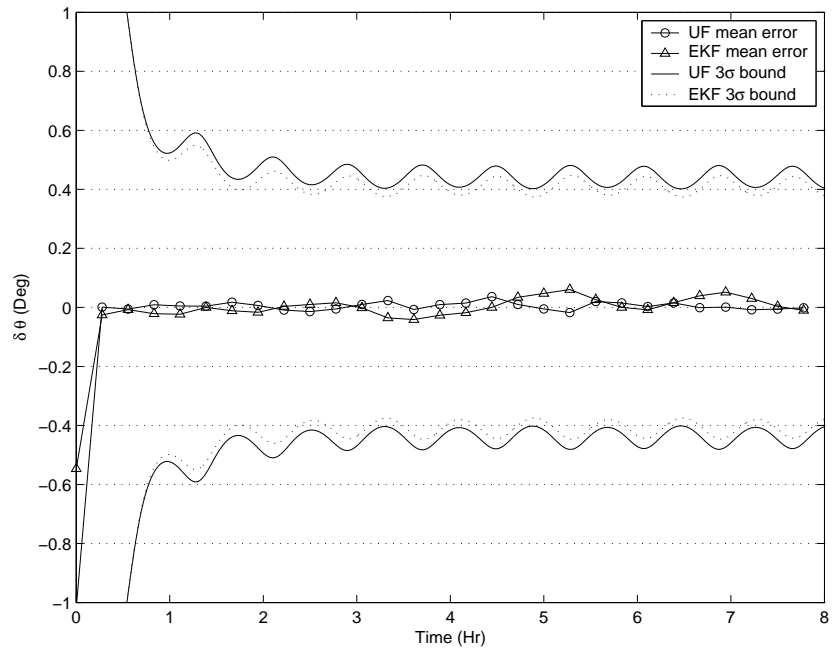


Fig. 6.26. EKF vs. UF Pitch Error

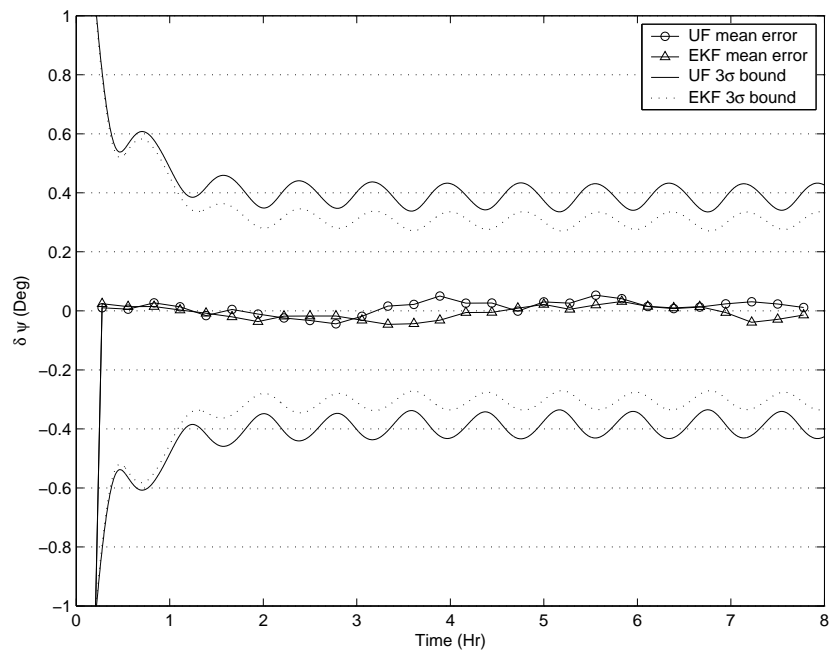
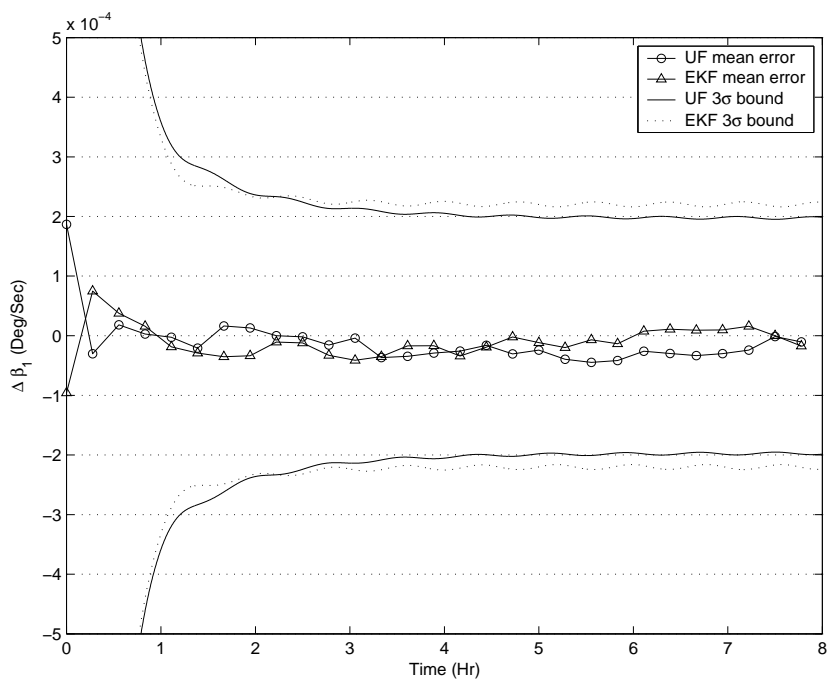
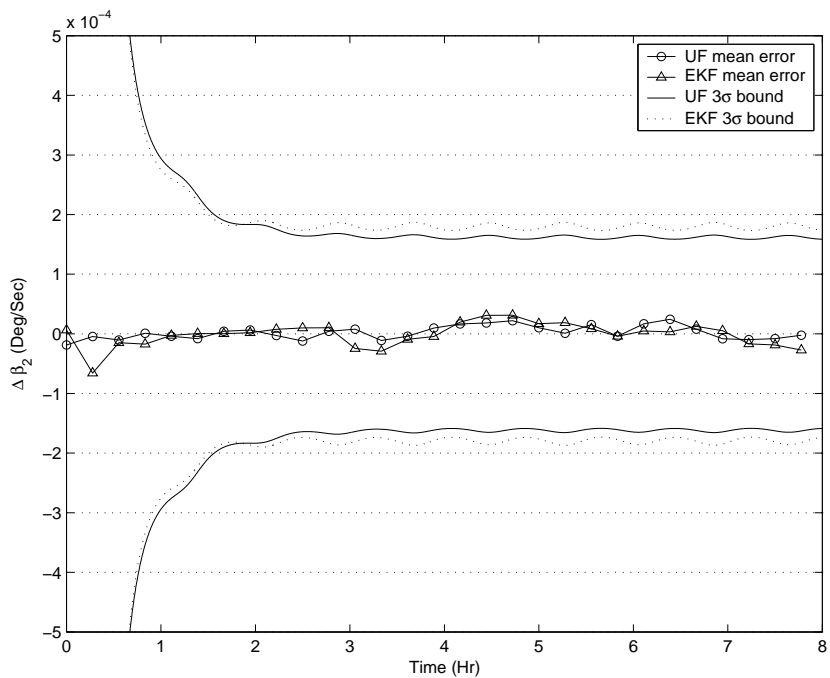


Fig. 6.27. EKF vs. UF Yaw Error

Fig. 6.28. EKF vs. UF  $\beta_1$  ErrorFig. 6.29. EKF vs. UF  $\beta_2$  Error

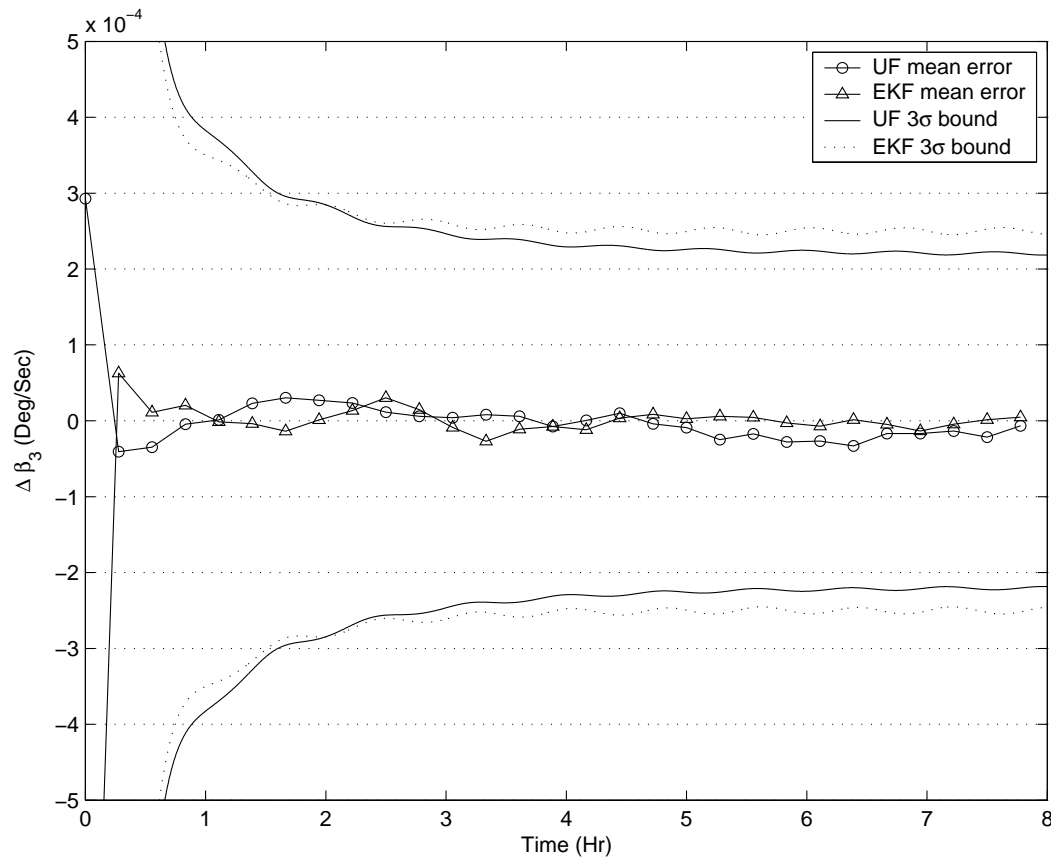


Fig. 6.30. EKF vs. UF  $\beta_3$  Error

### 6.5.3.2 Large Initial Errors

To compare the convergence behavior of the EKF and UF, a large initial error is considered as

$$\begin{bmatrix} \delta\phi \\ \delta\theta \\ \delta\psi \end{bmatrix} = \begin{bmatrix} 0 \\ -120^\circ \\ 0 \end{bmatrix}, \quad \Delta\boldsymbol{\beta} = \begin{bmatrix} -0.0001 \\ 0.0003 \\ 0.0002 \end{bmatrix} \quad (\text{rad/sec})$$

With the given initial guesses, the Euler angle estimation errors are compared in Figs. 6.31 and 6.32. As can be seen, the estimation of the EKF fails while the UF estimation errors are well within their  $3\text{-}\sigma$  bounds, although the convergence of the covariance and estimation error requires an hour. The failure of the EKF is caused

by the linearization approximation of the EKF that works only for small, first-order, errors.

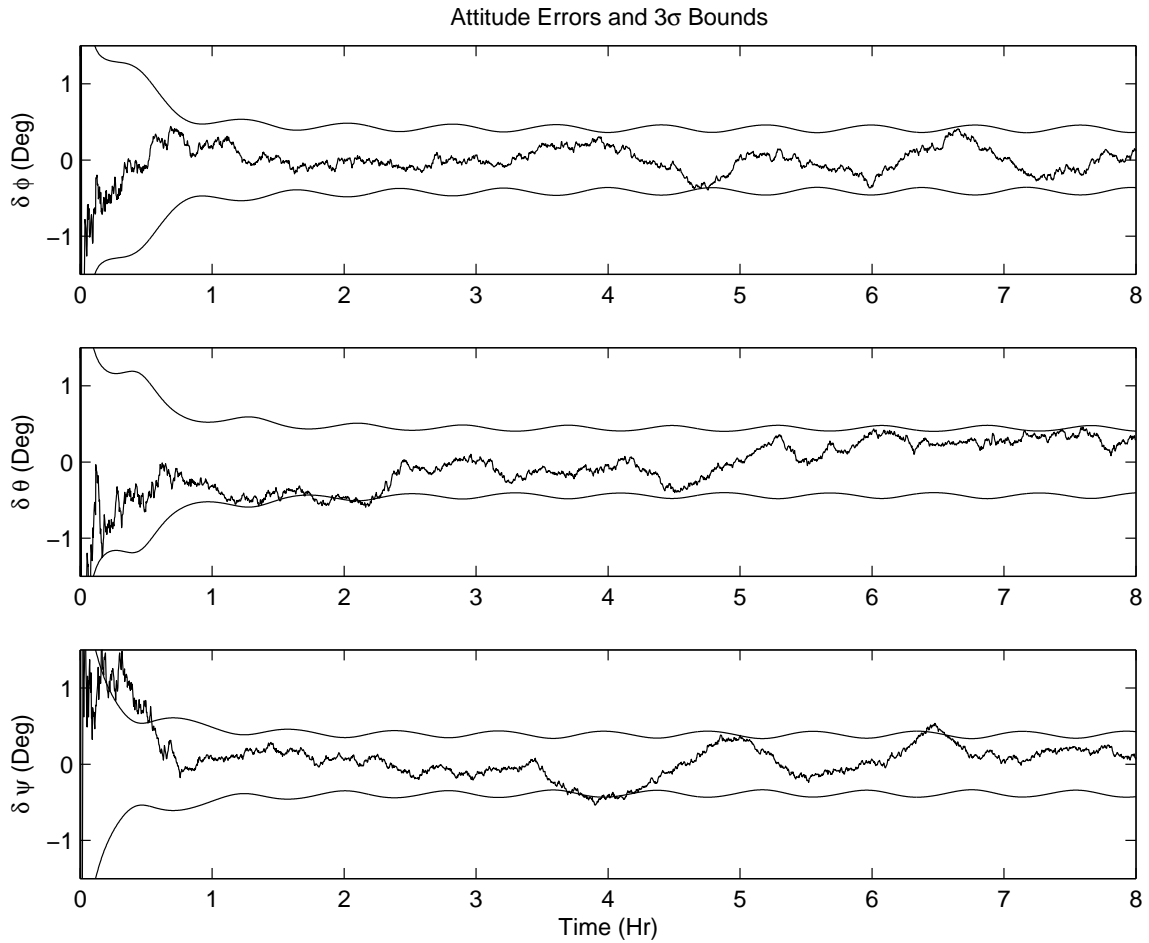


Fig. 6.31. UF Attitude Estimation Errors

Similar to Euler angle errors, the gyro drift estimation of the EKF fails. However, the estimation errors of the UF seem to be within  $3\sigma$  bounds. Also, the convergence of the drift errors requires more time than Euler angle estimation. The comparison is shown in Figs. 6.33 and 6.34.

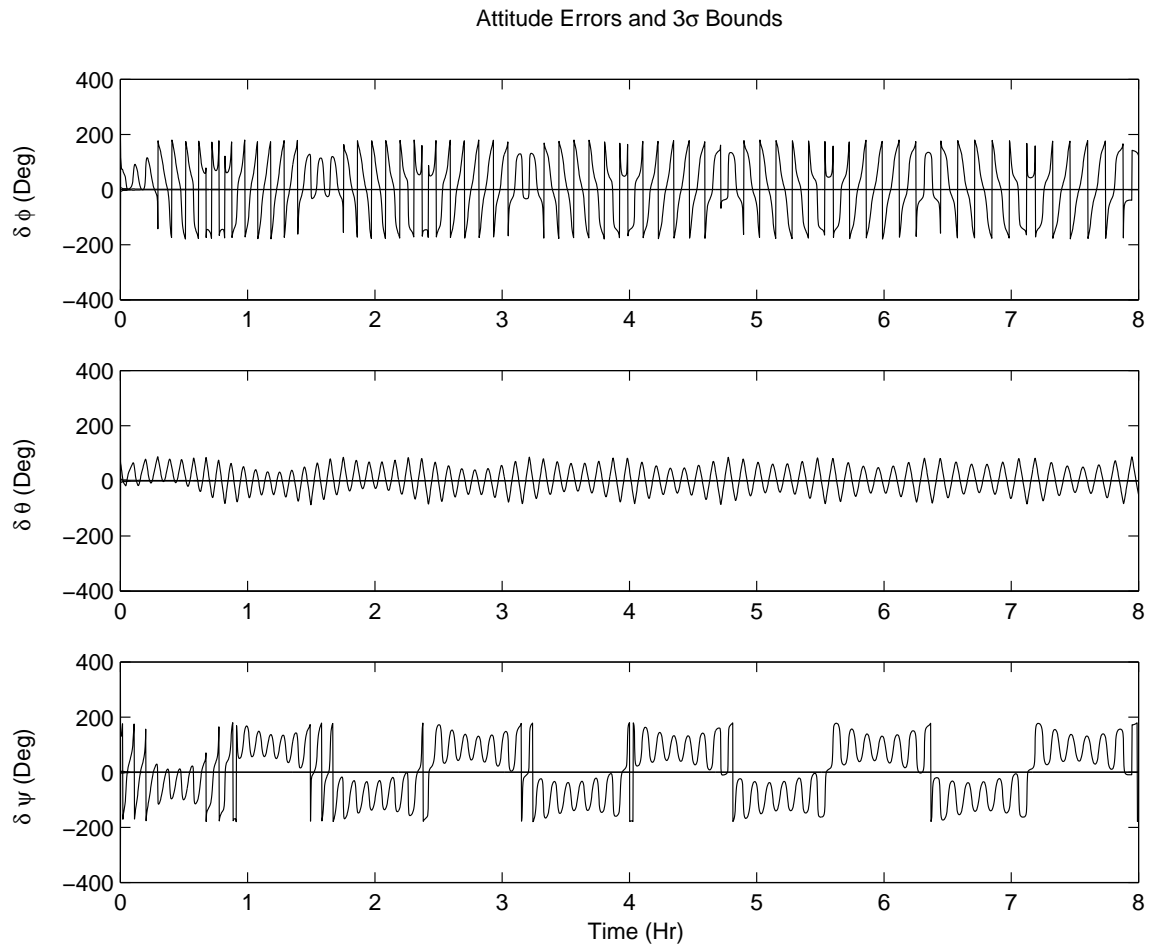


Fig. 6.32. EKF Attitude Estimation Errors

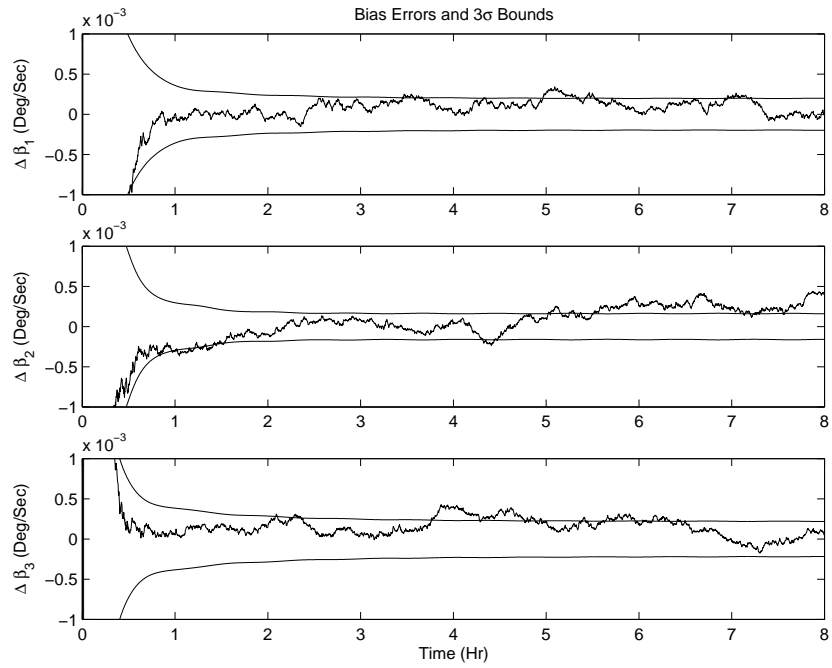


Fig. 6.33. UF Bias Estimation Errors

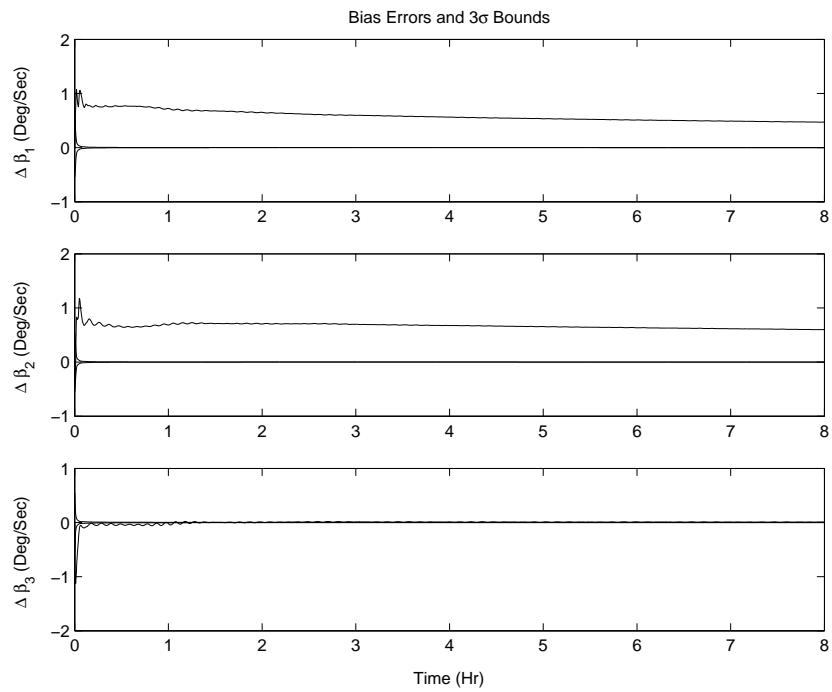


Fig. 6.34. EKF Bias Estimation Errors

## 6.6 Summary

Attitude estimation algorithms using Pseudolite signals are developed and compared in this section. The comparison is separated into two cases, the static and the moving cases. For the static case, nonlinear least squares as well as the Levenberg-Marquardt algorithm are compared with the nonlinear predictive filter. As a result, the nonlinear predictive filter with large weighting shows the smallest estimation errors while the estimation error covariance of all methods satisfies the Cramér-Rao lower bounds.

For moving cases, we consider a LEO spacecraft motion. Since the iterative algorithms, NLS and LM, are not efficient, only nonlinear predictive filter, EKF, and UF are compared. The estimation errors of the nonlinear predictive filter seem to be decreasing as weighting increases. However, unlike the static case, the estimation error of nonlinear predictive filter increases as the weight increases after a certain value of weighting which is varying due to sampling interval,  $\Delta t$ , and spacecraft angular motion. To enhance the estimation error characteristic, two filtering algorithms, the EKF and UF, are compared as well. As a result, both the EKF and UF determine the attitude well within 0.5 degrees Euler angle errors. However, the UF shows more robust results for large initial errors.

## CHAPTER VII

### CONCLUSION

In this dissertation, two tasks are accomplished. First, a self survey algorithm for GPS receiver is developed. Baselines, line biases, integer ambiguities, and attitude are determined successfully, although the phase measurements contains line biases and cycle slips. Both simulated and real data are used to verify the algorithm. Since cycle slips or jumps are frequently contained in the phase measurements, a real-time cycle slip detection and repair algorithm is developed for correct estimation. Then, a double difference scheme is used to cancel line biases errors which are also contained in the measurements. To determine the attitude, a nonlinear estimation problem is solved by using nonlinear least squares and the Levenberg-Marquardt algorithm. Simulations are used to compare the two methods. It is demonstrated that the LM method is more robust to large initial errors while NLS converges fast.

Then, attitude determination algorithms using spherical wavefront Pseudolite signals are developed and compared with simulations. A covariance analysis of the nonlinear predictive filter demonstrates it is an optimal estimator. For the static case, the estimation error is decreased as weighting is increased. However, the estimation error of the predictive filter is increased after a certain value of weighting for moving cases. To enhance the attitude determination performance, two filtering methods, the EKF and UF, are developed. Monte Carlo like simulations are used to compare the two filters for small initial errors. It is demonstrated that both filters work well. The differences between them cannot be differentiated. However, the covariance of UF is more reliable than that of the EKF. In the comparison of large initial errors, the UF determines attitude parameters and gyro drifts successfully while EKF fails. For the future work, real Pseudolite data application needs to be accomplished.



In addition, a new GPS constellation is proposed by using the Flower Constellation design scheme since the self survey and attitude determination rely on the geometry of sightlines. The proposed GNFC shows the better GDOPs and ADOPs than the existing or the upcoming GPS constellations.

## REFERENCES

- <sup>1</sup> Wertz, J., ed., *Spacecraft Attitude Determination and Control*, D.Reidel Publishing Company, Dordrecht, Holland, 1978.
- <sup>2</sup> Shuster, M. and Oh, S., “Three-Axis Attitude Determination from Vector Observations,” *Journal of Guidance and Control*, Vol. 4, No. 1, Jan. 1981, pp. 70–77.
- <sup>3</sup> Mortari, D., *Attitude Determination and Star Navigation*, Book in preparation.
- <sup>4</sup> Markley, F., “Attitude Determination Using Vector Observations: A Fast Optimal Matrix Algorithm,” *The Journal of the Astronautical Sciences*, Vol. 41, No. 2, April 1993, pp. 261–280.
- <sup>5</sup> Park, K. and Kim, J., “Performance Analysis of Four Attitude Determination Methods Using Line of Sight Vectors,” *Journal of Korean Society for Aeronautical and Space Sciences*, Vol. 26, No. 3, May 1998, pp. 140–147.
- <sup>6</sup> Bar-Itzhack, I., “Polar Decomposition for Attitude Determination from Vector Observations,” *Proceedings of the Flight Mechanics/Estimation Theory Symposium*, NASA-Goddard, Greenbelt, MD, 1992, pp. 201–215.
- <sup>7</sup> Crassidis, J., Andrews, S., Markley, F., and Ha, K., “Contingency Designs for Attitude Determination of TRMM,” *Proceedings of the Flight Mechanics/Estimation Theory Symposium*, NASA-Goddard Space Flight Center, Greenbelt, MD, May 1995, pp. 419–433.
- <sup>8</sup> Wahba, G., “A Least Squares Estimate of Spacecraft Attitude,” *SIAM Review*, Vol. 7, No. 3, July 1965, pp. 409.
- <sup>9</sup> Mortari, D., “Second Estimator of the Optimal Quaternions,” *Journal of Guidance, Control, and Dynamics*, Vol. 23, No. 5, Sept.–Oct. 2000, pp. 885–888.
- <sup>10</sup> Markley, F. and Mortari, D., “New Developments in Quaternion Estimation from Vector Observations,” *The Richard H. Battin Astrodynamics Symposium*, College Station, TX, March 2000, pp. 373–394.
- <sup>11</sup> Kalman, R., “A New Approach to Linear Filtering and Prediction Problems,” *Transactions of the ASME Journal of Basic Engineering*, Vol. 82 (Series D), March 1960, pp. 35–45.
- <sup>12</sup> Crassidis, J. and Junkins, J., *Optimal Estimation of Dynamic Systems*, Chapman & Hall/CRC, Boca Raton, FL, 2004.

- <sup>13</sup> Gelb, A., *Applied Optimal Estimation*, MIT Press, Cambridge, MA, 1974.
- <sup>14</sup> Stengel, R., *Optimal Control and Estimation*, Dover Publications, New York, 1994.
- <sup>15</sup> Jazwinski, A., *Stochastic Processes and Filtering Theory*, Vol. 64 of *Mathematics in Science and Engineering*, Academic Press, New York, 1970.
- <sup>16</sup> Farrell, J. and Barth, M., *The Global Positioning System & Inertial Navigation*, McGraw-Hill, New York, 1998.
- <sup>17</sup> Crassidis, J. and Markley, F., "Attitude Estimation Using Modified Rodrigues Parameters," *Proceedings of the Flight Mechanics/Estimation Theory Symposium*, NASA-Goddard Space Flight Center, Greenbelt, MD, May 1996, pp. 71–83.
- <sup>18</sup> Lefferts, E., Markley, F., and Shuster, M., "Kalman Filtering for Spacecraft Attitude Estimation," *Journal of Guidance, Control, and Dynamics*, Vol. 5, No. 5, Sept. 1982, pp. 417–429.
- <sup>19</sup> Crassidis, J., Markley, F., Kyle, A., and Kull, K., "Attitude Determination Improvements for GOES," *Proceedings of the Flight Mechanics/Estimation Theory Symposium*, NASA-Goddard Space Flight Center, Greenbelt, MD, May 1996, pp. 151–165.
- <sup>20</sup> Crassidis, J. and Markley, F., "Unscented Filtering for Spacecraft Attitude Estimation," [CD-ROM] *AIAA Guidance, Navigation, and Control Conference and Exhibit*, Austin, TX, Aug. 2003.
- <sup>21</sup> Creamer, G., "Spacecraft Attitude Determination Using Gyros and Quaternion Measurements," *The Journal of the Astronautical Sciences*, Vol. 44, No. 3, July 1996, pp. 357–371.
- <sup>22</sup> Deutschmann, J. and Bar-Itzhack, I., "Extended Kalman Filter for Attitude Estimation of the Earth Radiation Budget Satellite," *Proceedings of the AAS Astrodynamics Conference*, Portland, OR, Aug. 1990, pp. 786–796.
- <sup>23</sup> Gebre-Egziabher, D., Hayward, R., and Powell, J., "A Low-Cost GPS/Inertial Attitude Heading Reference System (AHRS) for General Aviation Application," *IEEE Position Location and Navigation Symposium '98*, Rancho Mirage, CA, April 1998, pp. 518–525.

- <sup>24</sup> Hayward, R., Gebre-Egziabher, D., and Powell, J., “GPS-Based Attitude For Aircraft,” *International Conference on Integrated Navigation Systems*, St. Petersburg, Russia, May 1998, [http://waas.stanford.edu/~wwu/papers/gps/PDF/att\\_for\\_aircraft\\_rch1998.pdf](http://waas.stanford.edu/~wwu/papers/gps/PDF/att_for_aircraft_rch1998.pdf).
- <sup>25</sup> Kim, J., *ISS Leak Localization Using Attitude Response*, Ph.D. dissertation, Texas A&M University, College Station, TX, Aug. 2002.
- <sup>26</sup> Markley, F., “Attitude Estimation or Quaternion Estimation?” *The John L. Junkins Astrodynamics Symposium*, College Station, TX, May 2003, pp. 113–128.
- <sup>27</sup> Shuster, M., “Kalman Filtering of Spacecraft Attitude and the QUEST Model,” *Journal of Astronautical Sciences*, Vol. 38, No. 3, July 1990, pp. 377–393.
- <sup>28</sup> Sorensen, J., Schmidt, S., and Goka, T., “Application of Square-Root Filtering for Spacecraft Attitude Control,” *Journal of Guidance and Control*, Vol. 2, No. 5, Sept.–Oct. 1979, pp. 426–433.
- <sup>29</sup> Bernelli-Zazzera, F. and Campana, R., “Adaptive Kalman Filtering for Multipath Rejection in GPS Based Attitude Determination,” *1999 AAS/AIAA Space Flight Mechanics Conference*, Breckenridge, CO, Feb. 1999, pp. 995–1010.
- <sup>30</sup> Crassidis, J. and Markley, F., “Predictive Filtering for Attitude Estimation Without Rate Sensors,” *Journal of Guidance, Control, and Dynamics*, Vol. 20, No. 3, May-June 1997, pp. 522–527.
- <sup>31</sup> Gai, E., Daly, K., Harrison, J., and Lemos, L., “Star-Sensor-Based Satellite Attitude/Attitude Rate Estimator,” *Journal of Guidance*, Vol. 8, No. 5, Sept.–Oct. 1985, pp. 560–565.
- <sup>32</sup> Junkins, J., Hughes, D., Wazni, K., and Pariyapong, V., “Vision-Based Navigation for Rendezvous,” *22nd Annual AAS Guidance and Control Conference*, Breckenridge, CO, Feb. 1999, pp. 203–220.
- <sup>33</sup> Schierman, J., Schmidt, D., and Deutschmann, J., “Attitude and Trajectory Determination Using Magnetometers and Estimated Rates,” *Proceedings of the Flight Mechanics/Estimation Theory Symposium*, NASA-Goddard Space Flight Center, Greenbelt, MD, May 1997, pp. 319–330.
- <sup>34</sup> Crassidis, J. and Markley, F., “Unscented Filtering for Spacecraft Attitude Estimation,” *Journal of Guidance, Control, and Dynamics*, Vol. 26, No. 4,

- July–Aug. 2003, pp. 536–542.
- <sup>35</sup> Julier, S. and Uhlmann, J., “A General Method for Approximating Nonlinear Transformations of Probability Distributions,” Online, 1996, <http://citeseer.ist.psu.edu/julier96general.html>.
- <sup>36</sup> van der Merwe, R. and Wan, E., “Sigma-Point Kalman Filters for Probabilistic Inference in Dynamic State-Space Models,” *Proceedings of the Workshop on Advances in Machine Learning*, Montreal, Canada, June 2003, <http://www.iro.umontreal.ca/~kegl/CRMWorkshop/paperMerweWan.pdf>.
- <sup>37</sup> Shuster, M., “A Survey of Attitude Representations,” *Journal of Astronautical Sciences*, Vol. 41, No. 4, Oct. 1993, pp. 439–517.
- <sup>38</sup> Schaub, H. and Junkins, J., *Analytical Mechanics of Space Systems*, American Institute of Aeronautics and Astronautics, Inc., Reston, VA, 2003.
- <sup>39</sup> Julier, S., Uhlmann, J., and Durrant-Whyte, H., “A New Method for the Non-linear Transformation of Means and Covariances in Filters and Estimators,” *IEEE Transactions on Automatic Control*, Vol. 45, No. 3, March 2000, pp. 477–482.
- <sup>40</sup> Wan, E. A. and van der Merwe, R., “The Unscented Kalman Filter for Non-linear Estimation,” *IEEE Proceedings of Symposium 2000 on Adaptive Systems for Signal Processing, Communication and Control (AS-SPCC)*, Lake Louise, Alberta, Canada, Oct. 2000, pp. 153–158.
- <sup>41</sup> Lai, K., Crassidis, J., and Harman, R., “In-Space Spacecraft Alignment Calibration Using the Unscented Filter,” [CD-ROM] *AIAA Guidance, Navigation, and Control Conference and Exhibit*, Austin, TX, Aug. 2003.
- <sup>42</sup> Lightsey, E. and Crassidis, J., “Real Time Attitude Independent GPS Integer Ambiguity Resolution,” *The John L. Junkins Astrodynamics Symposium*, College Station, TX, May 2003, pp. 145–164.
- <sup>43</sup> Crassidis, J. and Markley, F., “Predictive Filtering for Nonlinear Systems,” *Journal of Guidance, Control, and Dynamics*, Vol. 20, No. 3, May-June 1997, pp. 566–572.
- <sup>44</sup> Axelrad, P. and Behre, C., “Satellite Attitude Determination Based on GPS Signal-to-Noise Ratio,” *Proceedings of the IEEE*, Vol. 87, No. 1, Jan. 1999, pp. 133–144.

- <sup>45</sup> Azimi-Sadjadi, B. and Krishnaprasad, P., "Approximate Nonlinear Filtering and Its Applications for GPS," *Proceedings of 39th IEEE Conference on Decision and Control*, Sydney, Australia, Dec. 2000, pp. 1579–1584.
- <sup>46</sup> Bar-Itzhack, I., Montgomery, P., and Garrick, J., "Algorithms for Attitude Determination Using GPS," *Proceedings of the AIAA Guidance, Navigation, and Control Conference*, Reston, VA, Aug. 1997, pp. 841–851.
- <sup>47</sup> Cohen, C., *Attitude Determination Using GPS*, Ph.D. dissertation, Stanford University, Dec. 1992.
- <sup>48</sup> Crassidis, J., Markley, F., Lightsey, E., and Ketchum, E., "Predictive Attitude Estimation Using Global Positioning System Signals," *Proceedings of the Flight Mechanics/Estimation Theory Symposium*, NASA-Goddard Space Flight Center, Greenbelt, MD, May 1997, pp. 107–120.
- <sup>49</sup> Crassidis, J. and Markley, F., "A Predictive Attitude Determination Algorithm," *Proceedings of the Flight Mechanics/Estimation Theory Symposium*, NASA-Goddard Space Flight Center, Greenbelt, MD, May 1997, pp. 249–263.
- <sup>50</sup> Crassidis, J. and Markley, F., "A New Algorithm for Attitude Determination Using Global Positioning System Signals," *Journal of Guidance, Control, and Dynamics*, Vol. 20, No. 5, Sept.-Oct. 1997, pp. 891–896.
- <sup>51</sup> Crassidis, J., Markley, F., and Lightsey, E., "Application of Vectorized Attitude Determination Using Global Positioning System Signals," *Proceedings of the AIAA/AAS Astrodynamics Specialist Conference*, Boston, MA, Aug. 1998.
- <sup>52</sup> Crassidis, J., Lightsey, E., and Markley, F., "Efficient and Optimal Attitude Determination Using Recursive Global Positioning System Signal Operations," *AIAA Journal of Guidance, Control, and Dynamics*, Vol. 22, No. 2, March–April 1999, pp. 193–201.
- <sup>53</sup> Park, K. and Crassidis, J., "Autonomous Attitude Determination for ISS Applications Using Pseudolite Signals," Tech. Rep. , NASA Johnson Space Center, Houston, TX, June 2003.
- <sup>54</sup> Gaylor, D. and Lightsey, E., "GPS/INS Kalman Filter Design for Spacecraft Operating in the Proximity of the International Space Station," [CD-ROM] *AIAA Guidance, Navigation, and Control Conference and Exhibit*, Austin, TX, Aug. 2003.

- <sup>55</sup> Hayward, R. and Powell, J., “Real Time Calibration of Antenna Phase Errors for Ultra Short Baseline Attitude Systems,” *ION GPS-98*, Nashville, TN, Sept. 1998, pp. 1753–1762.
- <sup>56</sup> Madsen, J. and Lightsey, E., “Attitude Determination Using GPS Signal to Noise Ratio and Carrier Phase Measurements,” [CD-ROM] *AIAA Guidance, Navigation, and Control Conference and Exhibit*, Austin, TX, Aug. 2003.
- <sup>57</sup> Peng, H., Chang, F., and Wang, L., “Rotation Method for Direction Finding via GPS Carrier Phases,” *IEEE Transactions on Aerospace and Electronic Systems*, Vol. 36, No. 1, Jan. 2000, pp. 72–84.
- <sup>58</sup> Psiaki, M., “Attitude Sensing Using a GPS Antenna on a Turntable,” *AIAA Guidance, Navigation, and Control Conference and Exhibit*, Denver, CO, Aug. 2000.
- <sup>59</sup> Pendergrass, J., Treder, A., and Gomez, S., “GPS-Updated Attitude Determination Performance on ISS Despite Rich Multipath,” *AIAA Guidance, Navigation, and Control Conference and Exhibit*, Denver, CO, Aug. 2000.
- <sup>60</sup> Brown, A. and Stolk, K., “Rapid Ambiguity Resolution using Multipath Spatial Processing for High Accuracy Carrier Phase,” *Proceedings of ION GPS-2002*, Portland, OR, Sept. 2002, pp. 973–980.
- <sup>61</sup> Crassidis, J., Markley, F., and Lightsey, E., “Global Positioning System Integer Ambiguity Resolution Without Attitude Knowledge,” *AIAA Journal of Guidance, Control, and Dynamics*, Vol. 22, No. 2, March–April 1999, pp. 212–218.
- <sup>62</sup> Gabor, M. and Nerem, R., “A New Approach to GPS Carrier Phase Ambiguity Resolution,” *1999 AAS/AIAA Astrodynamics Specialist Conference*, Girdwood, AK, Aug. 1999, pp. 1009–1027.
- <sup>63</sup> Lightsey, E., Crassidis, J., and Markley, F., “Fast Integer Ambiguity Resolution for GPS Attitude Determination,” *Proceedings of the AIAA Guidance, Navigation, and Control Conference*, Portland, OR, Aug. 1999, pp. 403–412.
- <sup>64</sup> Teunissen, P., “A Canonical Theory for Short GPS Baselines Part II: The Ambiguity Precision and Correlation,” *Journal of Geodesy*, Vol. 71, No. 7, May 1997, pp. 389–401.
- <sup>65</sup> Teunissen, P., “A Canonical Theory for Short GPS Baselines Part III: The Geometry of the Ambiguity Search Space,” *Journal of Geodesy*, Vol. 71, No. 8,

- May 1997, pp. 486–501.
- <sup>66</sup> Weisenburger, S., *Effect of Constraints and Multiple Receivers for On-The-Fly Ambiguity Resolution*, M.S. thesis, University of Calgary, Alberta, Calgary, April 1997.
- <sup>67</sup> Hofmann-Wellenhof, B., Lichtenegger, H., and Collins, J., *Global Positioning System: Theory and Practice*, 4th ed., Springer-Verlag, New York, 1997.
- <sup>68</sup> Comp, C. and Axelrad, P., “Adaptive SNR-Based Carrier Phase Multipath Mitigation Technique,” *IEEE Transactions on Aerospace and Electric Systems*, Vol. 34, No. 1, Jan. 1998, pp. 264–276.
- <sup>69</sup> Parkinson, B. and Spilker Jr., J., ed., *Global Positioning System: Theory and Applications*, Vol. I–II, American Institute of Aeronautics and Astronautics, Washington, DC, 1996.
- <sup>70</sup> Altmayer, C., “Enhancing the Integrity of Integrated GPS/INS Systems by Cycle Slip Detection and Correction,” *Proceedings of the IEEE Intelligent Vehicles Symposium*, Miami, FL, Oct. 2000, pp. 174–179.
- <sup>71</sup> Cohen, C., “Attitude Determination,” *Global Positioning System: Theory and Applications*, Vol. II, edited by B.W. Parkinson and J.J. Spilker, Jr., American Institute of Aeronautics and Astronautics, Washington, DC, 1996, pp. 519–538.
- <sup>72</sup> Alonso, R. and Shuster, M., “A New Algorithm for Attitude-Independent Magnetometer Calibration,” *Proceedings of the Flight Mechanics/Estimation Theory Symposium*, NASA-Goddard Space Flight Center, Greenbelt, MD, May 1994, pp. 513–527.
- <sup>73</sup> Fujikawa, S. and Zimbelman, D., “Spacecraft Attitude Determination by Kalman Filtering of Global Positioning System Signal,” *Journal of Guidance Control and Dynamics*, Vol. 18, No. 6, Nov.–Dec. 1995, pp. 1365–1371.
- <sup>74</sup> Melvin, P. and Hope, A., “Satellite Attitude Determination with GPS,” *Advances in the Astronautical Sciences*, Vol. 85 - Part I, 1993, pp. 59–78.
- <sup>75</sup> Melvin, P., Ward, L., and Axelrad, P., “The Analysis of GPS Attitude Data from a Slowly Rotating, Symmetrical Gravity Gradient Satellite,” *Advances in the Astronautical Sciences*, Vol. 89 - Part I, 1995, pp. 539–558.
- <sup>76</sup> Lightsey, E., Cohen, C., Feess, W., and Parkinson, B., “Analysis of Spacecraft Attitude Measurements Using Onboard GPS,” *17th Annual American Astro-*



- nautical Society (AAS) Guidance and Control Conference*, Feb. 1994, pp. 521–532.
- <sup>77</sup> Lightsey, E., Ketchum, E., Flatley, T., Crassidis, J., Freesland, D., Reiss, K., and Young, D., “Flight Results of GPS-Based Attitude Control on the REX-II Spacecraft,” *Proceedings of ION GPS-96*, Kansas City, MO, Sept. 1996, pp. 1037–1046.
- <sup>78</sup> Brock, J., Fuller, R., Kemper, B., Mleczo, D., Rodden, J., and Tadros, A., “GPS Attitude Determination and Navigation Flight Experiment,” *Proceedings of ION GPS-95*, Palm Springs, CA, Sept. 1995, pp. 545–554.
- <sup>79</sup> Zimmerman, K. and Cannon Jr., R., “Differential Carrier Phase GPS Techniques for Space Vehicle Rendezvous,” *Proceedings of ION GPS-94*, Salt Lake City, UT, Sept. 1994, pp. 1693–1700.
- <sup>80</sup> Zimmerman, K. and Cannon Jr., R., “Experimental Demonstration of GPS for Rendezvous Between Two Prototype Space Vehicles,” *Proceedings of ION GPS-95*, Palm Springs, CA, Sept. 1995, pp. 1905–1913.
- <sup>81</sup> The MathWorks, “Documentation for MathWorks Products (Release 13 with Service Pack 1),” Online, <http://www.mathworks.com/access/helpdesk/help/helpdesk.shtml>.
- <sup>82</sup> Junkins, J. and Kim, Y., *Introduction to Dynamics and Control of Flexible Structures*, AIAA Educational Series, American Institute of Aeronautics and Astronautics, Inc., Washington, DC, 1993.
- <sup>83</sup> Bryson, Jr., A. and Ho, Y., *Applied Optimal Control* (Revised Printing), Taylor & Francis, Levittown, PA, 1975.
- <sup>84</sup> Altmayer, C., “Accuracy Improvements of Pseudolite Systems - First Results,” *Proceedings of National Technical Meeting 2001*, Long Beach, CA, Jan. 2001, pp. 491–500.
- <sup>85</sup> van der Merwe, R., de Freitas, N., Doucet, A., and Wan, E., “The Unscented Particle Filter,” Tech. Rep. CUED/F-INFENG/TR380, Cambridge University Engineering Department, Aug. 2000.
- <sup>86</sup> van der Merwe, R. and Wan, E. A., “The Square-Root Unscented Kalman Filter For State And Parameter-Estimation,” Online, <http://citeseer.ist.psu.edu/vandermerwe01squareroot.html>.

- <sup>87</sup> Stanley, W., “Quaternion from Rotation Matrix,” *Journal of Guidance and Control*, Vol. 1, No. 3, May 1978, pp. 223–224.
- <sup>88</sup> Markley, F., “Matrix and Vector Algebra,” *Spacecraft Attitude Determination and Control*, edited by J.R. Wertz, D.Reidel Publishing Company, Dordrecht, Holland, 1978, pp. 744–757.
- <sup>89</sup> Farrenkopf, R., “Analytic Steady-State Accuracy Solutions for Two Common Spacecraft Attitude Estimators,” *Journal of Guidance and Control*, Vol. 1, No. 4, July–Aug. 1978, pp. 282–284.
- <sup>90</sup> Navigation Center, “GPS Almanac Information,” Online, <http://www.navcen.uscg.gov/gps/almanacs.htm>.
- <sup>91</sup> Gurtner, W., “RINEX: The Receiver Independent Exchange Format Version 2.10,” Online, June 2001, <http://www.ngs.noaa.gov/CORS/instructions2/>.
- <sup>92</sup> Lechner, W. and Baumann, S., “Global Navigation Satellite Systems,” *Computers and Electronics in Agriculture*, Vol. 25, Issues 1-2, Jan. 2000, pp. 67–85.
- <sup>93</sup> European Communities, “Galileo Technical Documents,” Online, [http://europa.eu.int/comm/dgs/energy\\_transport/galileo/doc/galilei\\_brochure.pdf](http://europa.eu.int/comm/dgs/energy_transport/galileo/doc/galilei_brochure.pdf).
- <sup>94</sup> Mortari, D., Wilkins, M., and Bruccoleri, C., “The Flower Constellations,” *The John L. Junkins Astrodynamics Symposium*, May 2003, pp. 269–290.
- <sup>95</sup> Vallado, D., *Fundamentals of Astrodynamics and Applications*, McGraw-Hill, New York, 1997.
- <sup>96</sup> NASA Laboratory of High Energy Astrophysics, “Ask a High Energy Astronomer,” Online, [http://imagine.gsfc.nasa.gov/docs/ask\\_astro/ask\\_an\\_astronomer.html](http://imagine.gsfc.nasa.gov/docs/ask_astro/ask_an_astronomer.html).
- <sup>97</sup> Park, K., Wilkins, M., and Mortari, D., “Uniformly Distributed Flower Constellation Design Study for Global Navigation System,” *The 14th AAS/AIAA Space Flight Mechanics Meeting*, Maui, Hawaii, Feb. 2004.
- <sup>98</sup> The Analytical Graphics, Inc., “STK 4.4 Online Help,” Online, <http://www.agi.com/resources/help/help/stk44/overview.htm>.
- <sup>99</sup> Dai, L., Wang, J., Tsujii, T., and Rizos, C., “Pseudolite Application in Positioning and Navigation: Modeling and Geometric Analysis,” *Int’l Symposium on Kinematic Systems in Geodesy, Geomatics & Navigation (KIS2001)*, Banff, Canada, June 2001, pp. 482–489.

- <sup>100</sup> LeMaster, E. and Rock, S., “Self-Calibration of Pseudolite Arrays Using Self-Differencing Transceivers,” *Proceedings of ION GPS-99*, Nashville, TN, Sept. 1999, pp. 1549–1558.
- <sup>101</sup> LeMaster, E. and Rock, S., “Field Test Results for a Self-Calibrating Pseudolite Array,” *Proceedings of ION GPS-2000*, Salt Lake City, UT, Sept. 2000, pp. 1046–1055.
- <sup>102</sup> LeMaster, E., Matsuoka, M., and Rock, S., “Mars Navigation System Utilizes GPS,” *IEEE Aerospace and Electronic Systems Magazine*, Vol. 18, No. 4, April 2003, pp. 3–8.
- <sup>103</sup> Stone, J., LeMaster, E., Powell, J., and Rock, S., “GPS Pseudolite Transceivers and Their Applications,” *Proceedings of National Technical Meeting 99*, San Diego, CA, Jan. 1999, pp. 415–424.
- <sup>104</sup> Teague, E., How, J., Lawson, L., and Parkinson, B., “Carrier Differential GPS for Real-Time Control of Large Flexible Structures,” *Proceedings of ION GPS-96*, Kansas City, MO, Sept. 1996, pp. 1355–1365.
- <sup>105</sup> Moehlis, J., “A Beginner’s Guide to Simulating Stochastic Differential Equation,” Online, <http://www.math.princeton.edu/~apc514/tutorials/tutorial7/tutorial7/tutorial7.html>.

## APPENDIX A

## COLORED NOISE

Non-Gaussian error, such as multi-path error, is known to be contained in the GPS phase measurement. This colored noise,  $\xi(t)$ , may be calculated by<sup>53,105</sup>

$$\frac{d\xi}{dt} = -\frac{1}{\tau}\xi + \frac{\epsilon}{\tau}\eta(t) \quad (\text{A.1})$$

where  $\eta(t)$  is a Gaussian white noise and  $\tau$  is a time constant. A colored noise used in the simulation is shown in Fig. A.1. A time constant of twenty minutes is used.

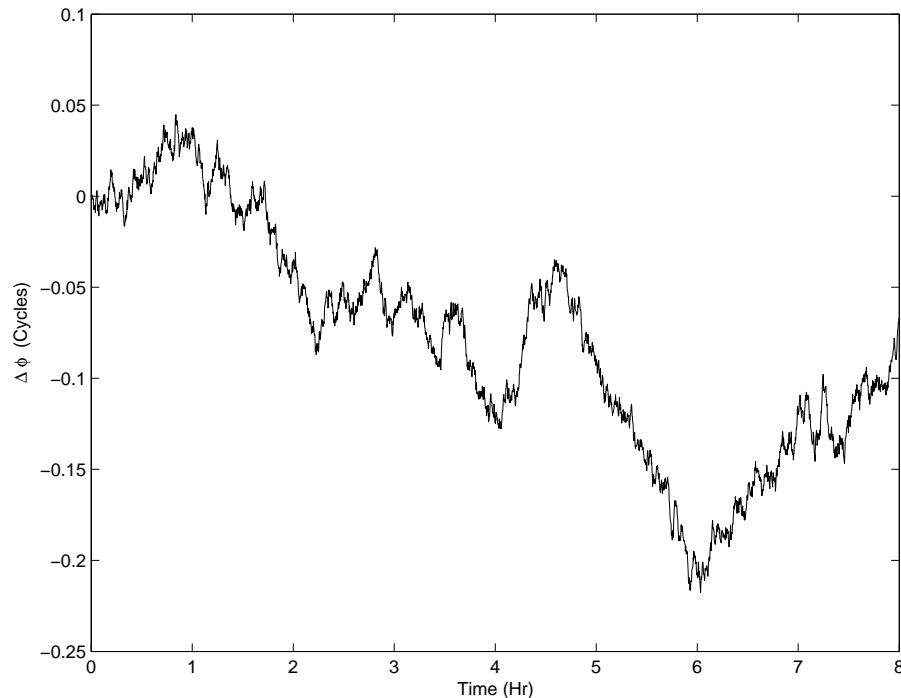


Fig. A.1. Colored Noise

By using these colored noises, the phase measurements are simulated. Then, NLS and PF estimation results are compared in Fig. A.2. as well as  $3\text{-}\sigma$  bounds. The thick solid line represents the roll angle estimation error that is determined by the PF. Small circles correspond to the NLS estimation error. As can be seen, the PF shows slightly the better results.

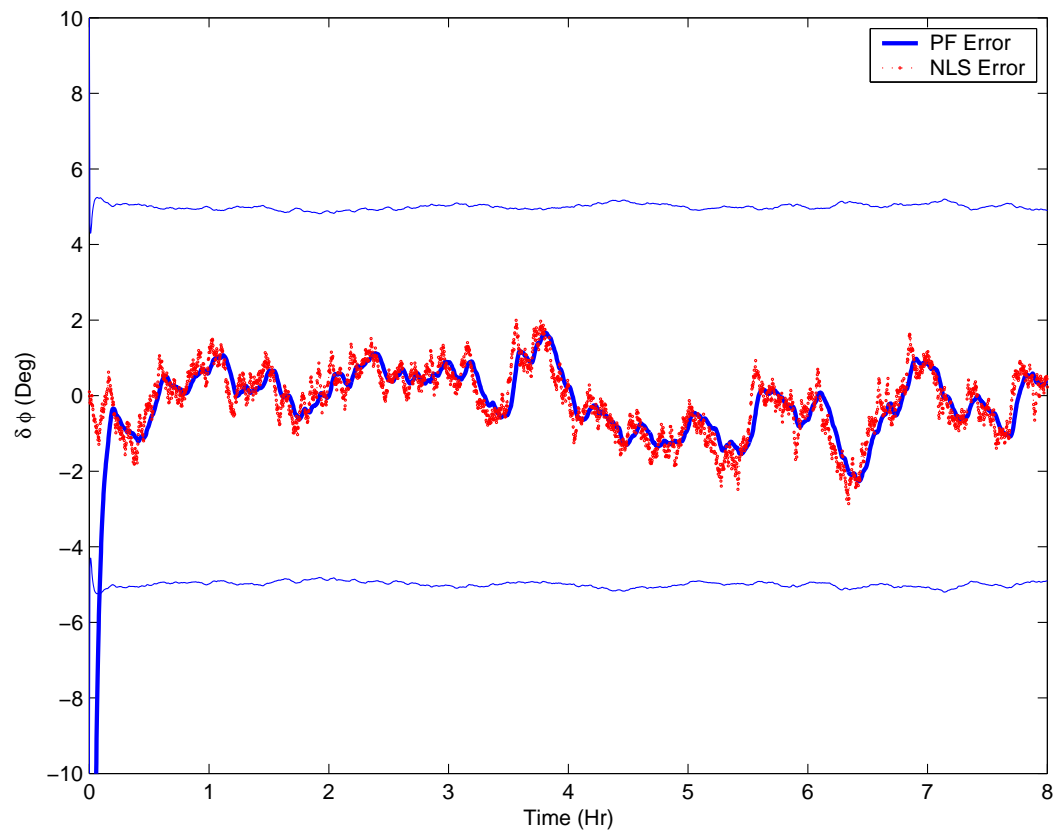


Fig. A.2. Roll Angle Estimation Error Comparison (Colored Noise)

## VITA

Keun Joo Park graduated from Inha University, Incheon, South Korea with a Bachelor of Science degree in aerospace engineering in February 1995 and a Master of Science degree in aerospace engineering in February 1997. After his graduation, he worked as an engineer in the Satellite Business Division of Hyundai Electronics Industries, Inc., Icheon, South Korea from June 1997 to March 1998. In the fall of 1999, he joined the Ph.D. program in the Department of Aerospace Engineering at Texas A&M University. His professional interests include optimal nonlinear filtering and control techniques, space mission design and analysis, and software development.

Permanent address:

406-2003 Hyundai APT, Okryundong, Yunsugu, Incheon, South Korea, 406-050  
(email: [kj\\_park@hotmail.com](mailto:kj_park@hotmail.com))

This dissertation was typed by the author.